On the Utility of Nonthermal Plasmas

Michael J. Hay

A Dissertation
Presented to the Faculty
of Princeton University
in Candidacy for the Degree
of Doctor of Philosophy

Recommended for Acceptance
by the Department of
Astrophysical Sciences
Program in Plasma Physics
Adviser: Nathaniel J. Fisch

November 2016

Abstract

Nonthermal plasmas have properties which can differ substantially even from thermal plasmas of the same density and energy. In practical applications, many of these differences have utility that can be exploited, often with waves. The goal of this thesis is to explore three such applications of nonthermal plasma for the purposes of wave amplification and, ultimately, controlled nuclear fusion.

First, we discuss the outstanding potential for a shaped plasma technology that relies on ionizing a beam of aerosol particles. This ionization results in a Coulomb explosion, yielding a highly nonthermal distribution for the plasma in the target volume. Homogeneous, high aspect ratio plasma couplers such as these could be used in a Raman amplification scheme to attain the next generation of laser intensities. Such a powerful laser could be used to study radiation reaction and vacuum pair production, among many other applications. We describe the conditions under which sufficiently dense aerosol beams can be prepared and provide some experimental validation of these claims.

Second, we survey the prospects for controlled p-^{11}B fusion in both magnetic and inertial confinement schemes. Whereas most studies have focused on mitigating the bremsstrahlung loss channel, we focus on nonthermal manipulations of the bulk plasma which could improve the reactivity. In particular, we present upper bounds on the p-^{11}B reactivity using alpha channeling to efficiently heat the proton distribution in both schemes.

Finally, we place a sharp limit on the energy that can be extracted from a nonthermal particle distribution using waves. In the quasilinear regime of wave-particle

interaction, waves rearrange the densities of states in phase space in a diffusive fashion. A salient consequence is that only certain, generally nonthermal, plasma states can be reached. We characterize this restricted state space and thereby reduce the problem of maximizing energy extraction to linear programming. Varying the connectedness of the phase space so that e.g. particles may only be diffused to parts of phase space close in energy, we describe the implications for the state space and the solution of the optimization problem.

Acknowledgements

First and foremost I need to acknowledge the support and mentorship of my adviser, Nat Fisch. His creativity and intuition for posing and solving complex problems is unmatched in my experience. It has been a singular pleasure to work with him, and I hope that we remain collaborators far into the future.

Thanks to Barbara Sarfaty and Beth Leman for making the department feel like my second home. I sincerely appreciate all your help with university policies and paperwork and, more to the point, your assistance in tracking down Nat over the years.

This thesis has benefitted greatly from my time spent in the Dissertation Boot Camp on main campus. Thanks especially to Amanda Irwin Wilkins and Mariana Campos-Horta for the coaching and snacks.

It goes without saying that I could not have succeeded in pursuing a Ph.D. without the influence, kindness, and instruction of many teachers, past and present. From my formative years as a high school student in Minnesota, I thank David Bassett, Abdo Karimi, Doug Hoverson, Joe Koch, Lori Pearce, Mitch Taraschi, and Frank Blankley. From my time as a Berkeley undergraduate, I thank Ivan Matic, Raluca Scarlat, Heath Pearson, Susan Schweik, Francesco Ganda, Philippe Bardet, Per Peterson, Martin White, Susan Muller, Richard Klein, Raymond Jeanloz, Ed Morse, Raphael Bousso, and Rick Norman. During my time at Princeton, I have been lucky to know Ron Davidson, Ernie Valeo, Ilya Dodin, Honq Qin, Roscoe White, John Krommes, Bill Tang, and many more.

I spent many years collaborating with scientists at Lawrence Berkeley and Lawrence Livermore, and I am both grateful for their friendship and proud of the work we completed together. Thank you to John Barnard, Grant Logan, John Perkins, Larry Suter, Dan Clark, Alex Friedman, Richard Town, Debbie Callahan, Steve Lund, Peter Seidl, and Joe Kwan. Being a member of Action Carpool made the commute to Livermore enjoyable and enlightening: thanks to Matt Terry, Mordy Rosen, and Judy Harte for conversation and camaraderie.

Thanks to my readers Hong Qin and Roscoe White for their diligence and poignant suggestions: this thesis was much improved by their efforts. Of course, all errors remaining are my own. Hong was my first mentor at Princeton, and our collaboration continued while I completed my undergraduate work. It has been a pleasure being your colleague for the past eight years, and I'm looking forward to enjoying more of the brilliant and insightful work you and your students regularly produce. Roscoe was like a second advisor to me throughout my time here, and his sage perspective was always welcome. I'm sorry I dropped your class.

Particular thanks are due to my collaborators Ernie Valeo, Daniel Ruiz, Lee Gunderson, Enrique Merino, Stewart Zweben, and Jeremy Schiff for their contributions and insight into much of the work presented here.

Of course my friends made this whole thing possible. It was a pleasure to spend six years in the Theory Nub with the likes of Andrey Zhmoginov, Jono Squire, Josh Burby, Lei Shi, Ben Faber, Seth Davidovits, Eric Shi, Daniel Ruiz, Ian Ochs, Yao Zhou, Chang Liu, Paul Schmit, Zeev Toroker, Clayton Myers, John Rhoads, Jeff Parker, and Renaud Gueroult.

Thanks to Eric Shi, Kenan Qu, Seth Davidovits, Eero Hirvijoki, Julian Kates-Harbeck, and Tim Stevenson for making the Princeton Plasma Physiques Laboratory an excellent place to work out.

Finally, I thank my parents for their support, counsel, and unconditional love. I am here today because of you.

All work herein was performed under DOE Contract No. DE-AC02-09CH11466, the DOE management and operating contract for the Princeton Plasma Physics Laboratory. I was supported for four years by a Department of Energy NNSA Stewardship Science Graduate Fellowship under Grant No. DE-FC52-08NA28752. Other support came from the DOE NNSA Stewardship Science Academic Alliances program under Grant No. DE274-FG52-08NA28553.

For Kipper

Contents

List of Tables

List of Figures

Chapter 1

Introduction

Nonthermal plasmas have properties which can differ substantially even from thermal plasmas of the same density and energy. In practical applications, many of these differences have utility that can be exploited, often with waves. The goal of this thesis is to explore three such applications of nonthermal plasma for the purposes of wave amplification and, ultimately, controlled nuclear fusion.

Due perhaps to their altered properties, or out of necessity, nonthermal distributions have been the subject of extensive study in plasma physics. Virtually all interesting plasma phenomena arise from distributions which are at least weakly nonthermal, in the quasilinear approximation [Vedenov et al., 1962]. Nonthermal distributions may variously result in elevated reaction rates due to quantum interference [Wigner, 1932, Savchenko et al., 1999, Starostin et al., 2000, Fisch et al., 2012] and electron screening [Salpeter, 1954, Lapenta and Quarati, 1993, Son and Fisch, 2005], or depressed ones [Kaniadakis et al., 1996, Molvig et al., 2012, Davidovits

and Fisch, 2014]. Regarding tokamak performance, nonthermal distributions can be a blessing, supporting confining currents [Karney and Fisch, 1979, Fisch and Karney, 1985, Fisch, 1986] and alpha channeling [Valeo and Fisch, 1994, Fisch and Rax, 1992b], or a curse, as in the case of runaway electrons [Dreicer, 1959, Guan et al., 2010].

Moreover, it is necessary to capture the nonthermal physics in order to accurately describe transport processes in both magnetic and inertial fusion [Hinton and Hazeltine, 1976, Ichimaru, 1993, Atzeni and Meyer-ter-Vehn, 2004]. Nonthermal effects in laser plasmas are responsible for the acceleration of fast particle beams [Porshnev et al., 1994, Snavely et al., 2000] and x-ray lasing [Rosen et al., 1985]. Nonthermal plasmas enjoy many applications apart from fusion in healthcare and industry [Lieberman and Lichtenberg, 2005, Desmet et al., 2009, Yamamoto and Okubo, 2007]. In this thesis, we will emphasize the utility of imposed nonthermal conditions, using waves to create shaped plasmas, increase reactivity, and extract energy.

Chapter 2 reviews the physics of quasilinear diffusion, which underlies the wave-particle couplings exploited throughout this thesis, and provides some mathematical context for the problem of optimizing the plasma free energy (discussed below).

Chapter 3 introduces the design and production of freestanding dense plasma slabs. Shaped plasmas such as these represent an outstanding technical challenge due to the difficulty of producing them, as well as their many anticipated applications in radiation generation [Rosen et al., 1985], laser amplification [Malkin et al., 1999, Toroker et al., 2012, Malkin et al., 2012, Malkin and Fisch, 2016], and perhaps fusion [Ditmire et al., 1997, 1999, Slutz and Vesey, 2012, Hay et al., 2013]. It was

necessary to extend the technique of aerodynamically focusing aerosols [de la Mora and Riesco-Chueca, 1988, Liu et al., 1995a] to conditions in which the solid phase density exceeds that of the carrier fluid. In this regime, new, deleterious effects on the focusing appear which are analogous to optical aberrations. It is shown how these effects can be mitigated so that dense aerosols may be rapidly ionized to form nonthermal plasmas of the desired shape and composition. Over time, these evolve as Coulomb explosions [Tkachev and Yakovlenko, 1993, Bychenkov and Kovalev, 2005, Grech et al., 2011, Mason et al., 2015].

Due to their large aspect ratio, these plasma couplers could prove useful in attaining and surpassing laser powers in the exawatt regime, permitting on-target intensities in excess of $10^{25}\,\mathrm{W/cm^2}$ [Mourou et al., 2012]. Lasers in the ultrarelativistic regime, driving electron quiver energies much greater than mc^2, have a host of applications, from probing fundamental physics (e.g. radiation reaction [Dirac, 1927] and vacuum pair production [Schwinger, 1951, Di Piazza et al., 2012]), to the production of electron beams [Tajima and Dawson, 1979, Gordienko and Pukhov, 2005, Esarey et al., 2009, Geyko et al., 2010] and radiation [Ditmire et al., 1995, Brabec and Krausz, 2000, Nakamura et al., 2012], as well as fusion [Tabak et al., 1994].

Chapter 4 addresses the prospect of controlled p-^{11}B fusion in both magnetic and inertial confinement schemes. Because bremsstrahlung precludes the ignition of optically thin, thermal p-^{11}B plasmas [Dawson, 1981, Nevins, 1998], alternative approaches are needed. Those studied include reducing bremsstrahlung losses, either by direct suppression with an applied magnetic field [Lauer et al., 1983, Miller et al.,

1987] or by searching for an ignition regime characterized by substantial electron degeneracy [Leon et al., 2001, Son and Fisch, 2004]. Likewise, procedures for preparing optically thick targets of enormous density (or with a high-Z tamper [Nuckolls et al., 1974]) have been considered but discarded as impractical [Hora, 1975, Rider, 1995]. The direct conversion of bremsstrahlung radiation into electricity is an active area of research [Lerner and Blake, 2007, Binderbauer and Tajima, 2013].

Another approach relies on maintaining a nonthermal velocity distribution in the p-^{11}B plasma. In field-reversed configurations, nonthermal distributions may prove useful in curtailing MHD instabilities [Binderbauer et al., 2015, Guo et al., 2015]. [Labaune et al., 2013, 2016] demonstrated a record-breaking rate of fusion events using a beam on target configuration. Our own work bounds the utility of maintaining a monoenergetic beam of protons located near a p-^{11}B fusion cross section resonance. This configuration is able to evade the conclusions of [Rider, 1995] due to upward revisions of the p-^{11}B fusion cross section [Nevins and Swain, 2000].

Using injected waves to diffuse fusion alpha particles in the phase space, i.e. alpha channeling [Fisch and Rax, 1992b, Herrmann and Fisch, 1997], it is possible to maintain a cold ion beam at the desired particle energy. Such a beam would improve the plasma reactivity at constant pressure, at the cost of injecting mediating waves [Fisch and Herrmann, 1994]. A detailed accounting of this delicate power balance is given. Optimistic constraints on the possible gains are given for both DT and p-^{11}B plasmas, in both confinement schemes. Areas of parameter space which are most promising for sustained fusion reactions are described.

The balance of the thesis, Chapters 5, 6, and 7, places a sharp limit on the energy that might be extracted with waves from the birth alpha particle distribution in an infinite, homogeneous plasma. A resolution would hold particular significance for the channeling of alpha particle energy in fusion devices as well as laser-plasma interactions [Bernstein, 1958, Gardner, 1963, Fisch and Rax, 1993, Dodin and Fisch, 2005, Fisch, 2014, Levy et al., 2014]. In Hamiltonian systems, the 'restacking' algorithm for the redistribution of particle density in phase space provides a bound consistent with Liouville's theorem [Gardner, 1963].

However, in dissipative systems far from thermodynamic equilibrium, the phase space evolution is more complicated and the bound is unknown. In the ubiquitous quasilinear regime of wave-particle interaction [Vedenov et al., 1962], waves effectively diffuse particles throughout the phase space. We bound the extractable energy in an N-level system under the action of general diffusive processes that equalize two levels' populations. The space of states accessible with similar level-mixing operations has been considered in many other contexts, ranging from economic inequality [Thon and Wallace, 2004] to chemical reaction kinetics [Horn, 1964].

Morrison and Pfirsch have performed refined stability calculations for perturbations about Maxwell-Vlasov equilibria that include the contribution of resonant particles to the perturbation energy [Morrison and Pfirsch, 1989, 1990, 1992]. They treated an initial value problem for a perturbation embedded in an infinite, homogeneous plasma which, crucially, could evolve only according to a dynamic accessibility criterion. To wit, this criterion demands that the forces giving rise to the perturbation evolution are Hamiltonian in nature [Morrison and Pfirsch, 1992]. This problem

should be distinguished from the boundary value problem considered here, in which externally-driven waves pass through a finite plasma. As such, we are not concerned with the local stability of the waves, but rather a global quantity, the plasma free energy [Fisch and Rax, 1993]. Moreover, the accessibility criterion for the quasilinear diffusion problem admits exclusively dissipative forces.

Apart from bounding the free energy, it is shown which particular diffusion paths set up by injected waves are optimal. These techniques are extended to a more general class of diffusion problems in which the connectedness of the phase space is modified.

Chapter 8 concludes the thesis and offers some ideas for for further pursuing the work described herein.

Chapter 2

Preliminaries

2.1 Wave-induced diffusion

Taken together, the waves and particles of plasma form a dynamical system. If the waves are treated as quasiparticles ('plasmons'), a natural analogy to quantum mechanics is revealed [Dragoman and Dragoman, 2004, Tracy et al., 2014, Dodin, 2014, Barth et al., 2015]. Particles satisfying a resonance condition may interact with waves by absorbing and emitting wave quanta [Tsytovich, 1970]. A particularly important process is the Cherenkov emission of a particle moving with the wave's phase velocity v_{ph}. If, prior to emission, the particle energy and momentum are ϵ_p and $\mathbf{p}$, and the emitted wave has energy $\hbar\omega$ and momentum $\hbar\mathbf{k}$, the final particle

state is

$$\mathbf{p}' = \mathbf{p} - \hbar\mathbf{k}$$

$$\epsilon_p' = \epsilon_p - \hbar\omega.$$

The resonance condition $\omega - \mathbf{k} \cdot \mathbf{v}_p = 0$ can be recovered from these relations under the assumption $\hbar k \ll p$.

Many fundamental plasma processes may be characterized in this way, as a result of the detailed balance between absorbing and emitting processes [Tsytovich, 1970]. (The formalism is also well-suited to describing wave-wave interactions, e.g. parametric decay.) For example, wave damping results from an excess of absorbing particles (i.e. those with $v \lesssim v_{ph}$). If the wave amplitude is sufficiently large, the number of absorbing and emitting particles equilibrates, resulting in a flattening of the distribution function around $v = v_{ph}$. Another immediate consequence is that particles are constrained to absorb and emit wave energy and momentum in exactly the proportions satisfying the wave's dispersion relation $D(\omega, \mathbf{k}) = 0$.

Consider the interaction of an electrostatic wave with a single particle embedded in a background magnetic field, Fig. 2.1 [Fisch, 2012, Fetterman, 2012]. In the absence of the wave, the particle executes circular motion in the x-y plane with frequency $\Omega = eB/mc$ and constant speed $v_\perp$. Now, suppose that the particle and wave interact through a Landau resonance: $\omega - k_y v_y = 0$. The guide and wave fields are considered to be imposed, supported by the bulk ion distribution; only a small number of ions in the tail are resonant [Karney, 1979]. If, as depicted in Fig. 2.1,

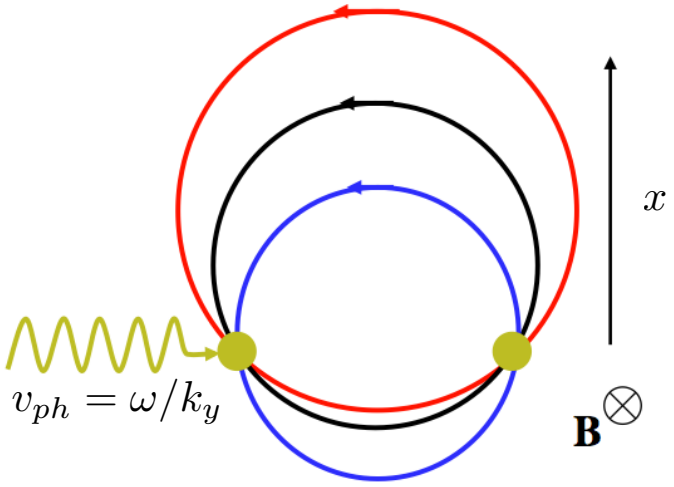

Figure 2.1: Wave interaction picture for a single particle.

the particle velocity $v_\perp$ exceeds the phase velocity ω/k_y, there are two resonances in the particle orbit (gold circles). Likewise, if $v_\perp = \omega/k_y$ there is one resonance and in the case of $v_\perp < \omega/k_y$ there are no resonances because $v_\perp \geq v_y$.

At a point of resonance, the particle receives an instantaneous kick from the wave, amounting to a Δv_y. Then the particle energy W also changes by the amount $\Delta W = \Delta(mv_\perp^2)/2 = mv_y\Delta v_y$. The guiding center location (x_{gc}, y_{gc}) consequently moves to $(x_{gc} - \Delta v_y/\Omega, y_{gc})$. The effect is due to the instantaneous change in gyroradius $v_\perp/\Omega$ when the kick occurs. If the particle of interest had the orbit following the black line before interaction, an energy increase would move the particle to larger x_{gc} (red line), and smaller x_{gc} otherwise (blue line). In this way, the wave-particle interaction couples motion in the configuration space to motion in the velocity space:

$$\frac{\Delta x_{gc}}{\Delta W} = -\frac{1}{m\Omega v_y} = -\frac{k_y}{m\Omega\omega}, \tag{2.1}$$

because $v_y = \omega/k_y$ at the moment of resonance.

Particles will trace out the diffusion path defined by Eq. (2.1) in x_{gc}-W space. Notably, the path depends only on imposed parameters: the strength of the applied magnetic field and the wave frequency and wavenumber. If, for example, the wave was to be used to extract cold alpha particles from the edge of a plasma, radius a, these parameters should be chosen so that

$$\frac{\Delta x_{gc}}{\Delta W} = -\frac{k_y}{m\Omega\omega} \approx \frac{a}{\epsilon_\alpha}, \tag{2.2}$$

because the alpha particles (birth energy ϵ_α) are born chiefly at the dense, hot center of the plasma, $r = 0$. In this way, there is a population inversion in the alpha distribution along the diffusion path, and the wave is amplified.

This result is one example of constrained diffusion in Hamiltonian dynamical systems [Chirikov, 1979]. If there exist constants of the motion, all particle motion, including diffusion, takes place on a subset of the coordinates in the phase space $\mathbb{R}^6$. Our single wave-particle system has two constants of the motion in the wave frame moving with $\mathbf{v}_{ph}$: the particle energy and the quantity $v_x^2 + v_z^2 + (v_y - \omega/k_y)^2$ [Smith and Kaufman, 1975, Zhmoginov and Fisch, 2008]. The particle motion then has only one degree of freedom, tracing out a so-called diffusion path embedded in the higher-dimensional phase space. The regime characterized by Fig. 2.1 relies on the wave field being weak enough so that particles execute uniform cyclotron motion outside of resonances. Increasing the field strength leads to island formation in phase space, resulting in diffusion [Chirikov, 1979, Stix, 1992].

The quasilinear theory offers a self-consistent description of these effects in the continuum limit [Vedenov et al., 1962, Krall and Trivelpiece, 1973, Stix, 1992]. The bulk plasma distribution function f_0 evolves slowly in time due to the emission and absorption of a full spectrum of waves. The aggregate effect is velocity-space diffusion:

$$\frac{\partial f_0}{\partial t} = \nabla_{\mathbf{v}} \cdot \mathsf{D}_{\mathbf{v}} \cdot \nabla_{\mathbf{v}} f_0(t), \tag{2.3}$$

$$\mathsf{D}_{\mathbf{v}} = 8\pi \left(\frac{q}{m}\right)^2 \int \frac{\mathcal{E}_{\mathbf{k}}(t)}{i(\mathbf{k}\cdot\mathbf{v}-\omega)} \frac{\mathbf{kk}}{|k^2|}\, d\mathbf{k}, \tag{2.4}$$

where $\mathcal{E}_{\mathbf{k}}$ is the time-dependent spectral energy density governed by

$$\frac{\partial \mathcal{E}_{\mathbf{k}}(t)}{\partial t} = 2\omega_i(\mathbf{k},t)\mathcal{E}_{\mathbf{k}}(t), \tag{2.5}$$

following the linear dispersion relation $D(\omega,\mathbf{k}) = 0$ (now allowing for the slow evolution of $f_0(t)$).

The classic "bump-on-tail" problem is instructive for us, concerning the evolution of a maxwellian distribution function to which a warm beam has been added, with drift velocity $v_b \approx v_{th}$ (Fig. 2.2a) [Krall and Trivelpiece, 1973]. Initially, waves with phase velocity $v_{ph} \lesssim v_b$ grow in amplitude due to instability: $\partial f_0/\partial v > 0$ there. The resonant particles give up energy to the wave and diffuse,

$$\left.\frac{df_0}{dt}\right|_{v\approx\omega/|k|} = \frac{8\pi^2 e^2}{m^2}\mathcal{E}_{k=\omega/v}\frac{1}{v}\left.\frac{d^2 f_0}{dv^2}\right|_{v\approx\omega/|k|}, \tag{2.6}$$

leading to an increase in density for the region originally $\partial f_0/\partial v > 0$ and a decrease in density for the bump itself. The right hand side of Eq. (2.6) has a first integral, yielding

$$f_0(v, t \to \infty) - f_0(v, t = 0) = 2\frac{\omega_p}{nm}\frac{d}{dv}\frac{1}{v^3}\mathcal{E}_{k=\omega/v}(t \to \infty). \tag{2.7}$$

Then the distribution function in the resonant region will change until it flattens, asymptotically: $\partial f_0/\partial v \to 0$, Fig. 2.2b.

In the case of two 'bumps' on the tail of f_0 (see Fig. 2.3), the asymptotically stable state is less clear. The general problem treated by Chapters 5, 6, and 7 is the calculation of the free energy of such a distribution under manipulation by injected waves. In the boundary value problem, we are concerned with the energy remaining after waves have left the plasma such that there is no oscillatory motion left behind in the nonresonant particles [Fisch and Rax, 1993]. Rather than allowing the system to relax, an optimal sequence of waves effecting pointwise quasilinear flattenings will extract the resonant particles' energy.

Using networks of diffusion paths to amplify plasma waves and extract alpha energy represents a prodigious opportunity for controlled fusion power [Fisch and Rax, 1992a,b, Emmert et al., 1994, Fisch and Herrmann, 1999, Zhmoginov and Fisch, 2008, Ochs et al., 2015a,b, Fisch, 2016]. By choosing different injected waves, one can divert the alpha energy to increase plasma reactivity or drive current [Fisch and Herrmann, 1994, Fisch, 1987]. Although one wave imposes a strict constraint on the particle motion, cf. Eq. (2.1), injecting multiple waves with overlapping resonances allows for more flexibility in constructing diffusion paths [Fisch and Herrmann, 1995,

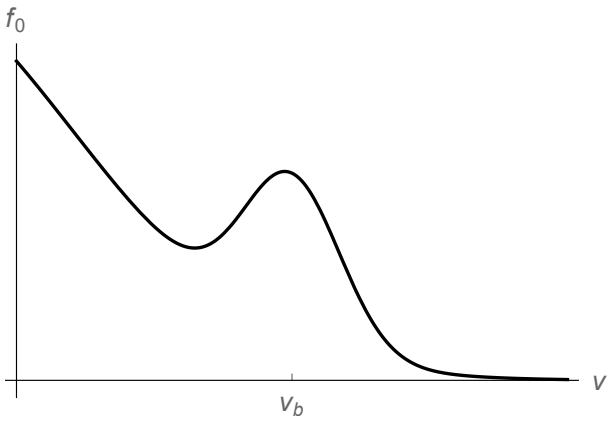

(a) $t = 0$

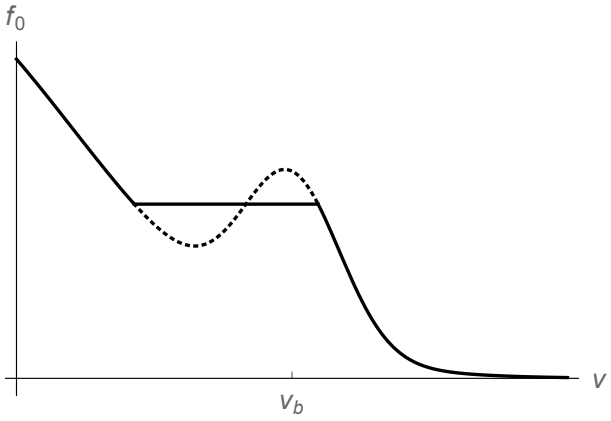

(b) $t \to \infty$

Figure 2.2: Quasilinear evolution of the bump on tail instability

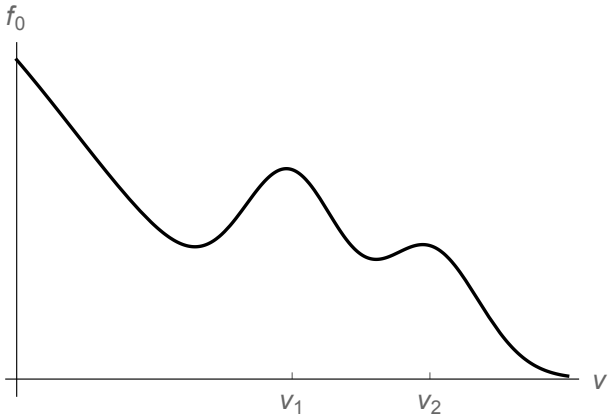

Figure 2.3: Distribution function with two minima

Herrmann and Fisch, 1997]. For example, one wave could be used to diffuse alphas in energy, while another could effect the diffusion in position. In the case of tokamaks, a pairing of the mode-converted ion-Bernstein wave and toroidal Alfvén eigenmode has been proposed for efficient alpha channeling [Fisch, 1995, Valeo and Fisch, 1994]. In general, the energy given up by an alpha particle will depend on its precise path through the network of diffusion paths (as established by the injected wave spectrum) [Fisch and Rax, 1993, Hay et al., 2015].

2.2 Mathematical background

In this section, we review some definitions and results from algebra, combinatorics, and graph theory that will prove useful in addressing the plasma free energy problem treated by Chapters 5, 6, and 7.

2.2.1 Algebra and combinatorics

A *monoid* is an algebraic structure consisting of a set S associated with an operation that maps any pair of elements in the set to another element [Lang, 2002]. As stated, the operation is a law of composition (mapping the set onto itself). This operation is associative and has a unit element e such that $ex = x$ for all $x \in S$. A *group* G is a monoid with the additional requirement that there exists an inverse $y \in G$ such that $xy = yx = e$ for all $x \in G$.

The operation satisfies the four group axioms: closure, associativity, identity, and invertibility. One elementary example is the integers $\mathbb{Z}$ under addition. In this case, the group operation is also commutative and so $(\mathbb{Z}, +)$ is an abelian group. A more provocative example for us is the free group with two generators, a and b. This group includes all distinct *reduced* words on the alphabet $\{a, a^{-1}, b, b^{-1}\}$; the group operation is concatenation. Reduced words cannot be further simplified by applying the group axioms, e.g. $aa^{-1}b = b$ is not reduced, but aba^{-1} is. The free group is non-abelian because concatenation is not commutative: $ab \neq ba$.

Our chief interest lies with the symmetric group on n symbols, denoted S_n. The elements of S_n are the $n!$ permutation operations that can be performed on n distinct symbols; the group operation is concatenation. It is expedient to think of permutations as bijections from a set onto itself. For example, the permutation $(312) \in S_3$ is the operation that replaces the first element with the third, the second with the

first, and the third with the second. In two-line notation,

$$(312) = \begin{pmatrix} 1 & 2 & 3 \\ 3 & 1 & 2 \end{pmatrix}.$$

The Coxeter generators of S_n are the adjacent transpositions $A_n = \{(i, i+1) : 1 \leq i \leq n-1\} = \{s_1, s_2, \ldots, s_{n-1}\}$. Each element of S_n can be expressed as a word on the alphabet A_n. For example, $(123)s_2s_1 = (123)(23)(12) = (132)(12) = (312)$. S_n is another non-abelian group: it is clear from the example that $(312) = (123)s_2s_1 \neq (123)s_1s_2 = (231)$. (We will omit the identity for conciseness; we presume all permutations are applied from left to right.) The s_i obey a few relations:

$$s_i^2 = 1,$$
$$s_i s_j = s_j s_i \text{ for } |i-j| > 1,$$
$$s_i s_j s_i = s_j s_i s_j \text{ for } |i-j| = 1.$$

The latter two relations suggest that a given permutation operation generally has multiple decompositions into adjacent transpositions. For example, $(321) \in S_3$ can be decomposed as $(12)(23)(12)$ or $(23)(12)(23)$. The pioneering work of [Stanley, 1984] succeeded in enumerating these reduced decompositions for each $\pi \in S_n$ [OEIS Foundation Inc., 2014b].

Now, let A_n^* denote the free group on A_n. Following [Stembridge, 1996, Berenstein et al., 1996, Bédard, 1999, Armstrong, 2009, Berkolaiko and Irving, 2016], introduce the equivalence relation $\sim$ induced by allowing commutations of disjoint cycles which

are adjacent in a word $\in A_n^*$. (We regard permutations connected by the second generator rule as equivalent: $s_i s_j \sim s_j s_i$ if $|i-j|>1$.) The equivalence classes for $\sim$ consist of the reduced decompositions for a particular permutation which can be obtained from each other by successively applying this generator relation.

Conversely, the quotient set $A_n^*/\sim$ can be identified with $\mathcal{I}_n$, the set of all inequivalent reduced decompositions in S_n. For example, the word (12)(34) in A_4^* belongs to the following equivalence class in $\mathcal{I}_4$, corresponding to the permutation (2143):

$$\{(12)(34),\ (34)(12)\}.$$

Skipping ahead, the key insight of Chapter 7 is that the extreme points of K correspond to the shortest possible factorizations of $\pi \in S_n$ expressed in terms of the A_n. In fact, each extreme point is associated with a set of *equivalent* factorizations under $\sim$. Therefore enumerating and characterizing the extreme points of a diffusion problem's state space is tantamount to studying the number and character of *inequivalent* reduced decompositions for the permutations in S_n. Because the plasma free energy is a linear functional on the level densities, there is a linear programming solution for the diffusion problem: evaluating the free energy at each extreme point.

2.2.2 Graph theory

A graph $G = (V, E)$ is a pair of sets such that the elements of E are two-element subsets of V. The set V lists the vertices (nodes) of the graph, and the elements of E are edges connecting pairs of vertices [Bondy and Murty, 2008, Diestel, 2010].

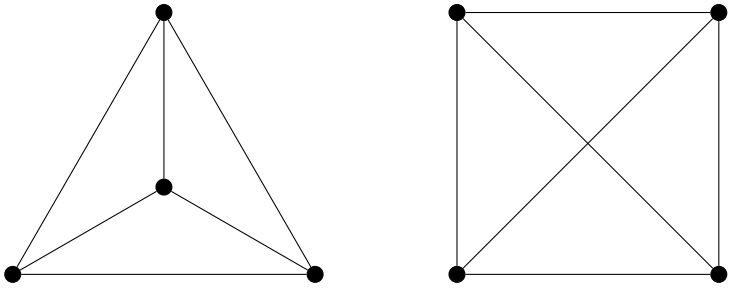

Figure 2.4: Two isomorphic representations of the complete graph on four nodes, K_4

Graphs have a ubiquitous pictorial representation which renders the vertices as dots and the edges as lines, Fig. 2.4. We say that two vertices v_1, v_2 are neighbors if there is an edge joining them: $v_1 v_2 \doteq \{v_1, v_2\} \in E$.

We will need the notion of graph isomorphism. If the graphs $G = (V, E)$ and $G' = (V', E')$ are isomorphic, $G \simeq G'$, there is a bijection $\varphi : V \to V'$ such that $xy \in E \Leftrightarrow \varphi(x)\varphi(y) \in E'$ for all pairs $xy \in E$. That is, by relabeling the vertices of G, one can obtain G'. Because a graph's properties are completely encoded in its vertex and edge sets, without reference to labeling or the drawn configuration of nodes, it is sufficient to study only one member of an isomorphism class.

This work examines the properties of a few common graphs in the context of diffusion problems. Different graphs are different realizations of the connectivity of the phase space. For example, the complete graph, $K_n = (V, E)$ has as its edge set all two-element subsets of V: $E = [V]^2$. In other words, $n - 1$ edges join each vertex with every other vertex. In this way, diffusion on the complete graph includes nonlocal effects, as even the most distant volumes in phase space are connected.

Graph-theoretic problems received much attention even before a formal theory of graphs was laid down. Perhaps the most famous is the Seven Bridges of Königsberg

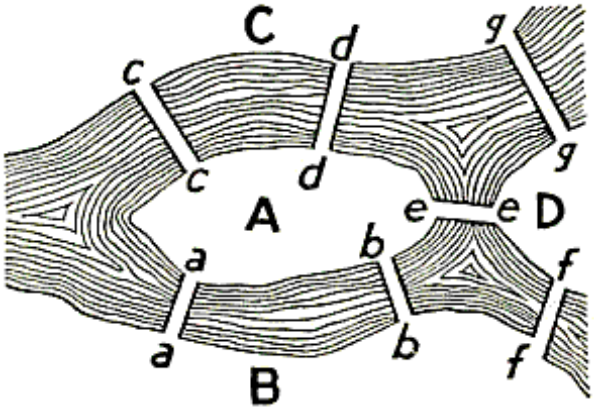

Figure 2.5: Seven bridges of Königsberg problem, Fig. 98 in [Kraitchik, 1942]. The seven bridges (edges) are represented by pairs of lowercase letters; the four nodes are designated with capital letters.

[Kraitchik, 1942, Biggs et al., 1976], Fig. 2.5. The question concerned the existence of a path through the town which visited each bridge precisely once, returning to the starting location. Euler answered in the negative, and such paths now bear his name: an Eulerian cycle is one which visits each edge in the graph once, beginning and ending at the same vertex.

By contrast, Hamiltonian paths visit each vertex exactly once. The familiar traveling salesman problem optimizes some objective function (e.g. the total time spent traveling) over all Hamiltonian paths through a list of cities. This exercise in combinatorial optimization has a very similar character to the diffusion problem in plasmas discussed by Chapters 5, 6, and 7.

Chapter 3

Geometrical optics of dense aerosols[1]

Assembling a free-standing, sharp-edged slab of homogeneous material that is much denser than gas, but much more rarefied than a solid, is an outstanding technological challenge. The solution may lie in focusing a dense aerosol to assume this geometry. However, whereas the geometrical optics of dilute aerosols is a well-developed field, the dense aerosol limit is mostly unexplored. Yet controlling the geometrical optics of dense aerosols is necessary in preparing such a material slab. Focusing dense aerosols is shown here to be possible, but the finite particle density reduces the effective Stokes number of the flow, a critical result for controlled focusing.

[1]This chapter is based on "Geometrical Optics of Dense Aerosols: Forming Dense Plasma Slabs," published in Physical Review Letters [Hay et al., 2013] and "Aerodynamic Focusing of High-Density Aerosols," published in the Journal of Aerosol Science [Ruiz et al., 2014].

3.1 Introduction

Certain applications in plasma physics require a dense plasma slab, but preparing an appropriately dense, shaped, and homogeneous plasma *in vacuo* is difficult. Rapidly ionizing a very dense aerosol jet offers a promising path to such a plasma, but the physics of focusing dense aerosols is entirely unexplored. In contrast, focusing effects in dilute aerosols have been the subject of extensive and fascinating work [de la Mora and Riesco-Chueca, 1988, Liu et al., 1995a]. Focusing of dilute aerosols occurs through the formation of particle caustics as the flow passes through simple plate orifices, in analogy with geometrical optics. In the dense aerosol regime, this picture is modified by the coupling of the particulate and continuous phases. Although this coupling has been investigated in other contexts, the focusing of highly-loaded flows is apparently unexplored. This Letter addresses such flows, uncovering new phenomena unique to the dense aerosol regime.

3.2 Dense Aerosol Regime

To describe these phenomena, we envision a two-stage device (Fig. 3.1) that assembles a dense jet of particulate from a dilute, homogeneous suspension. We specialize to a rectangular lens geometry with slit lenses and aerosol sheets. Passing through the first stage, the aerosol is focused into a narrow jet. Although the gas Mach number at the focusing nozzle is small enough that the gas compressibility is unimportant, the spherical aerosol particles themselves are highly supersonic with respect to their Brownian motion: immense compression is possible [de la Mora and Riesco-

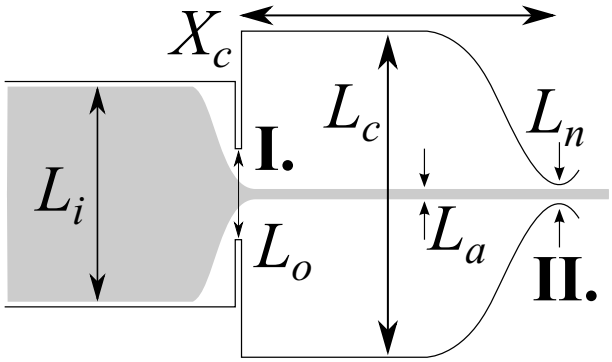

Figure 3.1: Schematic of two-stage system for compressing and extracting aerosol targets (gray). Stage I forms a jet from the isotropic suspension at the inlet. Stage II extracts this jet by dispersing the carrier gas. $\rho_{a,i}$ refers to the mean aerosol density upstream of Stage I, ρ_a is the density between stages, and ρ_t is the final target density downstream of Stage II.

Chueca, 1988]. In order to prepare high-density plasma targets, the aerosol phase will necessarily carry mass comparable to the carrier gas even prior to focusing. The second stage is a supersonic nozzle that greatly accelerates and expands the gas while imparting a small divergence angle and axial velocity kick to the aerosol sheet. Because the gas expansion is 2-D, the gas density becomes negligible compared to the aerosol beam density downstream of the nozzle throat. Thus a steadily flowing, bare aerosol sheet is formed. The sheet can be ionized downstream of the nozzle by an intense laser pulse that produces the shaped, dense plasma.

In the dilute limit, focusing requires Stokes number $\mathrm{S} \equiv \tau_d u_o / L_o \simeq 1$, where L_o is the size of the subsonic orifice, u_o is the gas flow speed there, and $\tau_d \equiv (2\rho_0 a^2/9\mu)(C_s/f_d)$ is a particle's velocity relaxation time due to drag on the carrier gas [Liu et al., 1995a]. ρ_0 is the bulk density of the particle material, a the particle radius, μ the fluid viscosity, and $C_s \equiv 1 + (\lambda/a)[A_1 + A_2 \exp(-A_3 a/\lambda)]$ is the

Cunningham correction for particle slip ($\lambda \propto 1/\rho_g$ is the gas-gas mean free path and the A_i's are order unity constants). $f_d \sim \mathcal{O}(1)$ corrects for finite particle Reynolds number. Additionally, unless the Reynolds number $\mathrm{Re} \equiv \rho_g u_o L_o/\mu \lesssim 10^3$, the resulting turbulent flow is expected to disrupt the deterministic particle trajectories and inhibit focusing.

The supersonic nozzle orifice must be larger than the aerosol beam as focused by the subsonic nozzle upstream. Because ANSYS FLUENT simulations indicate $L_o/L_a \lesssim 10$ at $\mathrm{S} = 1$, $L_o/L_n \lesssim 10$. Assuming an ideal gas equation of state for the carrier fluid and quasi-1D flow upstream of the supersonic nozzle throat, the Mach number in the central region must then exceed approximately 0.01 in order for $\mathrm{M} = 1$ flow at the throat. Operating at sufficiently large Knudsen number $\mathrm{Kn} \equiv \lambda/a \propto \mathrm{M/Re}$ subsumes the Reynolds and Mach constraints. In the $\mathrm{Kn} \gg 1$ regime,

$$\mathrm{S} \simeq 0.70\sqrt{\gamma}\frac{a\rho_0}{L_o\rho_g}\mathrm{M}_o \tag{3.1}$$

where $\mathrm{M}_o = u_o/c_g$ is the subsonic orifice Mach number, γ is the gas' adiabatic index, and $\mu = \bar{u}\lambda\rho_g/3$, c_g and $\bar{u}$ being the gas' sound and thermal speeds, respectively.

Together, these constraints on S, Re, and Kn impose an upper limit on the carrier gas density. The desired plasma electron density n_e determines the mean mass density of the spheres, $\rho_a \approx n_e(A/Z)M_p$, with A and Z denoting the aerosol material's mass and atomic numbers, respectively, and M_p the proton mass. Therefore

$$\frac{\rho_a}{\rho_g} \gtrsim \frac{L_o}{1\text{ cm}}\sqrt{\frac{1\ \mu\text{m}}{a}\cdot\frac{1\ \text{g/cm}^3}{\rho_0}}\left(\frac{n_e}{10^{19}/\text{cm}^3}\right) \tag{3.2}$$

In a homogeneous target ($n_a^{-1/3}/L_a < 10^{-2}$) suitable for compression of micron light, each factor will be $\mathcal{O}(1)$.

3.3 Aerodynamic Focusing

Several features of aerodynamic focusing were clarified by finite-volume FLUENT calculations. In the dilute regime, focusing was found to depend only two parameters, S and Re. Passing through a simple slit orifice, calculations indicated that the contraction of the aerosol beam L_a/L_o exhibited a $\mathrm{Re}^{-1/4}$ dependence with $\mathrm{S} = 1$ fixed.

Operating at finite ρ_a/ρ_g introduces aberrations that together result in shifting optimal focusing to larger S as compared with a dilute flow of identical particles. Fig. 3.2a shows $\mathrm{S} \approx 0.9$ particles focusing tightly in the upper half of the channel. The velocity field and particle tracks have been calculated by FLUENT in the dilute limit, $\rho_{a,i}/\rho_g \equiv \rho_p/\rho \approx 0.001$. Apart from a single trajectory, carrying little density, there is very little widening of the envelope of particle trajectories downstream of the orifice. Fig. 3.2b traces particles with τ_d identical to those in Fig. 3.2a, albeit with significant momentum coupling between the continuous and discrete phases. Mass loading lowers the orifice flow velocity and alters the gas streamline curvature, in turn reducing the 'true' S as compared to Fig. 3.2a—we are using the flow parameters from otherwise equivalent simulations of dilute aerosol flows to estimate S in the dense cases. Hence, both S and τ_d are constant between Figs. 3.2a and 3.2b although the orifice velocity changes. The energetic aerosol particles subsequently increase the

axial carrier velocity above the dilute calculation downstream of the orifice, resulting in small-divergence trajectories within $100L_o$.

Comparing Fig. 3.2b to Fig. 3.2c, it is evident that increasing S at high mass loadings can reduce the sheet's divergence in the region immediately downstream of the orifice. In both cases, the relatively dilute edge of the beam has the greatest divergence angle due to drag on the carrier flow filling the channel. Fig. 3.2d traces the larger-S particles' paths in the dilute limit, confirming that adjusting S is responsible for the change in dynamics. At finite S, the beam tends to a negligible divergence far downstream due to the underlying Poiseuille flow.

3.4 Coagulation

A severe operating constraint on the two-stage device is particle coagulation, which occurs upon a collision or approach within a distance characteristic of the van der Waals force. Upstream of the first stage, coagulation can destroy focusing and contribute to particle loss by altering the distribution of particle sizes. Downstream, where the residence time is very long and the particle density is large, coagulation reduces the homogeneity of the jet. The constraint pushes the operating regime to larger a, smaller L_a, and lower ρ_a.

Achieving, homogeneity at high focused densities motivates operation in a regime where the effective scattering length l_B of an aerosol particle's Brownian motion is large compared to a: $l_B \equiv v_{th}\tau_d \gtrsim a$, where $v_{th} \simeq \sqrt{k_B T_g/m_p}$. T_g is the ambient carrier gas temperature and m_p is the mass of an aerosol particle. This results in a

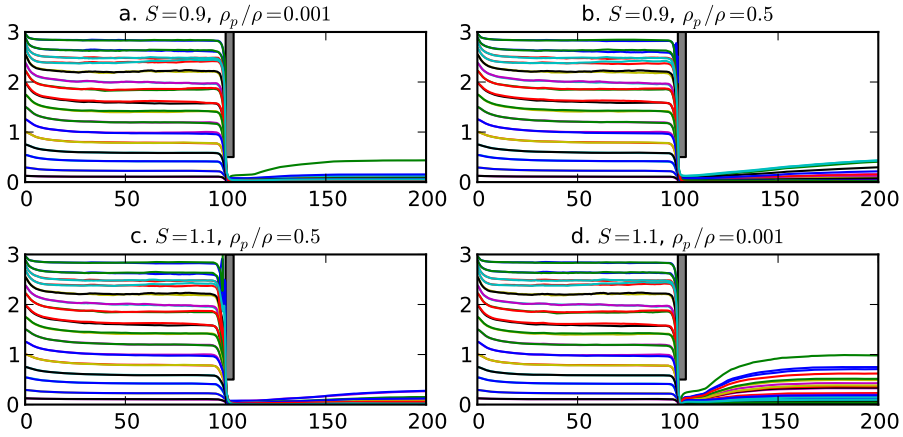

Figure 3.2: Representative particle tracks demonstrating aerodynamic focusing in four combinations of S and upstream $\rho_p/\rho = \rho_{a,i}/\rho_g$. In each frame, the abscissa is the horizontal displacement in multiples of L_o; the ordinate is the vertical displacement. The axial extent of the orifice is exaggerated for clarity.

longer collision time due to Knudsen flow in a layer of radial extent l_B surrounding each aerosol particle [Fuchs, 1964]. Most particle collisions occur between the two stages, so the constraint is determined there: $\tau_{\text{transit}}/\tau_{\text{coag}} \simeq (X_c/u_c)/\tau_{\text{coag}} < 1$. u_c is the axial gas speed in the central region and $\tau_{\text{coag}} \simeq (2\sqrt{2}\pi n_a a^2 v_{th}\delta)^{-1}$ where $n_a \equiv \rho_a/m_p$ is the number density of spheres [Fuchs, 1964]. $\delta \leq 1$ is the fraction of collisions resulting in coagulation. Note the strong dependence on particle size: $\tau_{\text{coag}} \propto a^{5/2}$ at fixed ρ_a. The need to avoid coagulation thus establishes a minimum particle size, above which beam divergence due to Brownian motion is also negligible.

3.5 Target Density and Aspect Ratio

We assume fluid descriptions for the coupled gas and aerosol flows in order to calculate the focused target's density and divergence. Although the particle Knudsen

number is large, the criterion for continuum flow is easily satisfied: $\lambda/L_o \ll 1$. Because the particle volume fraction $\rho_a/\rho_0 \ll 1$, the body force coupling the two fluids is $\propto \rho_a(\mathbf{u}_a - \mathbf{u}_g)/\tau_d$. Within the focused aerosol beam, $\rho_a/\rho_g \gg 1$, so we may neglect inertia in the gas momentum equation to obtain:

$$\mathbf{u}_g \simeq \mathbf{u}_a - \frac{\tau_d}{\rho_a}\nabla p_g \tag{3.3}$$

Assuming an equation of state $p_g = p_g(\rho_g)$, the gas continuity equation has the convection-diffusion form:

$$\frac{\partial \rho_g}{\partial t} + \nabla \cdot \rho_g \mathbf{u}_a = \nabla \cdot \frac{\tau_d}{\rho_a}\rho_g c_g^2 \nabla \rho_g \tag{3.4}$$

where $c_g^2 = \partial p_g/\partial \rho_g$. Near the subsonic orifice, the aerosol compression of order L_i/L_o can drive a corresponding $\Delta\rho_g$. In steady state, the gas diffusion compensates the convective aerosol compression:

$$\rho_g \frac{\hat{\mathbf{y}} \cdot \mathbf{u}_a}{L_o} \sim \frac{\tau_d \rho_g c_g^2}{\rho_a L_o^2}\Delta\rho_g \tag{3.5}$$

where $\hat{\mathbf{y}}$ is the transverse flow direction. Then

$$\frac{\Delta\rho_g}{\rho_g} \sim \alpha \equiv \frac{2L_o^2}{\gamma a^2} \cdot \frac{\rho_a \rho_g}{\rho_0^2} \ll 1 \tag{3.6}$$

if we can neglect the carrier gas compressibility. This is a consistency condition for the two-fluid model: $\alpha < 1$ restricts particle trajectory crossings due to coherent hydrodynamic motion. If $\alpha \ll 1$, the radial diffusion of gas in the focused beam is

faster than axial convection:

$$\nu_\perp \sim \frac{\tau_d \rho_g c_g^2}{\rho_a L_a^2} \gg \hat{\mathbf{x}} \cdot \mathbf{u}_a \frac{d}{dx} \log L_a \sim \nu_\parallel \tag{3.7}$$

and $\partial \rho_g / \partial y$ is accordingly negligible. Then $L_a \simeq$ const. and the summed momentum equations for the two phases have a first integral:

$$\frac{S_a}{L_a} u_a + p_g(\rho_g) \equiv \text{const.} \tag{3.8}$$

where $S_a \equiv \rho_a u_{a,x} L_a \simeq$ const. If $\mathrm{M} \gg 1$ downstream of the supersonic nozzle, $p_g \to 0$ and Eq. (3.8) implies that

$$u_{a,f} \leq \frac{L_a}{S_a} p_{g,i} \tag{3.9}$$

where $u_{a,f}$ is the final downstream aerosol speed and $p_{g,i}$ is the gas pressure far upstream of the focusing device. The acceleration of the aerosol beam is limited by a 'barreling' effect that depends on the contrast ratio ρ_a / ρ_g.

As $\rho_g(x)$ decreases through the supersonic nozzle, a transverse pressure gradient $\partial p_g / \partial y$ is established that can in turn develop a diverging $u_{a,y}$. Comparing the axial convection and radial diffusion terms of Eq. (3.4),

$$u_{a,x} \frac{\partial \rho_g}{\partial x} \sim \frac{\partial}{\partial y} \frac{\tau_d \rho_g c_g^2}{\rho_a} \frac{\partial \rho_g}{\partial y} \tag{3.10}$$

and substituting the y-component of the summed momentum equations,

$$\rho_a u_{a,x} \frac{\partial u_{a,y}}{\partial x} = -c_g^2 \frac{\partial \rho_g}{\partial y} \tag{3.11}$$

we estimate the divergence as

$$\frac{u_{a,y}}{u_{a,x}} \sim \frac{L_a/\tau_d}{u_{a,x}} \simeq \frac{L_a}{L_o}\alpha^{1/2} \tag{3.12}$$

where we have estimated $\partial/\partial y \sim 1/L_a$ and $u_{a,x} \sim (\rho_g/\rho_a)^{1/2} v_{th}$ from Eq. (3.9). The maximum aerosol speed limits the extracted target density:

$$\frac{\rho_t}{\rho_{a,i}} \simeq \frac{L_i u_i}{L_a u_{a,f}} = \frac{L_o^4(\rho_a\rho_g)_i}{a^2 L_a^2 \rho_0^2} = \frac{L_o^2}{L_a^2}\alpha \tag{3.13}$$

where $\mathrm{S} = 1$ to eliminate the upstream gas velocity u_i.

The consistency criterion for the two-fluid model is $\alpha \ll 1$, but the final target density is small in this limit per Eq. (3.13). Per Eq. (3.12), the target aspect ratio scales as $\alpha^{-1/2}$; intermediate α is necessary for high-quality targets. It is more important to operate in a large L_o/L_a regime, which occurs for $\mathrm{S} = 1$ and $\mathrm{Re} \gtrsim 10^2$.

3.6 Operating Points

Table 1 lists these and other pertinent constraints. Considering $n_e \simeq 10^{19}$ cm^{-3} plasmas suitable for Raman compression, the available targets are charted in Fig. 3.3. To compress intense light and attain large geometric convergence, large aspect ratio geometries are necessary. We estimate $AR \geq 10$ to be satisfactory, beyond what is available with gas jets. We note that 5-mm targets are available with good homogeneity: $a/L_a \sim 10^{-5}$. At fixed a, small-L_a targets below the boundary identified in Fig. 3.3 are too inhomogeneous. Likewise L_a above the region in Fig. 3.3, require

Stage I	$\mathrm{S} = 1$ $10 < \mathrm{Re} < 500$ $\alpha < 1$ $\mathrm{M}_o \equiv u_o/c_g < 0.3$ $\mathrm{Kn} \equiv \lambda/a > 1;\ \lambda/L_o < 1$
Between stages	$X_c > 10L_i$ $L_c > L_a$ $X_c/u_c < \tau_{\mathrm{coag}}$ $l_B/a > 1$
Stage II	$\mathrm{M}_n = 1$ $L_n > L_a$ $AR \equiv (L_a\alpha^{1/2}/L_o)^{-1} > 10$ $n_a^{-1/3}/L_a < 10^{-2}$ $\rho_t \simeq 0.017(\frac{A}{Z})\left(\frac{n_e}{10^{19}/\mathrm{cm}^3}\right)\ \mathrm{mg/cm}^3$

Table 3.1: Dense aerosol operating constraints

high-M and high-Re operation that could result in deleterious shocks, turbulence, etc. At fixed (a, L_a), a higher-density target is subject to those constraints; the (a, L_a) operating space tends to widen as ρ_t is reduced. Note that the particle trajectories between stages were assumed to have zero divergence before entering the second stage.

3.7 Alternative Techniques and Applications

Alternative techniques for producing a plasma slab suffer from limitations that might be overcome using the dense aerosol approach. Aerogels and foams are characterized

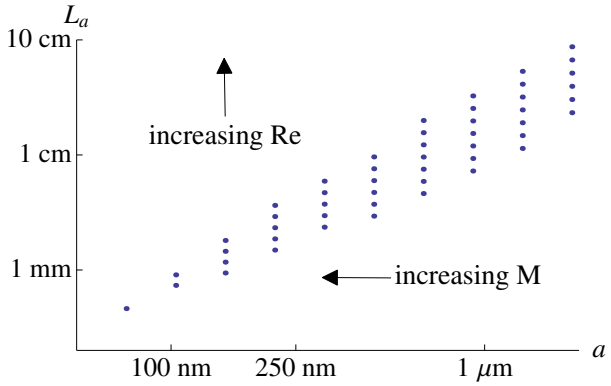

Figure 3.3: Possible operating points at $n_e \simeq 10^{19}$ cm^{-3} and $\rho_0 = 2\,\mathrm{g/cm^3}$ in (a, L_a) space. Each point is parametric in Re and M; the labeled arrows indicate tendencies.

by filamentary structures. In laser plasmas, the timescales over which the filaments vaporize and the target material homogenizes must be much shorter than the hydrodynamic timescale for the target edge to rarefact and expand. Because a typical filament has a large aspect ratio, it expands in 2D and such structures can persist late in the ionizing pulse [Bugrov et al., 1997, Caporaso, 1982]. Gas jets lack a solid matrix but are instead saddled with short hydrodynamic timescales associated with turbulent eddies and the propagation of shocks from the nozzle.

Fast Raman compression in plasma couplers may enable the next generation of laser intensities [Malkin et al., 1999]. Although first-generation experiments use capillary-shaped plasmas a few mm in length and transverse sizes of about 50 μm [Ping et al., 2004], ionized dense aerosols could be engineered to have the same length but much larger transverse sizes to accommodate more power [Toroker et al., 2012]. These pancake-shaped plasmas require good uniformity at electron densities greater than $10^{19}\,\mathrm{cm^{-3}}$, with transverse lengths of several cm.

Material	ρ_0 [g/cc]	max ρ_t [mg/cc]
CH	1.0	0.10
Fe	7.9	2.7
Ni	8.9	3.2
W	19.2	5.1
Au	19.3	5.2

Table 3.2: Accessible ρ_t for select materials. The maximum average mass density in the target was calculated for $100\,\text{nm} < a < 1\,\mu\text{m}$ and $1\,\text{mm} < L_a < 1\,\text{cm}$ using an optimization procedure constrained by the relations in Table 1.

Low-divergence aerosol targets could surpass the efficiencies of gas jets in radiator experiments on Z [Sze et al., 2005]. However, the homogeneity and aspect ratio requirements are relaxed somewhat compared to those required for Raman compression; here, a satisfactory design point is a 1-cm jet of 1-μm nickel particles, $\rho_0 = 8.9\ \text{g/cm}^3$. Larger particles are less susceptible to coagulation; the Reynolds constraint (3.2) guarantees operation in a moderately dense aerosol regime: $\rho_a/\rho_g \gtrsim 10^2$ at $\rho_t \approx 1\,\text{mg/cc}$. Table 2 below summarizes the target densities achievable with polystyrene (CH) and a few metals.

Similar dense aerosol schemes could offer structured targets to the MagLIF program, which is expected to rely on laser heating of annular targets [Slutz and Vesey, 2012]. FLUENT calculations suggest that a focus with $\text{S} \gtrsim 1$ will have a radial density profile peaking on axis; further increasing S will result in an annular density profile. By choosing different S for each phase, a single lens can yield gradients in material composition with differential focusing, e.g. an annulus of one phase ($\text{S} > 1$) filled by another ($\text{S} \approx 1$).

3.8 Experimental Results

[Ruiz et al., 2014] built a simple experimental device, Fig. 3.4, in order to study the properties of high-density aerosol focusing for 1 μm silica spheres. Preliminary results recovered previous findings on aerodynamic focusing at low densities [Liu et al., 1995b, Wang and McMurry, 2006]. At higher densities, it was demonstrated that the focusing properties change in a way which is consistent with a density-dependent Stokes number (cf. Sec. 3.3).

3.8.1 Effective Stokes number

The dimensionless Stokes number is defined

$$\mathrm{S} \equiv \tau_d \frac{U_0}{D_0} = \frac{\rho_p D_p^2}{18\mu} \frac{C_s}{f_d} \frac{U_0}{D_0} \tag{3.14}$$

where D_o is the size of the focusing orifice, U_o is the gas flow speed there, and τ_d is a particle's velocity relaxation time due to drag on the carrier gas [Liu et al., 1995a]. ρ_p is the bulk density of the particle material, a the particle radius, μ the fluid viscosity, and $C_s \equiv 1 + (\lambda/a)[A_1 + A_2 \exp(-A_3 a/\lambda)]$ is the Cunningham correction for particle slip ($\lambda \propto 1/\rho_g$ is the gas-gas mean free path and the A_i's are order unity constants). $f_d \sim \mathcal{O}(1)$ corrects for finite particle Reynolds number.

In the dense aerosol focusing regime, the particle focusing is modified by aberrations arising from the coupling of the particles with the background flowing gas. An intuitive example to illustrate high-density effects is the following: suppose that, in the dilute limit, the background gas parameters are set such that the aerosol is

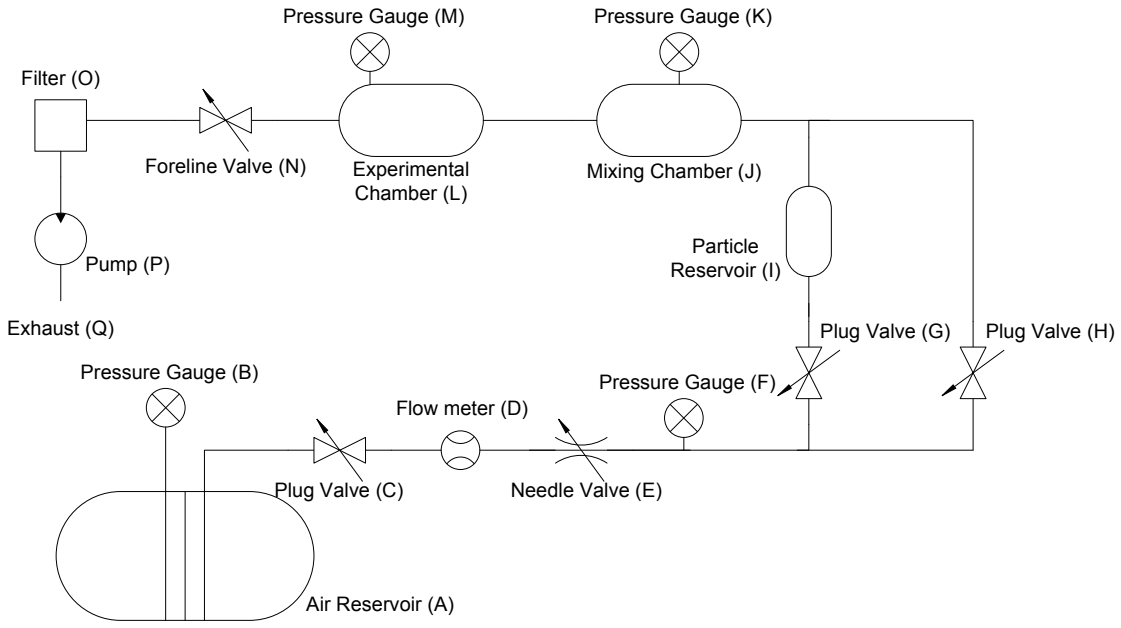

Figure 3.4: Schematic of device for preparing and focusing dense aerosols

aerodynamically focused after passing the orifice. Keeping the gas mass flow fixed, when the particle density increases, the background gas will encounter more of the (slow moving) particles in the orifice. Hence, the speed of the background gas at the orifice decreases. By inspection of Eq. (3.14), we note that the Stokes number S will also decrease at the orifice. Then, at high densities, the previously focused aerosol beam will become under-focused, i.e. the particle beam will have no focal point. Hence, finite aerosol densities can alter the focusing properties of the aerosol beam.

This leads to the notion of the effective Stokes number. The Stokes number shown in Eq. (3.14) is a function of the air flow velocity at the orifice. When no aerosol is present, one usually can infer the average velocity by measuring the air

mass flow and the pressure nearby the orifice and applying simple mass conservation. However, when aerosol particles are present, calculating the perturbed background gas velocity field at the orifice is more difficult because the particle spheres may significantly perturb the surrounding gas flow. However, by the previous thought experiment for fixed mass airflow, we know that the velocity of the airflow should decrease when the aerosol density is significant.

3.8.2 Methods

Before the experiment is pumped down to vacuum, the SiO_2 particles are inserted into the particle reservoir (I). (Alphabetical labels reference Figs. 3.4 and 3.5.) After the vacuum pump is turned on and the pressure at gauge (M) reaches its limiting pressure of approximately 600 mTorr, the main plug valve (C), the needle valve (E) and the foreline valve (N) are opened in order to establish the desired air mass flow rate. In this phase, the plug valve (G) leading to the particle reservoir is closed. Having the air mass airflow constant, the chamber pressure is varied. For a fixed mass airflow, when the pressure inside the experiment chamber is changed, the background gas density, the airflow speed at the orifice, and the slip correction factor C_s are modified. These factors cause a change in the Stokes number. Different aerosol focusing regimes are accessed by following this methodology.

Once the desired mass flux and pressure conditions are set, the valve (G) controlling the airflow to the particle reservoir (I) is opened, Fig. 3.5. The airflow then entrains particles from the reservoir and forms an aerosol. This effect only lasts for a few seconds, after which the easily entrained particles are spent, diminishing the

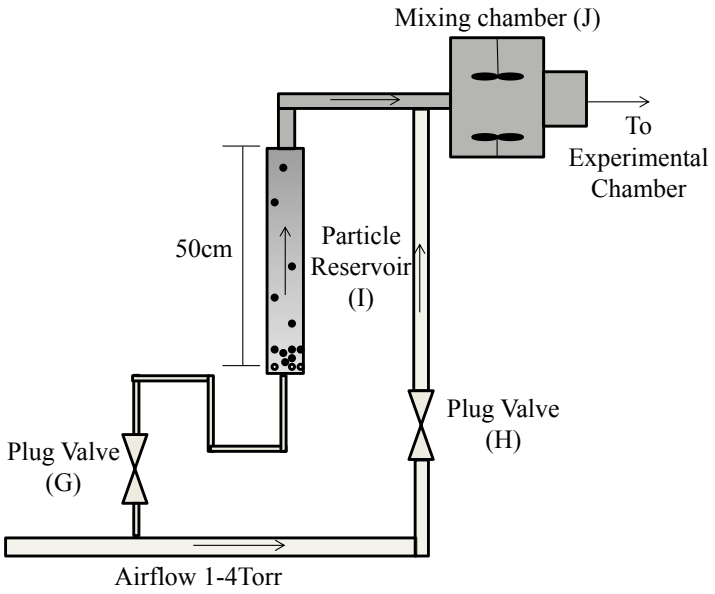

Figure 3.5: Schematic view of apparatus' aerosol production stage (not to scale). The airflow is divided into two flows. One flow passes through the particle reservoir (I) and entrains particles with it. An aerosol (shown in dark color) is formed. The aerosol then travels into the mixing chamber (J), where electrical fans further homogenize the aerosol cloud.

aerosol generation. In order to solve this problem, the exterior of the particle reservoir is manually vibrated in order to produce more aerosol particles. To access higher particle densities yet, the particle reservoir is tapped with a wrench causing more particles to be carried by the airflow stream. Although this rather crude method of producing the aerosol cannot directly control the aerosol mass density, it produces the wide variations of aerosol density needed to study the density effects on aerosol focusing.

Once the aerosol travels through the orifice inside the experimental chamber (L), the laser system illuminates the aerosol beam. The scattered light by the beam is recorded by the camera system. From the videos of the camera data, several proper-

ties of the focused beam are inferred, such as the beam diameter and the dispersion angle (aperture angle of the emerging aerosol beam). The light transmission measurement from the photodiode system located above the focusing orifice is used to infer the particle density inside the beam.

3.8.3 Discussion

The Stokes number in Eq. (3.14) is calculated by using the pressure and mass airflow measurements. By taking the mean of the pressure measurements given by gauges (K) and (M), one can approximate the pressure at the orifice. Then, we can obtain the air density at the orifice by using the expression $\rho_{\text{air}} = 1.225(P/1\,\text{atm})\ \text{kg}\cdot\text{m}^{-3}$. By combining the mass airflow measurement from (D), the calculated air density at the orifice and the orifice area, one can obtain the average velocity of the gas at the orifice by using mass conservation. Once the background gas velocity is calculated, the Stokes number can be easily obtained from Eq. (3.14). To measure the particle beam width, a 2D profile image of the particle beam is obtained via the camera system, Fig. 3.6. Fig. 3.7 illustrates three typical images in varying focusing regimes.

A 3-D surface of the normalized beam width $D_{\text{beam}} = D_{\text{beam}}(\text{S}, \rho_{\text{beam}})$ as a function of Stokes number and beam density was obtained by making a linear regression of the entire experimental data set. The contour plot of the constructed surface is shown in Fig. 3.8. As it can be seen, the optimal Stokes for focusing in the dilute regime is $\text{S} = 0.55$.

For larger Stokes numbers, it appears that when the beam density increases at a given Stokes parameter, the beam width decreases. Hence, a beam that is initially

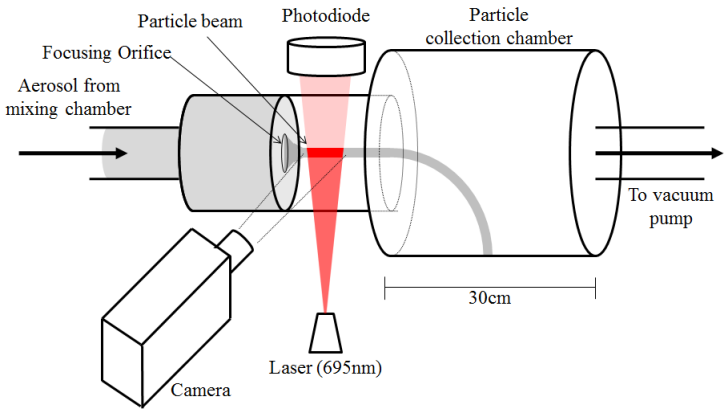

Figure 3.6: Schematic view of the apparatus' focusing stage. The aerosol beam is diagnosed by a laser transmission measurement and a high definition camera.

over-focused in the dilute regime can become better focused in the dense regime. From the interpolated surface in Fig. 3.8, a lineout at S = 1.55, is shown in Fig. 3.9. This figure illustrates the dependence of an over-focused beam width on the beam density. This effect might be useful for the design of aerosol beams that could serve as targets for plasma related experiments.

3.9 Summary

Self-consistent momentum coupling between aerosol and carrier flows changes the aerodynamic focusing properties of the system. The particle loading reduces the effective Stokes number in the first stage, shifting the focus; in the second stage, the aerosol is so dense that it dominates the flow field and the particles move ballistically.

The focusing properties of aerodynamic lenses permit the design of dense, homogeneous, high-aspect ratio targets. Jets of small spherical particles could be en-

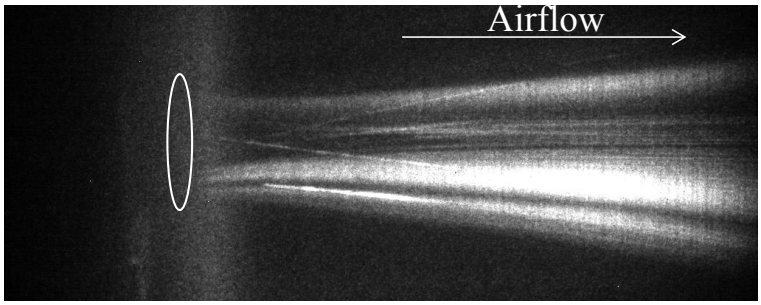

(a) Under-focused

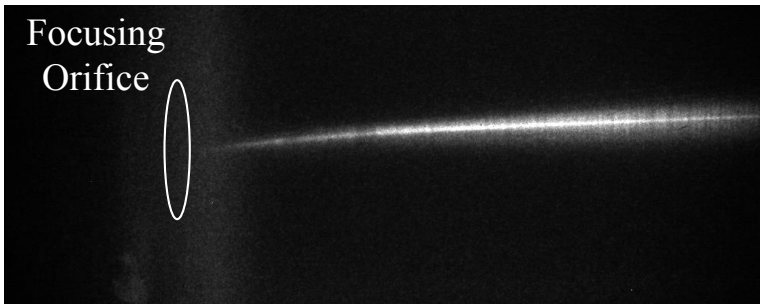

(b) Focused

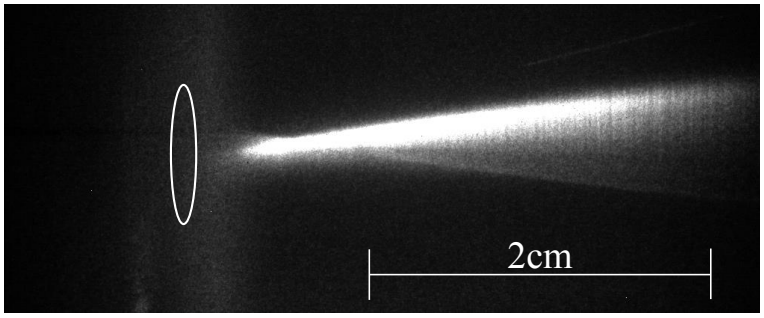

(c) Over-focused

Figure 3.7: Typical 2D profiles of the different aerosol focusing regimes. In these figures, the background gas flows from left to right. The focusing orifice is marked by the circles on the left hand side. (a) Example of under-focused regime. Particles still follow the flow streamlines. S $\approx$ 0.2. (b) Example of a good aerodynamic focusing regime. S $\approx$ 0.6. (c) Over-focused regime in which the aerodynamic focal point is clearly visible. S $\approx$ 1.6.

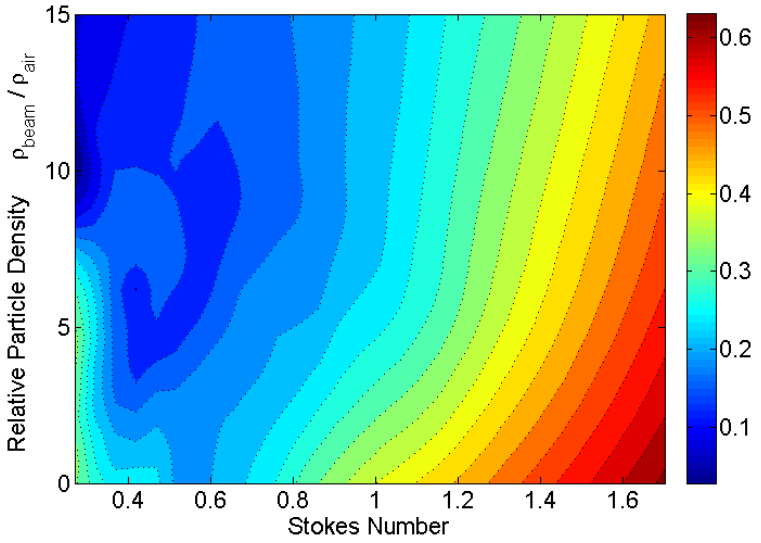

Figure 3.8: Contour plot of the normalized beam width (beam width/orifice size) vs. the Stokes number and the normalized aerosol density.

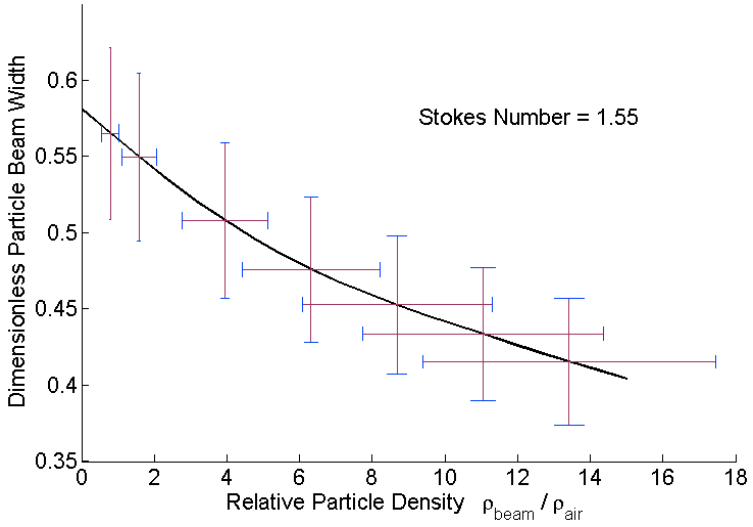

Figure 3.9: Lineout from Fig. 3.8 at Stokes number of 1.55

gineered to homogenize quickly with minimal turbulent features. Because so many solid and liquid species can be aerosolized, these targets open up the design space for plasma targets. Separating the target's assembly and ionization permits complex designs with tailored gradients that could improve current plasma technologies.

Chapter 4

α channeling in p-^{11}B plasmas[1]

An optically thin p-^{11}B plasma loses more energy to bremsstrahlung than it gains from fusion reactions, unless the ion temperature can be elevated above the electron temperature. In thermal plasmas, the temperature differences required are possible in small Coulomb logarithm regimes, characterized by high density and low temperature. Ignition could be reached more easily if the fusion reactivity can be improved with nonthermal ion distributions. To establish an upper bound for the potential utility of a nonthermal distribution, we consider a monoenergetic beam with particle energy selected to maximize the beam-thermal reactivity. Comparing DT and p-^{11}B, the minimum Lawson criteria and minimum ρR required for ICF volume ignition are calculated with and without the nonthermal feature. It turns out that channeling fusion alpha energy to maintain such a beam facilitates ignition at lower densities and ρR, improves reactivity at constant pressure, and could be used to remove he-

[1]This chapter is based on "Ignition threshold for non-Maxwellian plasmas," published in Physics of Plasmas [Hay and Fisch, 2015].

lium ash. Whereas the reactivity gains that could be realized in DT plasmas are significant, the excess electron density in p-^{11}B plasmas increases the recirculated power cost to maintain a nonthermal feature and thereby constrains its utility to ash removal.

4.1 Introduction

Fusion reactions which release most of their energy in charged particles are desirable for power applications. In particular, if the number of energetic neutrons produced is small, the power plant can be designed with less expensive shielding and with fewer material constraints [Kernbichler et al., 1987]. Also, direct conversion of charged particle energy could offer such a scheme much greater efficiency than a thermal cycle [Post, 1969]. This chapter addresses the fusion power prospects of the reaction $p + {}^{11}\mathrm{B} \rightarrow 3\alpha + 8.7$ MeV, which benefits from a low incidence of neutron-generating side reactions and the reactants' natural abundance. However, at typical densities, an optically thin p-^{11}B plasma loses more energy via bremsstrahlung radiation than it gains from fusion reactions, making sustained burn difficult [Dawson, 1981, Nevins, 1998]. Lacking sustained burn, or what is referred to as ignition, does not mean that fusion energy cannot be extracted, as in a wet wood burner. But the lack of ignition makes such a means of extracting energy technologically difficult and expensive [Manheimer, 2014].

Previous efforts toward p-^{11}B ignition have focused on mitigating the bremsstrahlung loss channel. One approach is embedding large magnetic fields in the fusing plasma,

restricting the motion of unbound electrons and reducing the bremsstrahlung emission both directly, by modifying electron-electron scattering, and indirectly, by modifying electron-ion scattering. The Landau wavefunctions differ considerably from the isotropic, field-free case and the electron-electron scattering assumes a 1-D character. In the aggregate, the spectrally integrated emission is reduced by about 20% [Lauer et al., 1983]. Likewise, by increasing the Landau energy level spacing ($\hbar\Omega$), a hot ion mode ($T_i > T_e$) can be preserved due to the suppression of ion-electron energy transfer; such a mode is characterized by low bremsstrahlung emission at a given plasma pressure [Miller et al., 1987].

In a plasma with substantial electron degeneracy, bremsstrahlung is also reduced. The main effect appears to be a reduction of the electron stopping power, enabling a large electron-ion temperature difference [Leon et al., 2001, Son and Fisch, 2004]. For the same reason, degenerate electrons are preferable in beam-initiated detonations of compressed p-^{11}B fuel that rely on rapidly heating the ion species in a small locus [Leon et al., 2001, Martinez-Val et al., 1996, Eliezer and Martinez-Val, 1998].

Ignition using p-^{11}B is possible when the ion temperature is raised significantly above the electron temperature, a circumstance realized only in high-density thermal plasmas. (Though this does occur naturally in low temperature plasmas because of electron degeneracy.) $T_i \gg T_e$ is necessary, but not sufficient: T_i itself must be on the order of several hundred keV due to the small p-^{11}B fusion cross section below that threshold. The resulting plasma is strongly collisional, but the robust fusion burn sustains ion temperatures above the electrons cooled by bremsstrahlung (note that $|T_i - T_e| \sim P_f/\nu_{ie}$ under these conditions).

Because high densities and temperatures are difficult to reach simultaneously, it is important to consider how either of these requirements might be relaxed. In equilibrium ignition-regime p-^{11}B plasmas, fusion alpha particles slow chiefly on the ions. Using waves to channel alpha energy [Fisch, 1987, Fisch and Rax, 1992b, Fisch and Herrmann, 1994, Herrmann and Fisch, 1997, Fisch and Herrmann, 1999] to the lighter fusing species (protons) could improve the reactivity at fixed pressure, but, in the case of p-^{11}B as opposed to DT, the net gain is limited by the small fraction diverted to electrons in equilibrium.

Nonthermal distributions offer a plausible means to ease ignition requirements, either by improving the MHD stability of the bulk plasma,[Binderbauer et al., 2015, Guo et al., 2015] or by increasing the number of reacting particles near the cross section peak in velocity space, as treated here. This work considers the effect of such a non-Maxwellian feature in the ion distribution, namely a monoenergetic beam with particle energy maximizing the beam-thermal reactivity.

In order to discover the minimal ignition criteria, it is assumed that a fraction of the fusion power is efficiently channeled to maintain the beam against collisions with thermal particles. By way of comparison, these ignition conditions are calculated for both DT and p-^{11}B plasmas, with and without the presence of the monoenergetic beam, in both magnetic and inertial fusion configurations.

In all instances, power flows from a 'hot' species (alphas, protons) to a cool one (protons, boron, respectively), and the extra power needed to maintain the nonthermal distributions is consistently included in the calculation. We explicitly include the effects of ion-ion and electron-ion drag in the energy balance.

However, we do neglect the power flow required to maintain the beam against velocity space diffusion. Consider a test particle born with energy slightly larger than that associated with the fusion cross section resonance. In both p-^{11}B and DT plasmas, this particle's fusion rate competes chiefly with slowing on light ions and electrons (boron excluded). Only after the particle slows out of the fusion resonance do the collisional drag and velocity space diffusion due to thermal ions become significant. Because the diffusion is especially small compared to drag at the beams' typical energies, we are justified in neglecting this term in the power balance (see Appendix A).

Likewise, we do neglect kinetic effects such as collisionless streaming instabilities. A cold beam in a warm plasma will be subject to a complex array of instability mechanisms, but the two-stream instability between the fast monoenergetic beam ions and warm bulk species is prognostic [Krall and Trivelpiece, 1973]. However, in both DT and p-^{11}B ignition-regime plasmas, the bulk species are sufficiently cool with respect to the beam that nearly monoenergetic beams are resilient to this instability (see Appendix A) [Fried and Wong, 1966].

Likewise, favorable assumptions and estimates are invoked to position the calculation as an upper bound on the feasibility of these fusion scenarios. For example, we explicitly assume that free energy in the alpha distribution can be transferred to the protons with perfect efficiency, whereas in practice rf power will likely be required to establish and maintain the mediating waves against collisions, etc. However, these beams do provide an upper bound on the gross gains (cf. net gains which would include the cost of maintaining a self-consistent distribution) realizable from

nonthermal distributions; each additional particle in the beam adds the maximum amount of reactivity that could be gained from an extra particle at any energy.

In all cases, the relative locations of the thermal and beam reactivities' maxima determine the possible advantages of a nonthermal scheme. In particular, a successful beam contributes excess reactivity at constant pressure, so a plasma burning at a temperature close to the peak cross section energy (as in the case of DT) reaps limited benefit from nonthermal features. Although the igniting operating regime is difficult to access, the maxima of the p-^{11}B thermal and beam reactivities are germane to a nonthermal configuration which substantially lowers the ignition threshold. This work suggests the existence of nonthermal regimes where p-^{11}B ignition may be possible.

In section II, the model used to analyze the equilibrium state of a nonthermal plasma is detailed. Sections III and IV apply this model to predict ignition thresholds in magnetically- and inertially-confined plasmas. Section V considers the potential benefits of non-Maxwellian features in these plasmas.

4.2 Thermal equilibration model

In the case of p-^{11}B , the proton population is modeled as a thermal bulk plus a fast monoenergetic beam located near the p-^{11}B fusion cross section peak at 592 keV [Nevins and Swain, 2000]. A 0-D equilibrium model provides self-consistent species

temperatures:

$$\beta_b P_{\text{fus}} = P_{\text{SD}} \tag{4.1a}$$

$$\beta_e P_{\text{fus}} + \nu_{ep}(T_p - T_e) + \nu_{eB}(T_B - T_e) - P_{\text{brem}} = 0 \tag{4.1b}$$

$$\beta_p P_{\text{fus}} + \nu_{pe}(T_e - T_p) + \nu_{pB}(T_B - T_p) = 0 \tag{4.1c}$$

$$\beta_B P_{\text{fus}} + \nu_{Bp}(T_p - T_B) + \nu_{Be}(T_e - T_B) = 0 \tag{4.1d}$$

$$G = G(\rho, \rho R;\, n_b, n_p, n_B;\, T_e, T_p, T_B) \tag{4.1e}$$

Eqs. (4.1a-d) describe the flow of fusion charged particle power to each species in a steady state ($\partial/\partial t = 0$) configuration. Eq. (4.1e) is independent of the first four and determines the volume gain G of an assembly with temperatures and densities characterized by (4.1a-d) once the scale of the system (ρ) is specified.

An effective frequency $\nu_{ij} = \nu_{ji}$ describes the drag of a thermal population i on thermal population j.[Huba, 2007] These coefficients are notably sensitive to the Coulomb logarithms characterizing the interacting species; the plasma electron density is an important parameter in establishing ignition criteria. The fusion power is the sum of a thermal reactivity [Nevins and Swain, 2000] and a beam-thermal reactivity, [Mikkelsen, 1989] viz. $P_{\text{fus}}/W_f = n_B n_p \langle \sigma v \rangle_{tt} + n_B n_b \langle \sigma v \rangle_{bt}$, where $W_f = 8.7\,\text{MeV}$ is the energy released in one reaction. The thermal bremsstrahlung emission P_{brem} is calculated as that from an optically thin medium, including relativistic corrections up to $(T_e/m_e c^2)^2$ [Rider, 1995].

The β_i denote the fraction of the fusion power $P_{\rm fus}$ deposited in the $i^{\rm th}$ species, such that $\sum_i \beta_i = 1$. In particular, β_b is the fraction of the fusion power spent preserving the proton beam velocity distribution, such that $\beta_b = P_{\rm SD}/P_{\rm fus}$, with $P_{\rm SD} = \sum_i n_b \nu_{bi} E_b$ the amount of power dissipated by fast protons slowing down in the plasma (see Appendix A). The ν_{bi}'s are effective frequencies describing the fast beam particles' energy loss to the $i^{\rm th}$ species [Huba, 2007]. The constant beam particle energy E_b is displaced from the cross section peak to maximize the beam-thermal reactivity at a specified T_B. In order to limit the anticipated damping of waves used to construct the beam, E_b was restricted to values at least twice as large as T_B.

In the large T_e limit anticipated here, fusion alpha particles slow chiefly on the ions, and the amount of alpha power diverted to electrons is of order 10%. In order to estimate the amount of alpha power absorbed by each species, consider a fast alpha particle born in a thermal p-^{11}B plasma with energy E_i. The amount of that particle's energy deposited in the protons is

$$\varphi_p = \frac{1}{E_i - E_f} \int_0^{t_f} \nu_{\alpha p} E(t)\, dt \tag{4.2}$$

where $E(t)$ is the instantaneous alpha particle kinetic energy. $\nu_{\alpha i}$ is the effective energy loss frequency for fast alpha particles slowing on the $i^{\rm th}$ species. $E_f = E(t_f)$ is the largest alpha energy at which energy flow from the particle to one species of field ions equals that from the field ions to the particle. As the typical alpha particle slows down from $\approx 3\,{\rm MeV}$ in a p-^{11}B plasma with $T_p = T_B = T_i$, it reaches this

dynamic equilibrium with the electrons first: although net energy exchange with the electrons has ended, the alpha particle continues to heat the proton and boron distributions at the t_f defined this way. Thus, $E_f \approx 1.5T_e$, such that $\nu_{\alpha e}(t_f)$ vanishes. Changing the variable of integration to the particle energy, note

$$\frac{dE}{dt} = -\sum_i \nu_{\alpha i} E \tag{4.3}$$

and find

$$\varphi_p = \frac{1}{E_i - E_f} \int_{E_f}^{E_i} \frac{\nu_{\alpha p}}{\nu_{\alpha p} + \nu_{\alpha B} + \nu_{\alpha e}} \, dE \tag{4.4}$$

φ_B and φ_e are defined analogously. This model satisfies $\varphi_B + \varphi_p + \varphi_e = 1$; the distribution of fusion product energy is sensitive to the three species' temperatures as well as their relative concentration, determined by $\epsilon = n_A/n_B$, the number ratio of the heavy species 'A' to the light species 'B' (here $\epsilon = n_B/n_p$).

In the model problem of an equilibrium p-^{11}B reactor, where a fraction β_b of the fusion power is devoted to counteracting the proton beam slowing down, only a fraction $\beta_p = (1 - \beta_b)\varphi_p$ is available to the protons. This β_b is extracted from alpha particles near their birth energies of several MeV. Because a temperature-dependent spectrum of birth energies peaking around 3.5 MeV is observed for the p-^{11}B reaction, it is assumed $E_i = 3\,\mathrm{MeV}$ qualitatively predicts the energy flow to the thermal ions [Stave et al., 2011]. The model includes species absorption fractions calculated accordingly.

4.3 Magnetic confinement

The four equilibrium equations (1a-d) describe the time rate of change of the species temperatures and the amount of power spent preserving the monoenergetic proton beam. Because the fusion reaction rates and bremsstrahlung emission both depend on n^2, only the ratios of species densities (n_b/n_p and $\epsilon = n_B/n_p$) are important. However, the temperature relaxation rates are sensitive to the Coulomb logarithm $\log\Lambda$, which in turn depends on the absolute electron density.

In order to explore the full space of igniting plasmas, consider a wide range of electron densities ($10^{10} < n_e < 10^{30}\,\mathrm{cm}^{-3}$) and disregard the boron temperature equation (1d), instead taking T_B as a specified parameter. The set (1a-c) can be solved for β_b, T_e, and T_p once n_e, T_B, n_b/n_p, and ϵ are chosen. This specification of T_B is tantamount to asserting an arbitrary ion energy confinement time.

With these assumptions, ignition thresholds can be defined for magnetically confined plasmas. It should be pointed out that such thresholds, while useful benchmarks for the model developed here, are still optimistic due to the neglected physics outlined in the introduction (e.g. instabilities and transport losses).

Lawson criteria are presented for thermal p-^{11}B and DT plasmas, followed by nonthermal p-^{11}B and DT plasmas. These latter calculations provide the upper bounds on the utility of maintaining a nonthermal distribution, abiding by the assumptions laid out in the Introduction. In the thermal cases, the numerical model predictions are compared to analytic calculations.

4.3.1 Lawson criterion

A common metric for the performance of fusion power systems is the criterion first obtained by [Lawson, 1957]. In steady state, a plasma ignites if the $n\tau$ product of number density and confinement time exceeds a specific value depending on the fusion reaction under consideration. The Lawson criterion is the statement of this minimum value, determined simply by $P_{\text{fus}} > P_{\text{loss}}$. Taking $P_{\text{fus}} = W_f n_A n_B \langle\sigma v\rangle$, with W_f the energy released in charged particles, and defining $\tau = W/(-dW/dt)$ where W is the thermal energy content of the plasma and $-dW/dt = P_{\text{brem}} = P_{\text{loss}}$ [Freidberg, 2007],

$$n_e\tau \geq \frac{T(Z_B + Z_A\epsilon)(1 + Z_B + \epsilon(1 + Z_A))}{W_f \langle\sigma v\rangle \epsilon} \tag{4.5}$$

where $\epsilon = n_A/n_B$, $n_e = Z_A n_A + Z_B n_B$, and T is the temperature common to all species. In general, the species temperatures differ, rendering the minimization of the right hand side nontrivial. It is however instructive to search numerically for those operating conditions which afford the least stringent Lawson criterion. The resulting numerical criterion is necessary but not sufficient for ignition. In pressure-limited systems, the triple product $nT\tau$ is a superior metric because it is proportional $T^2/\langle\sigma v\rangle$, in turn inversely proportional to the achievable fusion power $W_f p^2 \langle\sigma v\rangle / T^2$ [Shultis and Faw, 2007]. Thus the threshold igniting state has minimum $nT\tau$ and maximum power.

4.3.2 Minimum Lawson criterion for DT ignition

Assuming $T_e = T_i = T$, one can make a simple estimate of the threshold Lawson criterion for DT ignition. Because both deuterium and tritium carry the same number of electrons, P_{brem} does not depend directly on the number ratio ϵ. The fusion power, however, is maximized for $\epsilon = n_T/n_D = 1$, so the extremal ignition case will be located near that operating point. Using Eq. (4.5), we can form the triple product criterion for DT:

$$nT\tau \geq \frac{2T^2}{W_f \langle \sigma v \rangle} \frac{(1+\epsilon)^2}{\epsilon} = f(\epsilon)g(T). \tag{4.6}$$

In other words, the minimum triple product is a separable product of functions of ϵ and T. Considering minimization with respect to ϵ, we have

$$\min(nT\tau) \propto 2 + \epsilon + \frac{1}{\epsilon}, \tag{4.7}$$

which has its minimum at $\epsilon = 1$. The criterion is also proportional to $T^2/\langle \sigma v \rangle$, a function of temperature only. The numerical optimum temperature should be located close to the criterion's minimum at $T = 13.5\,\text{keV}$. The estimated lower bound is $1.9 \times 10^{21}\,\text{keV}\cdot\text{s/m}^3$.

Alternately, the consistent set given by Eqs. (1a-d) can be solved at various T_i to determine the threshold (minimum $nT\tau$) igniting configuration. A numerical search found the extremal point at a mass-weighted ion temperature $T_{\text{ion}} = 8.7\,\text{keV}$ and $\epsilon = 0.97$. The corresponding minimum value of $nT\tau$ is $2.6 \times 10^{21}\,\text{keV}\cdot\text{s/m}^3$, in close agreement with the estimated value. A slight excess of deuterons is explained by

their more efficient use of thermal energy. At fixed energy, the lighter particles have larger velocities, and for a thermal 9 keV DT plasma, larger cross sections (σ_f is monotone increasing up to $E_{CM} = 64\,\mathrm{keV}$). Balancing this effect are the fusion rate penalty with $\epsilon \neq 1$,

$$P_{\mathrm{fus}} \propto \frac{\epsilon}{1+\epsilon}, \tag{4.8}$$

and deuterons' larger drag losses to the electrons; the ratio of temperature equilibration rates is $\nu_{De}/\nu_{Te} \approx 1.5$.

4.3.3 Minimum Lawson criterion for p-^{11}B ignition

Following the approach of the previous section, the triple product criterion has the density scaling

$$\min(nT\tau) \propto 8 + \frac{1}{\epsilon} + 15\epsilon, \tag{4.9}$$

which takes its minimum value at $\epsilon = n_B/n_p = 1/\sqrt{15} \approx 0.26$. Likewise, the quantity $T^2/\langle\sigma v\rangle$ is minimized for $T = 138\,\mathrm{keV}$. This inconsistent optimization, regarding ϵ and T as totally independent quantities, returns an estimated lower bound of $5.1 \times 10^{23}\,\mathrm{keV{\cdot}s/m^3}$. However, a p-^{11}B plasma cannot ignite with $T_e = T_i$. (That is, unless a very substantial number of x-rays can be reflected off the walls and reabsorbed by the plasma. Here, we assume that for all practical purposes, this cannot be done. We likewise assume that the plasma is optically thin to bremsstrahlung.) Per the

analytic model, $P_{\text{fus}}/P_{\text{brem}}$ has a maximum value of 0.44 at $T_e = T_i = 204\,\text{keV}$ and $\epsilon = 0.11$.

A numerical search allowing for species-dependent temperatures found the extremal ignition point at a mass-weighted ion temperature $T_{\text{ion}} = 193\,\text{keV}$ and $\epsilon = 0.26$. The corresponding minimum value of $nT\tau$ is $2.2 \times 10^{23}\,\text{keV} \cdot \text{s/m}^3$, in close agreement with the estimated value. The numerical optimum is cooler and significantly more boron-rich than the naïve minimization of Eq. (4.5) would suggest. The extremal ignition state offsets a larger boron concentration (more fusions and bremsstrahlung) with a cooler $T_e = 59\,\text{keV}$.

4.3.4 Nonthermal gains: DT

Suppose there were some way, say by alpha channeling, to support a monoenergetic deuterium beam. In both the DT and p-^{11}B plasmas, the lighter species is chosen for the beam because of the lower energy investment required to achieve the high center of mass energy needed to access the fusion cross section peak. Operating points with $\lambda \doteq \log \Lambda < 3$ were discarded because the coupling coefficients ν_{ij} are accurate only to first order in λ^{-1}. Points with $\beta_b > 1$, signaling the need for injected power to maintain the beam, were discarded likewise.

The maximum reactivity subject to a pressure constraint is a good metric for comparing the effects of nonthermal distributions in fusion plasmas because the pressure a reactor can confine is limited by magnet strength. In the case of ITER, this figures to be about 10 bar, which we adopt as a standard value in order to compare DT and p-^{11}B MFE schemes. Nonthermal features which improve the fusion reactivity

at a fixed or reduced pressure are therefore desirable. In general, the plasma pressure includes contributions from any beam as well as the thermal populations and any alpha particles slowing down on thermal particles. Because the alpha particles whose energy is channeled to maintain the beam (fraction β_b) are 'lost' on a fast, collisionless timescale, their pressure can be assumed to be negligible. The total alpha pressure is estimated as

$$(1-\beta_b)n_\alpha \frac{W_f}{N_\alpha} = (1-\beta_b)\frac{P_{\text{fus}}}{N_\alpha \nu_{\text{SD}}} \tag{4.10}$$

where n_α is the number density of alpha particles, N_α is the number of alpha particles spawned by a single reaction, and ν_{SD} is the slowing down frequency on thermal particles. In practice, wave-mediated diffusion and device confinement could supersede Coulomb collisions with thermals as the salient processes limiting the average alpha lifetime. The reactivity includes contributions from both thermal-thermal reactions and beam-thermal reactions.

The ion number ratio which maximizes the reactivity of a pressure-limited, constant-temperature system (in the absence of a beam) is (see Appendix A)

$$\epsilon_0 = n_A/n_B = (1+Z_B)/(1+Z_A). \tag{4.11}$$

The temperature T_0 at the reactivity maximum satisfies

$$\frac{d}{dT}\langle\sigma v\rangle(T)\bigg|_{T=T_0} = 2\frac{\langle\sigma v\rangle(T_0)}{T_0} \tag{4.12}$$

Note that both of these conditions are independent of the limiting pressure. In the case of a constant-temperature DT plasma, the optimal reactivity is found at $T = 13.5\,\mathrm{keV}$ and $\epsilon = 1$. In the limit of small beam fraction $\varphi \to 0$, the numerical model locates the reactivity optimum under a 10-bar pressure constraint at $T_i = 15.3\,\mathrm{keV}$ and $\epsilon = 0.89$.

The introduction of a fast deuterium beam at the cross-section peak can improve the fusion reactivity at constant pressure. Fig. 4.1 indicates the possible gains up to a beam fraction of 1/2. The system pressure is held fixed at 10 bar.

As the beam fraction increases, the reactivity-optimizing temperature decreases and the ion ratio tilts toward the heavier target species. Both of these shifts tend to increase the beam reactivity at the expense of thermal reactivity. Such an optimized beam reduces the necessary thermal energy content of an igniting system because fewer fast particles are off-resonance; at constant pressure, a larger reactivity is possible. Likewise, a fast beam reduces the density and pressure required for an igniting plasma, substantially easing the minimum ignition conditions.

4.3.5 Nonthermal gains: p-^{11}B

In the beam-free, Maxwellian case, subject to a pressure constraint, the p-^{11}B reactivity is maximized at $T = 138\,\mathrm{keV}$ and $\epsilon = 1/3$. In the limit of small beam fraction, the reactivity maximum (under a 10-bar pressure constraint) occurs at $T_i = 137\,\mathrm{keV}$ and $\epsilon = 0.20$. The discrepancy in ϵ is due to the significant bremsstrahlung emission present in the full model at higher values of ϵ. The possible gains from the addition of a fast proton beam are indicated in Fig. 4.2, up to a beam fraction of 0.1.

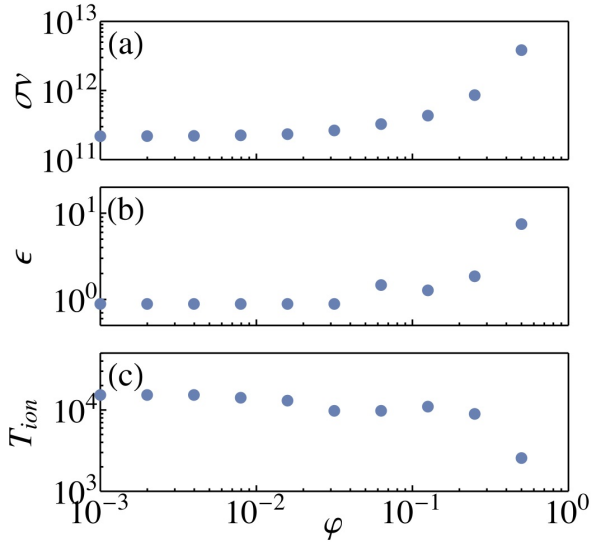

Figure 4.1: Optimized DT operating points with increasing nonthermal features in the light ion distribution function. The deuterium beam fraction φ varies from 10^{-3} to 0.5; the optima at larger beam fractions are characterized by greater reactivity (a) [cm^3/s], increased target ion concentration (b), and lower ion temperatures (c) [eV].

The energy cost of maintaining a given beam fraction against collisions with thermals is comparatively greater in p-^{11}B than DT, due primarily the abundance of electrons. Above about $\varphi = 0.2$, a proton beam cannot be maintained without injected power. In fact, above beam fractions of 0.02, these beams were only useful at higher temperatures, where the slowing down of beam protons is reduced, so the beams can be maintained at lower cost. Likewise, in the absence of a pressure constraint, fast beams can be used quite profitably. At sufficiently high temperature and density, the power required to counteract beam drag is a small fraction of the total thermal power.

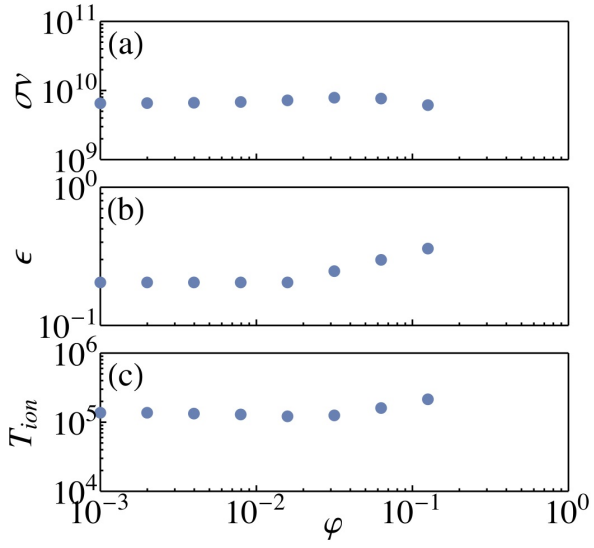

Figure 4.2: Optimized p-^{11}B operating points with increasing nonthermal features in the light ion distribution function. The proton beam fraction φ varies from 10^{-3} to 10^{-1}; the optima at larger beam fractions are characterized by greater reactivity (a) [cm^3/s], increased target ion concentration (b), and higher ion temperatures (c) [eV].

The removal of fast alpha particles in the channeling process is a significant boon to p-^{11}B ignition prospects. In a pressure-limited device, the enormous number of fusion alpha particles produced poisons the reaction by contributing pressure without also providing reactivity. Even a marginal increase in the reactant pressure, as would be the case with a small beam fraction of fast particles, could be helpful because the fusion power scales as p^2.

Consider the timescale defined by $\mathcal{T} = p_{th}/P_\alpha$, where p_{th} is the total pressure of all thermal particles in the plasma and $P_\alpha = \epsilon_\alpha \dot{n}_\alpha$ is the instantaneous fusion power released in alpha particles. If the pressure p_{th} varies slowly on the timescale

$\mathcal{T}$, for example in the case of continuous refueling, $\mathcal{T}$ is a reasonable estimate of the time a plasma can burn in quasi-steady state conditions (for which alpha poisoning is insignificant). The ratio $\mathcal{T}_{\rm DT}/\mathcal{T}_{pB}$ is of interest. Assuming equimolar DT with $T_D = T_T = T_i$,

$$\mathcal{T}_{\rm DT} = \frac{n_D T_D + n_T T_T + n_e T_e}{\epsilon_\alpha n_D n_T \langle \sigma v \rangle} \tag{4.13}$$

$$\approx \frac{4(T_i + T_e)}{\epsilon_\alpha n_e \langle \sigma v \rangle} \tag{4.14}$$

Supplying projected ITER plasma parameters, $\mathcal{T}_{\rm DT} \approx 1\,{\rm s}$, which indicates that controlling alpha pressure will be important during pulses expected to last several minutes. In comparison,

$$\mathcal{T}_{pB} = \frac{n_p T_p + n_B T_B + n_e T_e}{3\epsilon_\alpha n_p n_B \langle \sigma v \rangle} \tag{4.15}$$

$$= (1 + 5\epsilon)\frac{(T_p + T_B + (1 + 5\epsilon)T_e)}{3\epsilon_\alpha n_e \langle \sigma v \rangle}, \tag{4.16}$$

where $3\epsilon_\alpha = 8.7\,{\rm MeV}$. Note that in the case of the p-^{11}B reaction, $P_\alpha = P_{\rm fus}$. Supplying the parameters minimizing the Lawson criterion for a thermal p-^{11}B plasma (see section 4.3.3), $\mathcal{T}_{pB} \approx 10^{-16}\,{\rm s}$. Clearly an active means of removing alpha pressure (on a collisionless timescale) is crucial for any plausible p-^{11}B reactor.

Although the potential gains of a fast beam in p-^{11}B plasmas (due to the high reactivity of a beam near the thermal bulk) are limited by drag on the electron

densities required, alpha channeling may yet prove an invaluable means of controlling the alpha poisoning effect.

4.4 Inertial confinement

Here we describe the volume ignition scheme [Atzeni and Meyer-ter-Vehn, 2004] of inertial fusion and discuss how DT and p-^{11}B plasma parameters might be optimized to lower the ignition threshold. Although conservative in its predictions (cf. practical ICF schemes), the volume model is useful because of its simple structure (nearly neglecting hydrodynamic motion), highlighting the effect of a fast beam on ignition conditions. In particular, we will determine to what extent fast beams could reduce the assembly energies and ρR of DT and p-^{11}B volume targets.

The gain equation (1e) is independent of the equilibrium equations (1a-d). To solve the gain equation, however, the absolute density ρ and scale (ρR, or equivalently E_a) of the system must be specified. Together with the temperatures and beam density supplied by Eqs. (1a-d), these are sufficient to evaluate the volume gain (the yield of a homogeneous spherical assembly burning in a sound time divided by its initial thermal energy).

4.4.1 Volume ignition

The volume ignition scheme [Atzeni and Meyer-ter-Vehn, 2004] imagines a spherical target that has been prepared in a completely homogeneous state at the time of ignition. This provides a conservative estimate of the obtainable gain because the

entire fuel must be heated; more tractable ICF schemes rely on the heating of only a small portion of the burning mass, reducing the total thermal energy of the assembly, E_a. In practice, the driver energy required to assemble the target is greater than E_a due to backscatter, x-ray conversion losses, solid angle effects, rocket efficiency, etc.

The gain associated with a volume-ignited target can be expressed simply as (cf. Eq. (1e))

$$G = \frac{E\,\phi}{\frac{3}{2}\Gamma\,T_{\text{eff}}} \tag{4.17}$$

where E is the fusion energy released per unit mass ($3.39 \cdot 10^{11}$ J/g for DT, $7 \cdot 10^{10}$ J/g for p-^{11}B) and ϕ is the fraction of the target mass that burns before hydrodynamic disassembly. $\Gamma = k_B/m$ is the plasma's specific gas constant (m being the mean mass of the constituent particles) and T_{eff} is the number-weighted temperature. $\frac{3}{2}\Gamma\,T_{\text{eff}} = E_a/M_f$, where M_f is the total target mass. It is assumed that classical statistics suffice to describe each of the target's constituent species.

In order to operate in a high-gain regime, a typical ICF target will burn a significant fraction of its fuel [Lindl, 1995]. It is therefore necessary to integrate the fusion rate equation $\dot{n} \sim n^2$ over the confinement time to estimate the fraction of fuel consumed in fusion reactions. The result for a mixture of two species with initial number densities n_{A0} and n_{B0}, such that $\epsilon \doteq n_{A0}/n_{B0}$, is (see Appendix A)

$$\phi = \frac{2}{\epsilon+1}\left[1 - \frac{\epsilon-1}{\epsilon\exp\left(2\frac{\epsilon-1}{\epsilon+1}\frac{\rho R}{H_B}\right) - 1}\right] \tag{4.18}$$

where $H_B = 6c_s m/\langle\sigma v\rangle$, $c_s = (T_e/m)^{1/2}$ is the ion sound speed, and $m = (\epsilon m_A + m_B)/(\epsilon + 1)$. $\rho = m_A n_{A0} + m_B n_{B0}$ is the initial mass density. In the limit $\epsilon \to 1$, the familiar ρR formula for an equimolar target is recovered:

$$\phi \to \frac{\rho R}{\rho R + H_B} \tag{4.19}$$

In the limit $\rho R \to \infty$, burnup is limited to $2/(\epsilon + 1)$.

4.4.2 Optimization procedure

Along with ϵ, the initial ratio of boron to hydrogen nuclei, the proton beam fraction n_b/n_p is regarded as a parameter. With ϵ and n_b/n_p specified, the system of Eqs. (4.1) can be solved for T_e, T_B, T_p, and n_b. These state variables are used to evaluate the volume gain for the configuration, which is then a function of ρR only (through the burn fraction, ϕ). A large sampling space was considered to locate the minimum assembly energy E_a necessary for a volume gain of unity (Eq. (4.17)). E_a can be related directly to the equilibrium conditions determined by Eqs. (1a-d):

$$E_a \doteq \frac{3}{2} N T_{\text{eff}} = \frac{3}{2} \sum N_s T_s \tag{4.20}$$

$$= \frac{3}{2} \frac{M_f [T_e + T_p + \epsilon(5T_e + T_B)]}{m_e + m_p + \epsilon(5m_e + m_B)} \tag{4.21}$$

in the case of p-^{11}B with $n_{B0}/n_{p0} = \epsilon$ and $n_b/n_p = 0$ (no beam). M_f is the mass of the entire target; Boltzmann's constant k_B has been suppressed. Using

$$M_f = \frac{4\pi(\rho R)^3}{3\rho^2} \tag{4.22}$$

the burnup $\phi = \phi(\rho R, T_e, T_p, T_B)$ and therefore the volume gain are entirely specified by E_a once the assembled density ρ has been given (in addition to ϵ and β_b). To wit,

$$\rho R = \left(\frac{\rho^2 E_a}{2\pi} \frac{m_e + m_p + \epsilon(5m_e + m_B)}{T_e + T_p + \epsilon(5T_e + T_B)} \right)^{1/3} \tag{4.23}$$

The addition of a fast proton or deuteron beam is reflected by

$$E_a \to \frac{3}{2} \left(n_b \epsilon_b + \sum N_s T_s \right) \tag{4.24}$$

Thus, once equations (1a-d) have been solved consistently for the species temperatures with specified T_B, ϵ, beam fraction, and density, the gain equation (1e) can be solved for the minimum assembly energy resulting in a volume gain of unity. Using the above definitions, it is possible to express this criterion in terms of the assembly ρR.

4.4.3 DT ignition criterion

Assuming a constant temperature T for all species, it is straightforward to estimate a beam-free best case from the gain equation (1e). At $\rho = 10^3$, the result is a minimum

igniting ρR of $0.022\,\mathrm{g/cm^2}$ at $T = 18\,\mathrm{keV}$ and $\epsilon = n_T/n_D = 1.10$. This is equivalent to an assembly energy of 0.09 J.

A numerical search allowing for distinct, consistent species temperatures determined by the system (4.1a-e) located a minimum ρR of $0.07\,\mathrm{g/cm^2}$ at a mass-weighted ion temperature of $7.1\,\mathrm{keV}$ and $\epsilon = 1.13$. This is equivalent to an assembly energy of 1.1 J. In the full model, slowing of fusion alpha particles on the thermal electrons creates some separation in electron and ion temperatures ($T_e \approx 10\,\mathrm{keV}$ here), rendering the assumptions of the original estimate inaccurate.

In the presence of a fast deuteron beam, the ignition criteria are further relaxed. The typical minimal state features a fast beam colliding with a thermal plasma substantially cooler than the Maxwellian optimum. In DT, the potential utility of the beam is limited by the fact that the resonant beam energy is an order of magnitude greater than the optimal Maxwellian plasma temperature whereas the reactivity gain is limited to a factor of about 3.5. As Fig. 4.3 indicates, a fast deuteron beam nonetheless reduces the ρR required for ignition by a factor of 14, corresponding to a factor of 10^4 reduction in the total thermal energy of an igniting assembly. Above a beam fraction of about 4%, the shift towards large tritium concentrations (Fig. 4.3b) and low ion temperatures (Fig. 4.3c) is pronounced.

4.4.4 p-^{11}B ignition criterion

Assuming a constant temperature T for all species, it is straightforward to estimate a beam-free best case from the gain equation (1e). At $\rho = 10^3$, the result is a minimum

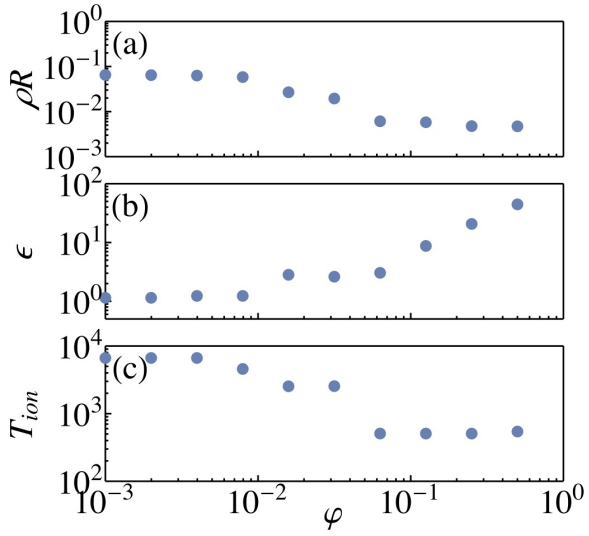

Figure 4.3: Optimized DT ICF operating points with increasing nonthermal features in the light ion distribution function. The deuteron beam fraction φ varies from 10^{-3} to 0.5; the optima at larger beam fractions are characterized by lower minimum igniting ρR (a) [g $\cdot$ cm^{-2}], increased target ion concentration (b), and lower ion temperatures (c) [eV].

igniting ρR of 9.95 g/cm^2 at $T = 153$ keV and $\epsilon = n_B/n_p = 1.30$. This is equivalent to an assembly energy of 59 MJ.

A numerical search allowing for distinct, consistent species temperatures determined by the system (1a-d) located a minimum ρR of 2.1 g/cm^2 at a mass-weighted ion temperature of 196 keV and $\epsilon = 1.8$. This is equivalent to an assembly energy of 0.28 MJ, showing marked improvement over the naïve estimate. At the high densities characteristic of ICF, the Coulomb logarithm is small enough that a large temperature difference can be sustained between electrons and ions. In the particular case of

p-^{11}B , the substantial bremsstrahlung emission keeps the electron temperature low. The resulting lower thermal content of the fusing plasma improves the volume gain.

In the presence of a fast proton beam, the ignition criterion is relaxed. In contrast to DT, the resonant beam energy (c. 592 keV) is only a factor of 2-4 greater than the optimal Maxwellian plasma temperature, whereas the reactivity gain is superior, about a factor of 6. Fig. 4.4 suggests that in p-^{11}B , the net effect of a beam is nevertheless less pronounced cf. DT. The minimum igniting ρR is reduced by nearly a factor of 3 (Fig. 4.4a), corresponding to a factor of 30 reduction in assembly energy. The optima eschew contributions from thermal reactions above a beam fraction of about 7%, as demonstrated by the shift to larger ϵ (Fig. 4.4b) and low ion temperature (Fig. 4.4c).

4.5 Possible implementation

The practical implementation of the effects considered here is really beyond the scope of this work. In all cases, it is necessary to identify a wave that persists on a long time scale that is capable of delivering its energy in such a way as to produce or maintain a non-Maxwellian feature or to make one species hotter than another species. Our intent here has been merely to bound from above how much could possibly be obtained by distortions to the distribution functions that do not violate thermodynamic principles. How the waves can be produced, and how the waves produce these distortions are beyond the scope of this work. But the hope is that if the upside potential would be large enough, then there would be incentive to

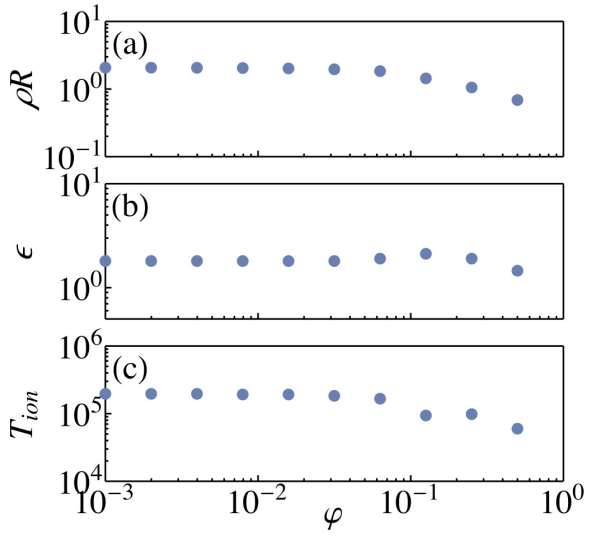

Figure 4.4: Optimized p-^{11}B operating points with increasing nonthermal features in the proton distribution function. The proton beam fraction φ varies from 10^{-3} to 0.5; the optima at larger beam fractions are characterized by lower minimum igniting ρR (a) [g $\cdot$ cm^{-2}], roughly equal target ion concentration (b), and lower ion temperatures (c) [eV].

look for specific waves and specific mechanisms, and to assess the consequences of effects neglected here. On the other hand, in regimes where the upside potential of these manipulations of the distribution functions through alpha channeling might be relatively modest, there would of course be no incentive to look further at detailed mechanisms—saving one the trouble of trying.

Nonetheless, in this section, we do discuss possible implementations of waves that would distort the Maxwellian distributions, but only to give a general sense of where there are reasons to believe that implementations may be at hand, and where

considerable ingenuity would need to be exercised to find them, even if they are not disallowed by thermodynamic principles.

While all implementations must be considered at present to be speculative, the most straightforward implementations, and the ones that have attracted the most theoretical attention, and even some experimental attention, would be those in the presence of a strong magnetic field, like in a magnetic confinement device such as a tokamak or a mirror. The mechanisms for alpha channeling in tokamaks were theoretically developed first through considerations of the lower hybrid wave [Fisch and Rax, 1992b,a]. It was later recognized that the mode-converted ion Bernstein wave offered greater possibilities [Valeo and Fisch, 1994, Fisch, 1995], and further optimizations might be enabled through a combination of several waves [Fisch and Herrmann, 1995, Herrmann and Fisch, 1997, Herrmann, 1998]. Aspects of the effect with the mode-converted ion Bernstein wave were verified in experiments [Fisch and Herrmann, 1999, Fisch, 2000]. The utility of these effects was quantified and deemed very substantial [Fisch and Herrmann, 1994].

Similar approaches are possible in mirror machines, where the boundary is more complicated, since particles can leave the mirror either at a physical boundary or at the trapped-passing boundary in velocity space [Fisch, 2006, 2007]. The effect can also be practiced in centrifugal mirror confinement fusion devices, where the channeling effect can be arranged to provide for direct support of the radial potential that produces the rotation [Fetterman and Fisch, 2008].

In inertial confinement fusion, alpha channeling scenarios are much harder to envision. The key issue is how can waves persist in such high-density plasma. It

would be necessary for the waves to capture the alpha particle energy and then to damp that energy on ions. The high densities make it difficult to catalyze the effect with waves, since the collision frequency may be so high that the wave energy is damped before mediating the energy transfer. One speculation in manipulating wave energy in an ICF target is to embed a wave in the hot spot early in time, possibly in a bit of an excavated, low-density hot spot, something like a bubble, before the compression happens, such that the wave grows in amplitude as a consequence of action conservation during the target compression [Schmit et al., 2010, Schmit and Fisch, 2012]. The amplified wave might then be available to mediate somehow energy exchange between fusion produced alpha particles and fuel ions, much like in magnetic fusion plasma. Langmuir waves would likely be sensitive to collisional damping, in these regimes, even in a bubble, but to if a magnetic field were generated in the target, a larger selection of waves might then be available for mediating the energy transfer.

In different devices, the alpha channeled energy might accomplish different things in addition to reducing ignition requirements through the hot ion mode: in tokamaks, significant practical advantages would be realized particularly if the alpha energy were diverted to current drive or ion heating; in case of centrifugal fusion, supporting the radial potential. And for p-^{11}B fusion, or for other low fusion density interactions, the greatest gains may come from prompt removal of fusion byproducts, once their energy is captured. However, these further advantages, as well as the real possibility of their practical implementation, like the possibility of maintaining the

non-Maxwellian features of the fuel ions in the first place, are beyond the scope of the present study.

4.6 Discussion

This work seeks to address, in broad strokes, the utility of non-Maxwellian features in both DT and p-^{11}B plasmas under magnetic and inertial confinement. Regardless of the scheme chosen, the relation between the thermal reactivity and resonant features in the fusion cross section is crucial in establishing this utility.

A natural criterion in both confinement schemes is the amount of pressure or thermal energy required for ignition because this quantity scales directly with the facility cost (magnet strength in MCF, driver energy in ICF). If a beam is to reduce the pressure requirement, it should provide excess reactivity without a disproportionate contribution to the system pressure. In particular, the beam-thermal reactivity ratio and the ratio of beam energy to the bulk temperature should be compared. Heuristically, the parameter

$$R = \frac{\langle \sigma v \rangle_{\text{beam}} / \langle \sigma v \rangle}{\epsilon_{\text{beam}} / T} \tag{4.25}$$

is indicative of the beam utility for specified plasma conditions.

In the case of DT, the fusion resonance is located far in the tail of most igniting plasmas (true 'thermonuclear' fusion). Because bremsstrahlung losses are minimal, the plasma energy content required for ignition is small (with respect to the resonance), but the distance of the resonance is a drawback when energy is supplied

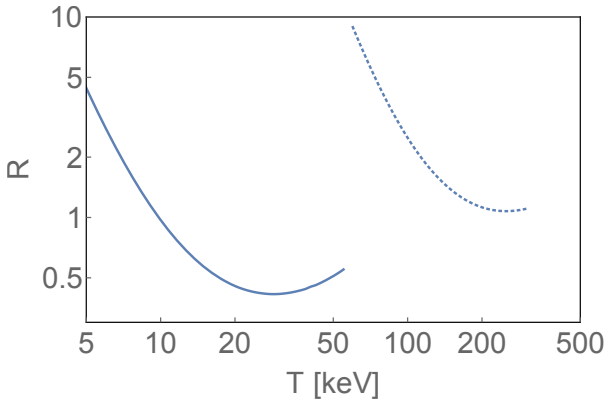

Figure 4.5: R metric plotted for constant-temperature DT (solid line) and p-^{11}B (dotted) plasmas. The plotting intervals are restricted by the validity of thermal reactivity fits and the incursion of the resonant beam into the bulk of the distribution function. We allow $\epsilon_{\text{beam}} > 2T$.

directly to heat particles at such large energies, as in the case of a resonant beam. Likewise, the broad DT resonance limits the achievable reactivity gain; the value of R in igniting thermal DT plasmas is about 1/2, indicating that channeling fusion power to a beam is not generally useful. Fig. 4.5 traces R for constant-temperature DT and p-^{11}B plasmas.

In contrast, the p-^{11}B cross section energy peak is close to the temperatures relevant to thermonuclear fusion. Likewise, due to the narrow resonance, substantial reactivity is gained by channeling fusion power to a resonant beam (e.g. the beam reactivity is 15.7X greater than thermal at $T = 100\,\text{keV}$). Typical values of R in an igniting p-^{11}B plasma are slightly larger than unity, suggesting that a beam is a potentially useful investment in these systems.

The equilibration model employed here alters these conclusions somewhat. At low temperatures, the pressure is reduced and the beam reactivity benefits from the re-

duced thermal broadening of the fusion resonance. R consequently improves, but the collisionality of the plasma increases simultaneously. Faster relaxation rates require the diversion of additional fusion power to maintain the beam and reduce the possible temperature separation between species, increasing the effective bremsstrahlung emission. Both of these effects limit the economic viability of a fast beam. However, the model excludes beam particles from the calculation of collision rates, reducing the collisionality of the plasma as the beam fraction is further increased. These competing collisional effects constitute the primary interactions of the beam with the thermal plasma.

Apart from the beam fraction, the other salient parameter in scanning plasma conditions is the number ratio ϵ, defined in all cases as the ratio of heavy ions to light ions, including beam ions. An interesting divergence arose between the two reactions: in DT, $\epsilon \gtrsim 1$ plasmas had lower ignition thresholds in both MCF and ICF. In p-^{11}B , $\epsilon < 1$ plasmas were favored for MCF and $\epsilon > 1$ plasmas were favored for ICF. In DT, the number of electrons does not depend on ϵ, so the bremsstrahlung emission is mostly independent of this parameter. The slight preference for tritium-rich plasmas is likely seen in extremal cases because the same center of mass energy is available at lower pressures in a deuterium-rich plasma. In p-^{11}B , the preference for boron-poor plasmas in MCF is explained by the balancing of bremsstrahlung emission (increasing with ϵ) and thermal reactivity (decreasing with ϵ).

The large boron density in the ICF optimum is harder to explain. The number ratio which maximizes the reactivity of a pressure-limited, constant-temperature system is $\epsilon = n_A/n_B = (1 + Z_B)/(1 + Z_A) = 1/3$, in the case of p-^{11}B. However,

if the species temperatures are allowed to float, a high electron density (due to the boron excess) could suppress the electron temperature enough via bremsstrahlung emission that the reduction in the thermal content of the plasma outpaces the loss of reactivity and improves the volume gain in the aggregate ICF accounting.

In the presence of a beam, the ϵ and T_i maximizing the total reactivity-pressure ratio should increase and decrease, respectively, as these changes create a rich environment of cold, resonant target ions for the lighter beam ions. The result is increased reactivity at fixed pressure. In p-^{11}B , the price of increasing ϵ is reduced thermal reactivity and, moreover, greater bremsstrahlung emission. In a constant-temperature model, both fuels behave as predicted; as the beam fraction rises from 0 to 1, there is a critical point where the beam reactivity exceeds the total thermal reactivity and the optimum operating point is an excess of very cold target ions.

Although the volume gain calculation is intrinsically conservative (cf. ignition in a hot spot), the assembly energies E_a have been systematically underestimated, thereby exaggerating the gains reported here. In practice, it will be necessary to prepare the target at the prescribed temperature, which will likely involve heating from low temperatures (perhaps cryogenic, ambient at best). This heating will have to overcome bremsstrahlung and conduction losses; a better estimate of the volume gain will require tracing the target's evolution in $\rho R - T$ phase space as Lindl has done for DT hot spots in NIF targets [Lindl, 1995].

Investing substantial recirculated power in a fast beam has the potential to reduce ignition threshold conditions and ameliorate various engineering difficulties. The encouraging results of the stability analysis suggest that because the bulk ions are

usually sufficiently cold, the necessary recirculated power can be regarded as small. In the case of DT plasmas, fast beams can increase the reactivity of a magnetically confined plasma at constant pressure or lower the ρR required for ignition by an inertially confined plasma. In p-^{11}B plasmas, the extra electron density increases the cost of maintaining a beam, limiting the gains which are possible in principle.

Indeed, this work found superior gains in DT with the introduction of a beam. In both MCF and ICF DT plasmas, these gains were substantial. A fast deuterium beam improved the DT reactivity by an order of magnitude while reducing the ion temperature to order-1 keV levels. However, the 10^4 reduction in the ICF igniting assembly energy is arguably even more impressive. In p-^{11}B ICF plasmas, the corresponding reduction was only a factor of 30. However, this reduction is more impressive than the gains realized in p-^{11}B MCF, where a beam improved the total reactivity by only 20%. However, the alpha channeling which could be used to power the beam is likely critical to any steady state, magnetically confined scheme as a reliable means of abating the pressure poisoning effect.

A key caveat to all the conclusions reached here, and the comparisons made between ICF and MFE as well as between DT and p-^{11}B fusion, is that these conclusions and comparisons are all based on an upper bound to a utility that in practice may be difficult to reach. However, the utility that can possibly be reached serves as impetus to try to find ways to reach it. The scenarios that we considered are in that respect at least not disallowed by the laws of physics, so they can serve at once not only as an impetus to achieve what is not disallowed, but also as a caution not to expect that more could be achieved.

Chapter 5

Energy extraction by diffusive exchange[1]

Waves propagating through a bounded plasma can rearrange the densities of states in the six-dimensional velocity-configuration phase space. Depending on the rearrangement, the wave energy can either increase or decrease, with the difference taken up by the total plasma energy. In the case where the rearrangement is diffusive, only certain plasma states can be reached. It turns out that the set of reachable states through such diffusive rearrangements has been described in very different contexts. Building upon those descriptions, and making use of the fact that the plasma energy is a linear functional of the state densities, the maximal extractable energy under diffusive rearrangement can then be addressed through linear programming.

[1]This chapter is based on "Maximal energy extraction under discrete diffusive exchange," published in Physics of Plasmas [Hay et al., 2015]

5.1 Introduction

Waves propagating through a bounded plasma can rearrange the densities of states in the six-dimensional velocity-configuration phase space. When the rearrangement is such as to cause particles to diffuse from higher energy states to lower energy states, the waves extract energy from the plasma. A particular case of this posing of the rearrangement problem is the case of alpha channeling, where the energy is deliberately extracted from the population of α-particles that are produced in a fusion reactor [Fisch and Rax, 1992b]. This energy is recovered as wave energy. In a reactor, this energy is more useful in the form of wave energy, which can be used to attain a hot-ion mode or to drive electrical current.

The rearrangements contemplated in plasma using waves are diffusive in nature, since the wave-particle mechanisms generally cannot maintain coherence, at least not for the leading way of using external rf sources to heat or drive current in plasma. However, depending on the wave frequency and wavenumber, the diffusion occurs in paths that link energy to the spatial dimensions. In the case of tokamak reactors, where α-particles are expected to be born at high energy in the plasma center, there is a natural energy inversion along the path that connects the dense phase space location at high energy in the center to the under-dense phase space location that is at low energy on the periphery. It is then only a matter of constructing the appropriate wave diffusion path to link these locations. How much energy can be released from α-particles is a matter of considerable practical interest, since if appreciable energy could be released in this manner, there then might be the opportunity to diminish substantially the cost of electricity through tokamak fusion.

A theoretical issue of academic interest, however, is the precise maximum available energy under diffusive rearrangements of phase space density when an arbitrary number of diffusion paths can be constructed [Fisch and Rax, 1993]. The energy extractable under diffusion was posed recently, in fact, as one of the interesting, outstanding problems in wave-particle physics in plasma [Fisch, 2014]. This issue also motivated to some extent approaches to other bounds on energy exchange between light and plasma, such as the extent to which bounds could be placed on the absorption of laser light at an interface [Levy et al., 2014]. There are, to be sure, also other formulations of free energy in plasma under phase space density rearrangements. For example, respecting phase space conservation, the Gardner restacking represents a precisely definable free energy that can be readily calculated [Gardner, 1963, Dodin and Fisch, 2005]. This energy is an upper bound on that which can be extracted through diffusive processes. However, because the Gardner restacking is without the realistic limitation of the diffusion constraint, the free energy available under this formulation represents a rather rarefied theoretical construct, even further from practical considerations than the academic issue posed here.

The free energy under the constraint of diffusive rearrangements has one well-known textbook example, the famous so-called "bump-on-tail" problem. The tail of the Maxwellian distribution is imagined to have a "bump" in velocity space, so that the distribution is no longer monotonically decreasing in energy. In that case, waves can diffuse particles so as to smooth out the bump, releasing the kinetic energy, until a distribution monotonically decreasing in energy is reached. The maximum extractable energy is obvious, and can be constructed from geometrical considerations;

for the 1-bump problem, it is just the energy change in flattening the bump. However, were there two bumps in the velocity space, then the optimal solution would no longer be obvious at all, since it is not clear which bump should be flattened first.

More generally, what is imagined here is that diffusion paths can be constructed that link any two phase space locations in the 6D velocity-configuration space, whether or not the locations are contiguous [Fisch and Rax, 1993]. The contiguous constraint can formally be realized, in any event, in the limit of vanishingly thin paths. Thus we imagine an ensemble of discrete phase space locations, each with an initial density, and each representing a certain energy. Then as population densities relax under diffusion, the total system energy relaxes as well. The free energy under the diffusion constraint is then defined as the maximum extractable energy, given the opportunity to diffuse particles between any two phase space locations, with any sequence of such two-location or what we might call two-state relaxations. It turns out, however, that while this pair-wise relaxation is a well-defined posing of the free energy, it has not been apparent at all how to calculate it efficiently when there are many states.

The problem thus posed in plasmas can similarly be posed with respect to stimulated emission by a set of lasers [Fisch and Rax, 1993]. Suppose, an atomic system with just three energy levels, the ground state at energy ϵ_1, the first excited state at ϵ_2, and the second excited state at ϵ_3, with initial population densities of, respectively, n_0^1, n_0^2, and n_0^3. The total energy can be put as $W = \vec{\epsilon} \cdot \vec{n}$, where $\vec{\epsilon}$ and $\vec{n}$ represent the energy levels and the population densities. Suppose further the availability of three lasers with frequencies ν_{10}, ν_{20}, and ν_{21}, that, respectively, can stimulate transitions

between the first level and the ground state, the second level and the ground state, and the second level and the first level. Suppose that these lasers are incoherent, so what they can accomplish is to equalize the populations in any two levels. The maximum energy is extracted when the correct sequence of laser pulses is applied.

To make the issues here clear, consider the following example [Fisch and Rax, 1993]. Suppose that the accessible states have energies with numerical values (0,1,4) and the initial state densities are (0,2/7,5/7), where the sum has been normalized to 1. Then the initial energy is $W_0 = 22/7$. The energy at step j can be put as W_j. The sequence of level-equalizing steps, $(\nu_{21}, \nu_{20}, \nu_{10})$, then gives

$$
\begin{array}{lll}
 & & \begin{array}{ccc} \epsilon_1 = 0 & \epsilon_2 = 1 & \epsilon_3 = 4 \end{array} \\
\text{initial} & W_0 = 22/7 & \left(\begin{array}{ccc} 0 & 2/7 & 5/7 \end{array} \right. \\
\text{step 1} & W_1 = 5/2 & \left(\begin{array}{ccc} 0 & 1/2 & 1/2 \end{array} \right. \\
\text{step 2} & W_2 = 3/2 & \left(\begin{array}{ccc} 1/4 & 1/2 & 1/4 \end{array} \right. \\
\text{step 3} & W_3 = 11/8 & \left(\begin{array}{ccc} 3/8 & 3/8 & 1/4 \end{array} \right)
\end{array}
$$

The energy extracted is thus $22/7 - 11/8 = 99/56$, or approximately 56% of the initial plasma energy. One can show, for this set of energy levels and initial populations, that the sequence used is the optimal sequence for extracting energy, resulting in the maximum extractable energy. What is of interest, however, is how exactly this can be proved, how the maximum extraction can be calculated efficiently, and how the complexity of the problem increases with the number of states.

It turns out that the answer to these questions lies in the mathematical developments in other fields (although these developments appear not to have received much attention). Similar level-mixing operations have been considered in chemical reaction kinetics [Horn, 1964]. More directly of use here, [Zylka, 1985] identified the set of accessible states through level-mixing operations, called the K set, using as an example the problem of attainable temperatures in heat reservoirs pairwise connected by heat pipes, with an arbitrary number of reservoirs. Thon and Wallace, in the context of characterizations of altruism as a pairwise relaxation correction to economic inequality, derived further features of the K set [Thon and Wallace, 2004].

Using these characterizations of the K set, the sequence of operations to extract maximal energy can be found. Although K, the set of states that can be reached from these level-mixing operations, is not convex [Zylka, 1985], one can imagine covering the entirety of K with a small convex polygon. This polygon (namely, the *convex hull* of K, denoted $ch(K)$ here) is determined by taking all possible convex combinations of the points found within K. Equipped now with a linear objective function (the total energy of a state) and a convex feasible region (the unique covering polygon, $ch(K)$), we may apply the fundamental theorem of linear programming to locate the minimum energy state at a vertex or edge joining two or more vertices of the convex hull of K. Crucially, K contains each of the vertices of its convex hull (by construction), and so the minimum energy state over the polygon *covering* K is identical to the minimum energy state found *within* K. Thus, using the results of [Zylka, 1985, Thon and Wallace, 2004] for the three-level system, we shall pose and answer the following five questions:

1. What sequence minimizes the energy?

2. What is the full set of sequences that must be considered before the optimal sequence can be found?

3. What are the full set of sequences that could possibly be a solution, for some values of the energy levels and the initial population densities?

4. If it were possible to partially relax the distribution between two states, rather than fully relax it, would that ever be a useful step?

5. Is it the case that it is ever useful to take a step that increases the energy rather than decreases it?

This chapter is organized as follows. In Sec. II, we define the diffusion model. In Sec. III, we reproduce results of the space of relaxation solutions, and show how this immediately answers the first three questions. In Sec. IV, we answer the fourth question, proving that partial relaxation is never a useful step, regardless of the number of states. In Sec. V, we demonstrate out that strategies previously considered [Fisch and Rax, 1993] can be put more precisely and further prove for any number of states that energy-increasing steps can never be part of the optimal sequence. In Sec. VI, we offer further discussion of the implications for N states and the degree of complexity of the problem. In Sec. VII, we summarize the main conclusions.

5.2 Diffusion model

Suppose a set of level energies $\epsilon = (\epsilon_1, \epsilon_2, \ldots, \epsilon_N)$ and a set of initial populations $n_0 = (n_0^1, n_0^2, \ldots, n_0^N)$. Here we understand the symbols ϵ and n_0, without superscripts, to represent vectors; the initial level density of state i is represented as n_0^i. In its discrete realization, Gardner's bound results from a permutation $\pi \in S_N$ of the initial level populations, where S_N denotes the symmetric group on $\{1, 2, \ldots, N\}$. The optimal final populations n_G are given by $n_G = P_\pi n_0$, where P_π is an $N \times N$ permutation matrix guaranteeing $\epsilon_i \geq \epsilon_j \Rightarrow n_G^i \leq n_G^j$. Thus the final populations are decreasing with increasing level energies. The Gardner permutation is not unique in cases of degeneracy in either the level energies or the initial populations. The associated bound on the final system energy is denoted $W_G \doteq \epsilon \cdot n_G$.

Now, consider a diffusion operation that equalizes the populations of a pair of levels (i, j) such that

$$\left(n_0^i, n_0^j\right) \rightarrow \left(\frac{n_0^i + n_0^j}{2}, \frac{n_0^i + n_0^j}{2}\right), \tag{5.1}$$

leaving all other level populations unchanged. We are interested here is the minimization of the system energy $W_d \doteq \epsilon \cdot n_f$ after repeated application of operations of this type on an initial state n_0 and reaching a state n_f.

The diffusion operation (5.1) can be represented by doubly stochastic matrices of the form $B_{ij} = \frac{1}{2}(I + Q_{ij})$, where I is the $N \times N$ identity matrix and Q_{ij} is the permutation matrix that exchanges the i^{th} and j^{th} level populations. Application of B_{ij} equalizes the i^{th} and j^{th} populations. For example, (5.1) could be styled $n_0 \rightarrow$

$n_0 B_{ij}$. The B_{ij} are symmetric, idempotent, and do not generally commute. (Two B_{ij} commute if neither of them operates on the same level.) They are a particular case of the T-transform: $T = (1-\alpha)I + \alpha Q$, $\alpha \in [0,1]$ and Q is a permutation of the identity matrix which exchanges only two rows [Marshall et al., 2009]. Like all doubly stochastic matrices, T-transforms are measure-preserving: $\sum_{ab} T_{ab} n_b = \sum_b n_b = 1$. It is important to distinguish between the cases of $0 \leq \alpha \leq 1/2$ and $1/2 < \alpha \leq 1$; the latter case corresponds to moving density from a less-populated level to a more-populated level. For now, we will consider only $\alpha = 1/2$ transforms, i.e. the B_{ij}.

5.3 The set of points K

[Zylka, 1985] was the first to identify the set of accessible states through level-mixing operations: the K set. K is determined by the provided set of level populations, represented as a length-N vector n_0, as well as the allowed diffusion operations. Without loss of generality, n_0 may be ordered increasing, as we assume throughout this work. As described previously, the diffusive B_{ij} operations equalize the populations of any pair of levels i and j. Each element contained in K is an N-tuple of level populations that can be reached by applying some sequence of the various B_{ij} to the initial state n_0.

The linear function W_d assumes its extremal values on the boundary of $ch(K)$. The three-level system is conveniently depicted in n_1-n_2 space. Due to normalization of the population vector, one coordinate is ignorable and a general state n may be written as $n = (n_1, n_2, 1 - n_1 - n_2)$; if the total density is say 1, the the density of

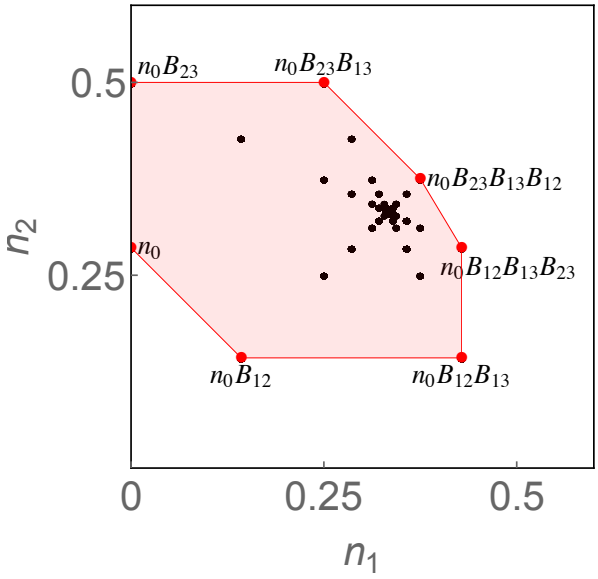

Figure 5.1: The set K for $n_0 = (0, 2/7, 5/7)$, depicted in n_1-n_2 space. The convex hull $ch(K)$ is illustrated by the pink region. Extreme points of $ch(K)$ are indicated with red dots and labeled by the by the series of transformations B_{ij} required to reach them. Interior points are labeled with small black dots. K itself is the union of the red and black dots.

the third is simply $1 - n_1 - n_2$. Following [Zylka, 1985], we will demonstrate that K is star-like.

To see this, first let us consider the example considered earlier, and previously in [Fisch and Rax, 1993], namely the case of $N = 3$ case with initial data $n_0 = (0, 2/7, 5/7)$ and $\epsilon = (0, 1, 4)$.

One can generate the entire set K by applying arbitrarily long sequences of the transforms B_{ij} to the initial point n_0. We denote the set of points generated by k arbitrary B_{ij} the k^{th} generation of K. The first six generations of K are plotted in Figure 1, overlaid with $ch(K)$. Except for the original point n_0, the entirety of K lies along three distinct line segments joining pairs of extreme points, as depicted in

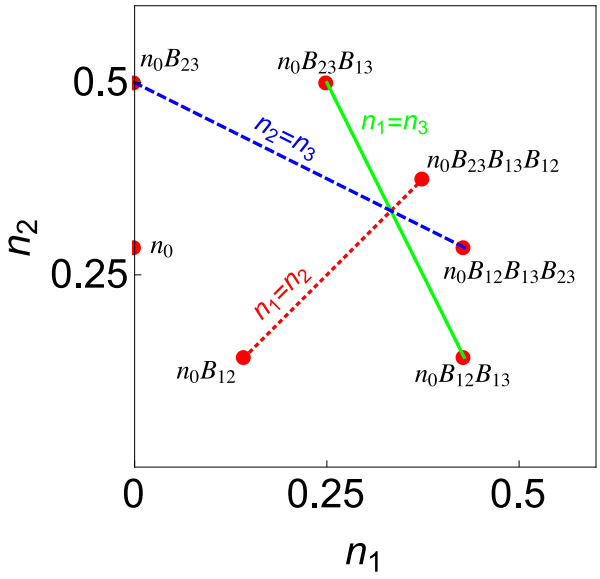

Figure 5.2: The three lines covering K are depicted for $n_0 = (0, 2/7, 5/7)$, emphasizing the star-shaped nature of K.

Figure 2. This arrangement is obvious if one considers that every state must have $n_i = n_j$, for some i and j, if the last transform applied in the sequence arriving at that state is B_{ij}.

The six extreme points (excepting n_0) can then be paired according to their final B_{ij}. For example, the extreme points $n_0B_{12}B_{13}$ and $n_0B_{23}B_{13}$ are so paired, and the line joining them satisfies $n_1 = n_3 = 1 - n_1 - n_2$, or $n_2 = 1 - 2n_1$. It is now clear that K must be star-shaped with respect to $e = (1/3, 1/3, 1/3)$ because the three lines joining pairs of extreme points satisfy $n_1 = n_2 = 1 - n_1 - n_2$ there [Zylka, 1985]. Likewise, $ch(K)$ for a three-level system is defined by at most seven extreme points (see Appendix B). Each generation approaches e more closely, and no extreme points are generated after the third generation. (Consider the effect of B_{ij} on a state $n = (n_1, n_2, 1 - n_1 - n_2)$. Then the Euclidean distance s of n from e

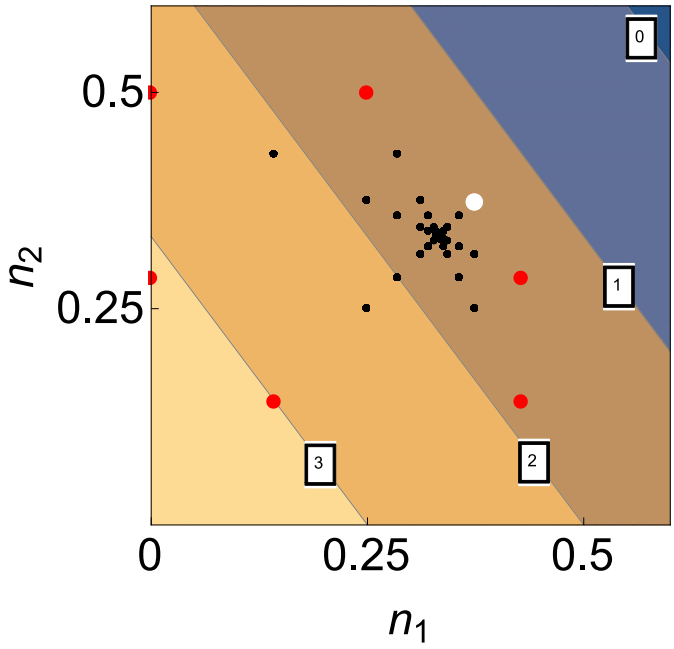

Figure 5.3: K superimposed on contours of $W_d = \epsilon \cdot n$ (labeled by energy). The minimum W_d is found at the extreme point $n_0 B_{23} B_{13} B_{12} = (3/8, 3/8, 1/4)$ (labeled by a red circle in Figs. 1 and 2) labeled here by a large white circle.

satisfies $s^2 = (n-e)\cdot(n-e)$. Comparing the distances of n and nB_{ij} from e, one finds $(n-e)\cdot(n-e) - (nB_{ij}-e)\cdot(nB_{ij}-e) = \frac{1}{2}(n_i - n_j)^2 \geq 0$. Thus each B_{ij} brings a state closer to e.)

Note that the set K is non-convex [Zylka, 1985] since not all of the points in $ch(K)$ can be reached by sequences of B_{ij} applied to n_0. Per the fundamental theorem of linear programming, the minimum W_d over the convex feasible region $ch(K)$ is found either at a single extreme point of $ch(K)$ or along an edge of $ch(K)$ joining two or more extreme points of $ch(K)$. (In the latter case, the minimum W_d multiplicity is equal to the number of collinear extreme points.) However, the extreme points of

$ch(K)$ are all contained in K. Thus the linearity of the objective function $W_d = \epsilon \cdot n$ ensures that it has the same minimum over K and $ch(K)$.

Having identified the set of extreme points of $ch(K)$, $\mathcal{E}(ch(K))$, in Fig. 1, the minimum W_d may be computed as $\min\{\epsilon \cdot \mathcal{E}(ch(K))\}$. Fig. 3 overlays contours of the state energy $\epsilon \cdot n$ on K, thereby illustrating the scheme and identifying the minimum energy state. In this case, the optimum level populations are $n_f = n_0 B_{23} B_{13} B_{12} = (3/8, 3/8, 1/4)$, yielding a minimum $W_d = 11/8$, as previously calculated by exhaustive search.

The sequence which minimizes the plasma energy can always be identified with this algorithm. Crucially, because we have not assumed any ordering of the level energies ϵ, the slope of the state energy contours is arbitrary in the general case (cf. Fig. 3). Therefore, each of the seven extreme points identified is a possible solution to the energy minimization problem.

5.4 Partial relaxation

The discussion so far has assumed complete pairwise equalization of levels at every step, corresponding to B_{ij} transforms with $\alpha = 1/2$. From a physical standpoint, densities could also be relaxed through a diffusion process that only partially equalizes population levels, corresponding to the case of T-transforms with $0 < \alpha < 1/2$.

The $\alpha = 1/2$ transforms B_{ij} can be reached by repeatedly applying a particular T-transform with $0 < \alpha < 1$ formed from the same Q_{ij}, since for all $0 < \alpha < 1$, $\lim_{n\to\infty} T_{ij}^n = \frac{1}{2}(I + Q_{ij}) = B_{ij}$. Thus, the $\alpha = 1/2$ state space is in the closure of

the state space for any fixed $0 < \alpha < 1$. At the same time, the $0 < \alpha < 1/2$ state space is contained entirely in the convex hull of the $\alpha = 1/2$ state space. To see this, simply observe that for $0 < \alpha < 1/2$,

$$T_{ij} = (1 - \alpha)I + \alpha Q_{ij} = (1 - 2\alpha)I + 2\alpha B_{ij}, \tag{5.2}$$

where $0 < 2\alpha < 1$. Thus any $0 < \alpha < 1/2$ transform (on a state in the $\alpha = 1/2$ state space) results in a state that is a convex combination of the initial state and the state resulting from the corresponding $\alpha = 1/2$ transform, i.e. an interior point of $ch(K)$. See Fig. 4 for a depiction of these possibilities. For any T_{ij} with $0 < \alpha < 1/2$, the new state is constrained to lie on the dashed line joining p and the corresponding pB_{ij}.

It follows that it is sufficient to consider only $\alpha = 1/2$ transforms to identify the extreme points of the $0 < \alpha \leq 1/2$ state space and accordingly solve the energy minimization problem.

5.5 Strategies for Finding the Optimum Sequence

Two strategies for determining the sequence of transforms B_{ij} required to attain the minimum-W_d state were conjectured [Fisch and Rax, 1993]. Reproduced here, these strategies are:

1. Diffusion of particles first between similar population levels, all other things being equal, eventually releases more energy.

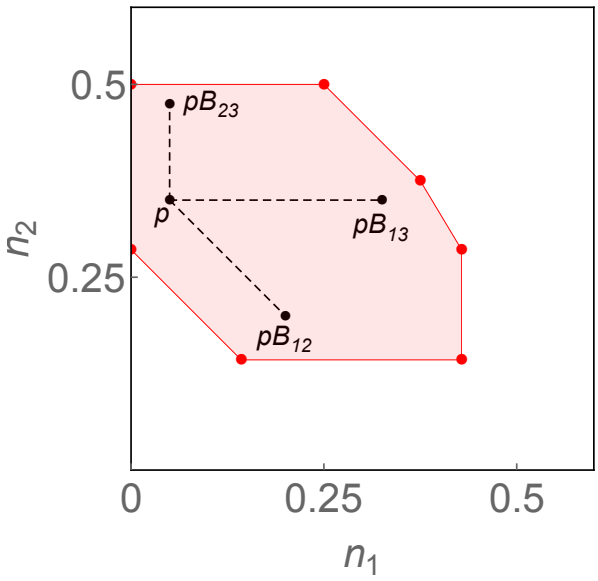

Figure 5.4: Result of partial relaxations (T_{ij} with $0 < \alpha < 1/2$) applied to a point p in the convex hull of K for $n_0 = (0, 2/7, 5/7)$, as before. Partial relaxations result in interior points constrained to lie along the dashed lines joining p to each pB_{ij}.

2. Depleting of particles the higher energy level first, all other things being equal, eventually releases more energy.

These strategies were only surmised based on trial-and-error experience. However, it turns out that they are intimately related to the more precisely put *Proposition 2*, proposed and proven by [Thon and Wallace, 2004]. It is worthwhile here to make use of the *permutation* of the set of initial populations, as introduced *ibid.* Given $n_0 = (n_1, n_2, n_3)$, the starting permutation is $\{1, 2, 3\}$ if $n_1 < n_2 < n_3$, as assumed throughout this work. Application of B_{ij} exchanges the level numberings, e.g. if n_0 has permutation $\{1, 2, 3\}$, $n_0 B_{12}$ has permutation $\{2, 1, 3\}$. For a more detailed exposition of these permutations and emergent combinatorial techniques, please refer to Appendix B.

Put briefly, *Prop. 2* states that extreme points can be obtained by equalizing only *adjacent* level pairs. That is, any sequence of B_{ij} resulting in an extreme point will effect only adjacent transpositions in the population permutation. More concretely, $n_0 B_{12}$ and $n_0 B_{23}$ are both extreme points, but $n_0 B_{13}$, which averages the nonadjacent first and third levels, is not. However, $n_0 B_{12} B_{13}$ is an extreme point because the later application of B_{13} equalizes two adjacent levels, viz. $n_0 \sim \{1,2,3\} \rightarrow n_0 B_{12} \sim \{2,1,3\} \rightarrow n_0 B_{12} B_{13} \sim \{2,3,1\}$.

Because the initial populations are assumed ordered increasing and the global minimum energy state will always be located at an extreme point, any correct first step must be consistent with Strategy 1: the B_{ij} chosen must mix two adjacent levels.

It is clear that there are 'dead ends' among the possible B_{ij} sequences, where a state is reached with level populations decreasing with level energy, such that no more energy can be extracted. Any such *stopping* state has the level population permutation which is the reverse of the energy level permutation. For example, given $\epsilon = (\epsilon_1, \epsilon_2, \epsilon_3)$ with $\epsilon_2 < \epsilon_1 < \epsilon_3 \sim \{2,1,3\}$, the *stopping permutation* is $\{3,1,2\}$, such that $n_3 \leq n_1 \leq n_2$. $n \sim \{3,1,2\}$ can be reached from $n_0 \sim \{1,2,3\}$ by the sequence $n_0 B_{23} B_{13}$.

The three-level system has two extreme points with permutation $\{3,2,1\}$, the stopping permutation if the level densities and energies are both ordered increasing. In one case, the two lower-energy levels are first diffused; in the other, the two higher-energy levels are first diffused. The state energies of the extreme points cannot be ordered using a reduced set of variables (i.e. only some of the initial populations or energy levels), so the correct first step can only be determined in retrospect after a full

calculation. The multiplicity of extreme points with a possible stopping permutation indicates that Strategy 2 is not generally applicable.

A further question of interest is the usefulness of an 'annealing' strategy whereby a diffusion operation heats the system, resulting in a state with extra energy. Subsequent B_{ij} would lower the system energy to its minimum value, presumably smaller than the minimum value possible without annealing. However, such a strategy cannot obtain a global minimum W_d. Note that any step which heats the system results in an inversion of the population permutation with respect to the correct stopping permutation. In order to obtain the stopping permutation, a subsequent diffusion operation is required on the two levels involved the heating step.

As an example, consider a case mentioned previously with level energy permutation $\epsilon \sim \{2,1,3\}$, initial population permutation $n_0 \sim \{1,2,3\}$, and stopping permutation $n \sim \{3,1,2\}$. Note that the initial permutation contains two inversions with respect to the stopping permutation. Applying B_{12} to the initial state results in the system absorbing energy,

$$\epsilon \cdot n_0 B_{12} - \epsilon \cdot n_0 = \frac{1}{2}(n_2 - n_1)(\epsilon_1 - \epsilon_2). \tag{5.3}$$

By construction, each difference on the right hand side of Eq. (5.3) is positive and the system absorbs energy. Now consider the number of inversions: $n_0 B_{12}$ results in the level population permutation $n \sim \{2,1,3\}$, containing a total of three inversions with respect to the stopping permutation $\{3,1,2\}$. The extra inversion changes the parity of the permutation and requires at least one additional diffusion operation to correct. In particular, the same diffusion operation B_{12} must be repeated at

some point in the relaxation process. Per *Prop. 3* of [Thon and Wallace, 2004], such a B_{ij} sequence does not generate an extreme point of $ch(K)$, even if both instances of the repeated B_{ij} correspond to adjacent transpositions. However, there exists at least one extreme point with the stopping permutation. Because K is star-shaped, any annealing strategy results in a non-optimal interior point (a convex combination of the uniform distribution e and an extreme point with the stopping permutation). Because the parity and number of inversions characterize any finite-length permutation, this conclusion holds in the general N-level case.

5.6 Complexity

Given length-N initial data, there are at most $\binom{N}{2}$ possible states after one transformation has been applied (fewer in case of degeneracy in the initial level populations). The second generation contributes up to $N(N-1)(N-2)(N+5)/8$ unique states [OEIS Foundation Inc., 2014c]. Although the number of possible unique states grows rapidly with the passing generations, these later states spiral quickly toward the uniform distribution $e = (1/N, 1/N, \ldots, 1/N)$. In fact, we can safely restrict our attention to the first $\binom{N}{2}$ generations, a nevertheless enormous set for large N.

[Thon and Wallace, 2004] presented an algorithm for generating the extreme points of $ch(K)$. In fact, the algorithm identifies the reduced (minimum length) sequences of adjacent transpositions (i.e. permutations exchanging only neighboring elements in the set) leading to each permutation in the N^{th} symmetric group $\mathcal{S}_N$. For example, if $N = 3$, the group $\mathcal{S}_3$ contains $N! = 6$ possible permutations. The

permutation $\{3,2,1\}$ can be reached from the initial $X = \{1,2,3\}$ by two distinct sequences of adjacent transpositions: $(1,2)(2,3)(1,2)$ and $(2,3)(1,2)(2,3)$. The other five possible permutations of X have unique reduced decompositions in adjacent transpositions; the total number of such decompositions for all of the permutations in $\mathcal{S}_3$ is therefore seven [OEIS Foundation Inc., 2014b]. As noted, each possible permutation in $\mathcal{S}_N$ is a stopping state for an appropriate permutation of ϵ.

Any sequence of diffusion operations with a repeated B_{ij} is not minimal and results in a permutation accessible with $\binom{N}{2}$ or fewer B_{ij}. This follows because the reverse permutation, the longest permutation when expressed in adjacent transpositions, requires precisely $\binom{N}{2}$ transpositions (corresponding to the number of inversions in the final permutation). For example, $nB_{23}B_{13}B_{12}B_{23}$ has the permutation $\{2,3,1\}$, which could also be reached with $nB_{12}B_{13}$.

In the $N = 3$ case, the minimization of W_d is straightforward. There are $\binom{3}{2} = 3$ unique B_{ij}: B_{12}, B_{13}, and B_{23}. Without loss of generality, the initial data n_0 is increasing, so the initial permutation is $\{1,2,3\}$. The set K is covered by $ch(K)$, which has seven extreme points: n_0, n_0B_{12}, n_0B_{23}, $n_0B_{12}B_{13}$, $n_0B_{23}B_{13}$, $n_0B_{12}B_{13}B_{23}$, and $n_0B_{23}B_{13}B_{12}$.

There are ϵ for which each of the seven extreme points can serve as the optimum system configuration. As noted, $\epsilon \sim \{1,2,3\}$ is a special case in which the decomposition has maximum length $\binom{3}{2} = 3$; there are two unique decompositions of the stopping permutation $\{3,2,1\}$ in adjacent transpositions. Equivalently, there are two extreme points with the stopping permutation: the minimum system energy is then $W_d = \min\{\epsilon \cdot n_0B_{23}B_{13}B_{12}, \epsilon \cdot n_0B_{12}B_{13}B_{23}\}$. This is the most general scenario

for the free energy optimization problem, in which multiple extreme points with the correct stopping permutation must be compared.

The problem has been reduced to evaluating the function $W_d = \epsilon \cdot n$ at a finite number of known extreme points. Unfortunately, the upper bound on the number of extreme points with stopping permutations is $\mathcal{O}(N^{N^2})$ [OEIS Foundation Inc., 2011, Stanley, 1984]. Because there is no *a priori* means of ordering these points in energy, the exponential depth of the state tree is intrinsic to the optimization problem [Yannakakis, 1991]. Thus calculating the system energy accessible with discrete diffusive exchanges is NP-hard.

5.7 Conclusions

The constrained evolution of physical systems obeying an H-theorem has important consequences for their thermodynamic state variables [Zylka, 1985, Gorban, 2013]. In particular, the free energy of an irreversible system is limited to those values associated with attainable states.

By utilizing the (mostly ignored) literature on pairwise relaxation transformations, it is a relatively simple matter to apply the techniques of convex optimization and combinatorics to answer the questions posed. In particular, we find that for the three-level case, only seven sequences need be considered. One further conclusion that can be drawn is that each of the sequences that must be considered will definitely be the solution at least for one energy vector. In general, a large but fi-

nite number of sequences must be checked to solve the energy extraction problem. Moreover, partial relaxation or annealing strategies are never useful.

The exposition here has also laid the foundation for analyzing the extremal properties of more complicated systems. One might make use of the results about K to extremize nonlinear objective functions, as would be necessary in e.g. systems with electrostatic self-energy. Alternately, formulating the optimization problem over a system of countable particles (as in integer programming) could shed light on the manipulation of degenerate matter. These systems and others like them could reveal the physical significance of the non-convexity of the state space.

Although we have shown that identifying the maximal energy extraction solution is impractical in most cases of interest, the results obtained along the way nonetheless provide useful constraints on diffusive schemes that should narrow the search for efficient strategies.

Chapter 6

On the extreme points of the diffusion polytope[1]

We consider a class of diffusion problems defined on simple graphs in which the populations at any two vertices may be averaged if they are connected by an edge. The diffusion polytope is the convex hull of the set of population vectors attainable using finite sequences of these operations. A number of physical problems have linear programming solutions taking the diffusion polytope as the feasible region, e.g. the free energy that can be removed from plasma using waves, so there is a need to describe and enumerate its extreme points. We review known results for the case of the complete graph K_n, and study a variety of problems for the path graph P_n and the cyclic graph C_n. We describe the different kinds of extreme points that arise, and identify the diffusion polytope in a number of simple cases. In the case of increasing

[1]This chapter is based on "Available free energy under local phase space diffusion," [Hay et al., 2016].

initial populations on P_n the diffusion polytope is topologically an n-dimensional hypercube.

6.1 Introduction

Consider a discrete-time conservative diffusion process on a graph. By this we mean a connected, simple graph G with vertices $\{V_i\}_{i=1}^n$, a set of initial "populations" $\{\rho_i\}_{i=1}^n$ at the vertices, and a set of rules that can be applied at each time step, with the understanding that the rules in some sense equalize the populations, while conserving the total $\sum_i \rho_i$. So, for example, in classical diffusion [Chung, 2009, Kondor and Lafferty, 2002], at each time step the populations at all the vertices are updated simultaneously via the rule

$$\rho_i \to \rho_i + h \sum_{\text{neighbors } j \text{ of } i} (\rho_j - \rho_i) \ , \qquad i = 1, \ldots, n \ ,$$

where h is a positive constant. Other relevant contexts are chip-firing [Björner et al., 1991] and sandpile models [Dhar, 1990, 1999]. In this chapter we will examine a diffusion process in which at each time step, the populations at any two vertices connected by an edge can be averaged. In some generality, for many reasonable sets of rules, there will a bounded set of attainable population vectors in $\mathbf{R}^n$. In various applications we may be interested in extremizing some linear function of the populations $\sum_i w_i \rho_i$, and to do this (using a linear programming approach) we need to identify the closure of the convex hull of the set of attainable population vectors. We call this the *diffusion polytope* of the diffusion process (associated with the graph

G, the relevant sent of rules and the initial set of populations). In some sense the diffusion polytope measures the diversity of behavior that can be attained in the diffusion process.

Our motivation comes from plasma physics. There is a class of diffusion problems associated with opportunities in extracting energy in plasma with waves. Waves can be injected into a fusion reactor such that high energy alpha particles, the byproducts of the fusion reaction, lose energy to the waves, as those alpha particles are diffused by the waves to lower energy [Fisch and Rax, 1992b,a, Fisch and Herrmann, 1999]. The extra energy in the waves can then be used, for example, to increase the reactivity of the fuel or to drive electric current [Fisch and Herrmann, 1994, Hay and Fisch, 2015, Fisch, 1987]. Choosing the correct sequence of waves to extract as much energy as possible is an optimization problem on a graph of the type described above. Because the wave-particle interaction is diffusive, particles in a given location in the 6D phase space of velocity and position are randomly mixed by the wave with particles in another location in the 6D phase space [Vedenov et al., 1962]. A graph encodes the connectedness of the phase space; each node denotes a volume element in phase space, and an edge between two nodes indicates that those two volume elements may be mixed. Wave-induced diffusion follows a path in the 6D phase space corresponding to an edge in the associated graph. If there is a population inversion in energy along the path, then the diffusive process releases energy. If there is only one wave and a specified diffusion path, the amount of extractable energy can be readily calculated. However, more energy can be extracted when several waves are employed [Fisch and Herrmann, 1995, Herrmann and Fisch, 1997]. When many

diffusion paths are possible, it turns out that the order in which these paths are taken affects the energy that can be extracted. We reach the situation described above, of a range of possible population distributions on the nodes. Determining the maximum amount of extractable energy under the constraint that the particle distribution function evolves only due to diffusion reduces to a linear programming problem on the diffusion polytope, the convex hull of all attainable population vectors, and we are concerned with identifying its extreme points and the edge sequences that give rise to these extreme points.

Arguably the simplest case of this diffusion problem is to allow, at every step, averaging of the populations at any two nodes. This is the full-connectivity, or the *nonlocal diffusion* problem, in which diffusion paths can be constructed between any two phase space locations, and the relevant graph is the complete graph K_n (see Figure 6.1). In the context of plasma, there are physical reasons why this arrangement is realizable on a macroscopic scale, despite the restriction of diffusion to contiguous regions of phase space on the microscopic scale [Fisch and Rax, 1993]. In this case the diffusion polytope, and the maximum energy extractable, or what we call the *free energy*, have been described previously [Hay et al., 2015]. The same optimization problem has been discussed in other fields, in the context of attainable states in chemical reactions and thermal processes [Horn, 1964, Zylka, 1985], and in the context of altruism and wealth distribution [Thon and Wallace, 2004].

However in all these settings, there are arguments to restrict the connectivity. In the context of plasma, possible reasons for restriction include that waves can only diffuse particles from one phase space position to a contiguous position, or between

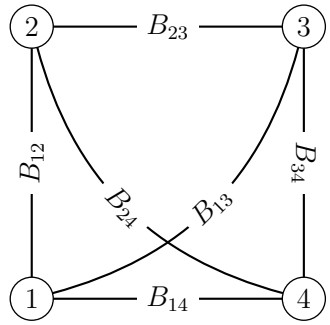

(a) Nonlocal diffusion: K_4

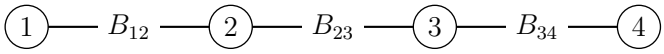

(b) Local diffusion: P_4

Figure 6.1: Graph representations of diffusion problems in two four-level systems, K_4 and P_4. The marking B_{ij} on an edge indicates that the populations of nodes i and j can be equalized.

pairs of states determined by selection rules. In the case of such a *local diffusion* problem, the free energy will be less, because there are fewer ways in which the energy might be released. As the simplest example of such a local diffusion problem we study diffusion when the connectivity is restricted from that of K_n to that of the path graph P_n (see Figure 6.1). In the context of alruism, the effects of other (retrospective) restrictions on the connectivity have also been studied [Aboudi and Thon, 2008].

The path graph context P_n arises naturally when the 6D phase space is projected to a 1D energy representation, and only transitions between adjacent energies are allowed. Many physical problems of interest are captured by the model of contiguity based on energy only. Other network problems can be defined which capture the spatial element [Zhmoginov and Fisch, 2008]. A different problem on P_5 arises in the context of maximizing the possible concentration of atoms in a specific state

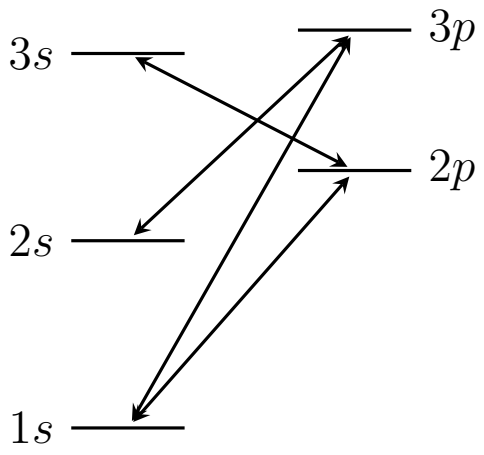

Figure 6.2: Truncated parahelium energy level diagram with all possible electric dipole transitions represented by arrows, $\leftrightarrow$. Energy scale is arbitrary. The s-p splitting is due chiefly to the partially screened Coulomb repulsion of the nucleus (a larger effect in p orbitals vs. s orbitals) [Schwabl, 2007].

in an ensemble of atoms of helium. Fig. 6.2 shows a truncated level diagram for parahelium ($S = 0$). Due to level splitting, each energy level is associated with a unique energy. We suppose processes are available which can mix levels joined by a dipole transition (such as spatially incoherent light at the appropriate frequency). For example, it is possible to average the number of atoms in $2s$ and $3p$, but it is not possible to do the same for $2s$ and $3s$. Thus four operators are allowed in this five-level system, $1s \leftrightarrow 2p$, $1s \leftrightarrow 3p$, $2s \leftrightarrow 3p$, $3s \leftrightarrow 2p$. We gain a clearer picture by redrawing the energy level diagram of Fig. 6.2 with vertices relabelled $1 = 1s, 2 = 2s, 3 = 2p, 4 = 3s, 5 = 3p$ (so the vertex label indicates the energy rank) to obtain Fig. 6.3. Thus we see this also gives a diffusion problem on P_n; however the allowed transitions are *not* between adjacent energies.

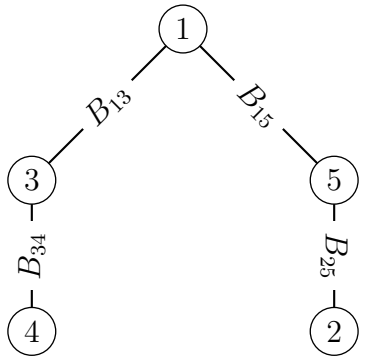

Figure 6.3: Graph representation for the diffusion problem on parahelium, cf. Fig. 6.2. Vertices are labeled by the rank of the corresponding energy eigenvalue (increasing). The graph is P_5, but the transitions are not between adjacent energy levels.

This chapter proceeds as follows: In Section 6.2 we give the precise statement of the diffusion model we study, the definition of the diffusion polytope, and state some elementary facts. In Section 6.3 we review known results for the case of the complete graph K_n, [Hay et al., 2015, Horn, 1964, Zylka, 1985, Thon and Wallace, 2004]. We show that for a general graph, whenever 3 vertices are connected to each other (i.e. form a triangle), extreme points of the diffusion polytope are obtained only by averaging over the pairs with consecutive populations. This generalizes a theorem of Thon and Wallace for case of the complete graph, and is a key result in characterizing the diffusion polytope. In Sec. 6.4, we study the diffusion polytope for the path graph P_n. There are different cases depending on the ordering of the initial populations. In the case $n = 3$ we describe the solution in all cases, emphasizing the location of the resulting polytopes inside the K_3 polytope, and the different kind of extreme points that arise. In the case of P_n with ordered initial populations we show the diffusion polytope is topologically an $(n-1)$-dimensional hypercube

with 2^{n-1} vertices. Whereas the extreme points of the K_n nonlocal problem can all be constructed by $\binom{n}{2}$ or fewer level mixings, some extreme points in the P_n local problem are only reachable by an infinite sequence of operations. Curiously, the number extreme points in the P_n local problem that are inherited from the nonlocal problem is a Fibonacci number, and the number of operations required to reach them is at most $\lfloor n/2 \rfloor$. Sec. 6.5 extends the analysis to diffusion on the cycle graph C_n, again focusing on the new types of extreme points that become available. We summarize in Sec. 6.6, and present open questions concerning more physically relevant graphs, and connections between ideas presented in this work and other notions in modern network theory.

6.2 Diffusion model

The diffusion model studied in this chapter is as follows: We are given a connected, simple graph G with vertices $\{V_i\}_{i=1}^n$, and a set of initial populations $\{\rho_i\}_{i=1}^n$ at the vertices. We assume without loss of generality that the population vector $\rho = (\rho_1, \rho_2, \ldots, \rho_n)$ is normalized: $\sum_i \rho_i = 1$.

To any edge in G we associate an operator. If the edge connects vertices V_i and V_j we indicate this operator B_{ij}, and this acts on the populations at the vertices i and j via

$$B_{ij} : (\rho_i, \rho_j) \to \left(\frac{1}{2}(\rho_i + \rho_j), \frac{1}{2}(\rho_i + \rho_j) \right)$$

while leaving the populations at all the other vertices unchanged.

We can write $B_{ij} = \frac{1}{2}(I + Q_{ij})$ where Q_{ij} is the operator that permutes the populations at the i'th and j'the vertices. In greater generality we could consider the action of operators $B_{ij;\alpha} = (1-\alpha)I + \alpha Q_{ij}$ for all $\alpha \in [0, \frac{1}{2}]$. This is the case in which "partial relaxation" is allowed as well as full relaxation. However, since we will only consider the convex hull of the population vectors generated by the B_{ij}, it is clear that this does not make any difference. However, it is important to distinguish between the cases of $0 \leq \alpha \leq 1/2$ and $1/2 < \alpha \leq 1$; the latter case corresponds to inversion of populations, and are not allowed.

We assume we are given an objective function $f = \sum_i w_i \rho_i$ which is to be extremized over the set $A(\rho_0)$ of attainable states, i.e. populations generated by finite sequences of the operators B_{ij} from the initial population vector ρ_0. The weights w_i are taken to be all positive and distinct. Without loss of generality we can assume either $w_1 < w_2 < \cdots < w_n$ or that the components of ρ_0 satisfy $\rho_1 \leq \rho_2 \leq \cdots \leq \rho_n$. Due to the linearity of f, this problem has a linear programming solution on $DP = \overline{ch\,(A(\rho_0))}$, the closure of the complex hull of $K(\rho_0)$. We call this the *diffusion polytope* of the problem; it is determined by the graph G and the initial population vector ρ_0.

Since we have assumed G is connected, the uniform population $\rho = \left(\frac{1}{n}, \frac{1}{n}, \ldots, \frac{1}{n}\right)$ is in DP. (To prove this, observe that the quantity $\max_{i,j}(\rho_i - \rho_j)$ is a strictly decreasing function under the application of the averaging operations, and it cannot have a non-zero minimum.)

Another immediate property of DP is that if the graph G' can be obtained from G by deletion of one or more edges (while still staying connected) then $DP(G') \subseteq$

$DP(G)$. Here the assumption is that we start with the same population vector on both G and G'. However, since G' has less edges, the set of attainable states is smaller compared to that for G (and in the plasma setting the free energy is reduced). Thus the diffusion polytope of *every* graph with n vertices is a subset of the diffusion polytope for K_n. Reducing the connectivity will restrict the diffusion polytope. This gives, for example, a way to identify "important" edges in a graph, as edges whose elimination causes a significant restriction diffusion polytope, or to define robustness of a network in terms of how the diffusion polytope responds to removal of edged, c.f. [Cohen et al., 2000, Tanizawa et al., 2005].

6.3 Diffusion on K_n: Nonlocal Diffusion

For the case of K_n, the case of nonlocal diffusion,[Thon and Wallace, 2004] presented a recursive algorithm to identify the extreme points of the diffusion polytope by applying different sequences of the B_{ij}. It was noted in [Hay et al., 2015] that this algorithm generates reduced (minimal length) decompositions of the elements in the symmetric group S_n [OEIS Foundation Inc., 2014b]. That is, the algorithm identifies every possible minimum-length way to generate each of the $n!$ permutations of a length-n word using only adjacent transpositions $\sigma_i = (i\ i+1)$. It turns out that the nonlocal extreme points are in bijection with equivalence classes of reduced decomposition, the equivalence classes being the sets of reduced decompositions obtainable from each other by the applying the commutation relation $\sigma_i\sigma_j = \sigma_j\sigma_i$, $|i-j| > 1$ [Berkolaiko and Irving, 2016].

It was noted that 'dead ends' exist among the possible sequences of diffusion operations, where a state is reached with level densities decreasing with level energy, such that no more energy can be extracted. Any such *stopping* state has the level population permutation which is the reverse of the energy level permutation. For example, given $w = (w_1, w_2, w_3)$ with $w_2 < w_1 < w_3 \sim \{2, 1, 3\}$, the *stopping permutation* is $\{3, 1, 2\}$, such that $\rho_3 \leq \rho_1 \leq \rho_2$.

In order to identify the extremal sequence of diffusion operations resulting in a minimum-energy state, it is generally necessary to evaluate the objective function for each inequivalent reduced decomposition of the stopping permutation. For the worst-case reverse permutation, there are a large number of states to check [OEIS Foundation Inc., 2014a]. We emphasize that each extreme point in the nonlocal problem is associated with a finite sequence of diffusion operations, with the limiting words being the identity (length 0) and the reverse permutation (length $\binom{n}{2}$).

Finally, all extremal sequences result in a monotone trend in the objective function: in our plasma example, we can exclude from consideration any operations which absorb energy from the injected waves.

A significant tool for these results was Prop.2 in [Thon and Wallace, 2004] and this has an extension to the diffusion problem on an arbitrary graph. Suppose the 3 vertices V_i, V_j, V_k form a triangle, i.e. that there are edges between the 3 possible pairs of these three vertices. Assume without loss of generality that $\rho_i < \rho_j < \rho_k$. Then *no extreme point can be obtained by immediate application of* B_{ik}. In other words, in any triangle, extreme points can only generated by averaging pairs with

adjacent populations. This fact follows from two following simple identities:

$$\begin{pmatrix} \frac{1}{2} & 0 & \frac{1}{2} \\ 0 & 1 & 0 \\ \frac{1}{2} & 0 & \frac{1}{2} \end{pmatrix} \begin{pmatrix} a \\ b \\ c \end{pmatrix}$$

$$= \lambda_1 \begin{pmatrix} \frac{1}{3} \\ \frac{1}{3} \\ \frac{1}{3} \end{pmatrix} + (1-\lambda_1) \begin{pmatrix} \frac{1}{2} & 0 & \frac{1}{2} \\ 0 & 1 & 0 \\ \frac{1}{2} & 0 & \frac{1}{2} \end{pmatrix} \begin{pmatrix} 1 & 0 & 0 \\ 0 & \frac{1}{2} & \frac{1}{2} \\ 0 & \frac{1}{2} & \frac{1}{2} \end{pmatrix} \begin{pmatrix} a \\ b \\ c \end{pmatrix}$$

$$= \lambda_2 \begin{pmatrix} \frac{1}{3} \\ \frac{1}{3} \\ \frac{1}{3} \end{pmatrix} + (1-\lambda_2) \begin{pmatrix} \frac{1}{2} & 0 & \frac{1}{2} \\ 0 & 1 & 0 \\ \frac{1}{2} & 0 & \frac{1}{2} \end{pmatrix} \begin{pmatrix} \frac{1}{2} & \frac{1}{2} & 0 \\ \frac{1}{2} & \frac{1}{2} & 0 \\ 0 & 0 & 1 \end{pmatrix} \begin{pmatrix} a \\ b \\ c \end{pmatrix}$$

Here it is assumed that $a < b < c$ and $a + b + c = 1$, and

$$\lambda_1 = \frac{3(c-b)}{b+c-2a} \quad \text{and} \quad \lambda_2 = \frac{3(b-a)}{2c-a-b} \ ,$$

so

$$1-\lambda_1 = \frac{2(2b-a-c)}{b+c-2a} \quad \text{and} \quad 1-\lambda_2 = \frac{2(a+c-2b)}{2c-b-a} \ .$$

If $a + c \leq 2b$ then $0 \leq \lambda_1 \leq 1$, and the first identity says that the population obtained by application of B_{ik} is a convex combination of the population obtained by averaging all three populations at V_i, V_j, V_k, with the population obtained by application of first B_{jk} and then B_{ik}. The latter two populations may or may not be extreme points of DP; but they are both in DP, and thus the population obtained by immediate application of B_{ik} is certainly *not* an extreme point. If $a + c > 2b$

then $0 \leq \lambda_2 \leq 1$ and the second identity is relevant, and the population obtained by immediate application of B_{ik} is a convex combination of the population obtained by full averaging, with that obtained by first applying B_{ij} and then B_{ik}.

In contrast, the other crucial result for understanding the case of K_n, viz. Prop.3 in [Thon and Wallace, 2004], seems to be specific to K_n.

6.4 Diffusion on P_n: Local Diffusion

Throughout our discussion of the P_n case we assume without loss of generality that $\rho_1 \leq \rho_2 \leq \cdots \leq \rho_n$.

For $n = 3$ there are three distinct cases to consider, when the allowed operators are (a) B_{12}, B_{23}, (b) B_{12}, B_{13}, (c) B_{13}, B_{23}. Figure 6.4 compares the diffusion polytopes in the three different cases with that of K_3, in the case $\rho_0 = (0, 2/7, 5/7)$.

The extreme points in the case K_3 are $\rho_0,\ \rho_0 B_{12},\ \rho_0 B_{23},\ \rho_0 B_{12} B_{13},\ \rho_0 B_{23} B_{13},\ \rho_0 B_{12} B_{13} B_{23}$, $\rho_0 B_{23} B_{13} B_{12}$. Writing $\bar{\rho} = \left(\frac{1}{3}, \frac{1}{3}, \frac{1}{3}\right)$, the extreme points in the three P_3 cases are

- $\rho_0, \rho_0 B_{12}, \rho_0 B_{23}, \bar{\rho}$.
- $\rho_0, \rho_0 B_{12}, \rho_0 B_{12} B_{13}, \bar{\rho}$.
- $\rho_0, \rho_0 B_{13}, \rho_0 B_{23}, \rho_0 B_{13} B_{23}, \rho_0 B_{23} B_{13}$.

Note first that any K_3 extreme point that can be attained in any of the P_3 cases is an extreme point in that case. We call such points "nonlocal extreme points" (of the local problem), as they are inherited form the nonlocal problem. However, there are also new extreme points. In the first two cases the point $\bar{\rho}$ is added. This is a limit

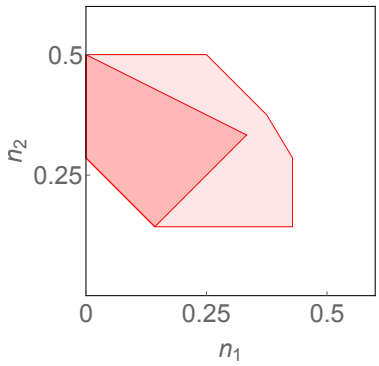

(a) B_{12}, B_{23} allowed (P_3)

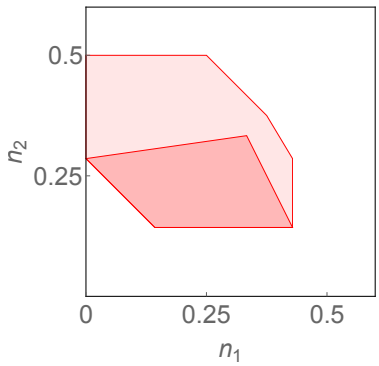

(b) B_{12}, B_{13} allowed

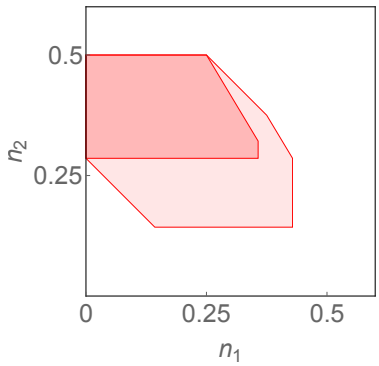

(c) B_{13}, B_{23} allowed

Figure 6.4: Comparison of polytopes for K_3, P_3, and two other restricted graphs for initial data $\rho_0 = (0, 2/7, 5/7)$, with permitted operators (a) B_{12}, B_{23}, (b) B_{12}, B_{13}, (c) B_{13}, B_{23}. All are superimposed on the polytope for K_3. (Due to normalization, the third coordinate is ignorable.)

point of the attainable populations — it cannot be attained by application of a finite sequence of the B_{ij} operators; we call such points "asymptotic extreme points". In the third case there are new extreme points that *can* be attained by application of a finite sequence of the B_{ij}, however these are not extreme points for the nonlocal K_3 case. In more general local diffusion problems all three kinds of extreme points coexist — nonlocal extreme points inherited from K_n, asymptotic extreme points (which do not appear in the case K_n) and other extreme points generated by finite sequences of operations that are *not* inherited from K_n.

In the case P_n in which the allowed operators are $B_{12}, B_{23}, \ldots, B_{n-1,n}$ the diffusion polytope can be identified explicitly. In Appendix C, we prove that there are 2^{n-1} extreme points in bijection with the power set of $\{1, 2, \ldots, n-1\}$. It follows that the diffusion polytope is topologically an $(n-1)$-dimensional hypercube Weisstein [n.d.b]. Any extreme point corresponding to a subset $A \subseteq \{1, 2, \ldots, n-1\}$ is connected (by edges, forming the 1-skeleton of the hypercube) to $n-1$ other extreme points corresponding to the $n-1$ subsets that differ from A in just one element. Fig. 6.5 illustrates the 3-cube hull for the four-level problem.

We ask the question how many nonlocal extreme points are there in this case? (i.e. how many points are inherited from the case of the complete graph K_n.) In the case $n = 3$ there are 3: ρ_0, $\rho_0 B_{12}$, and $\rho_0 B_{23}$ are all extreme points. In the case $n = 4$ there are 5: ρ_0, $\rho_0 B_{12}$, $\rho_0 B_{23}$, $\rho_0 B_{34}$ and $\rho_0 B_{12} B_{34}$. In general, the question is how many subsets of *commuting* operators are there in $\{B_{12}, B_{23}, \ldots, B_{n-1,n}\}$? For $n = 4$ and $n = 5$ only commuting 2-tuples are possible. For $n = 6$, a commuting 3-

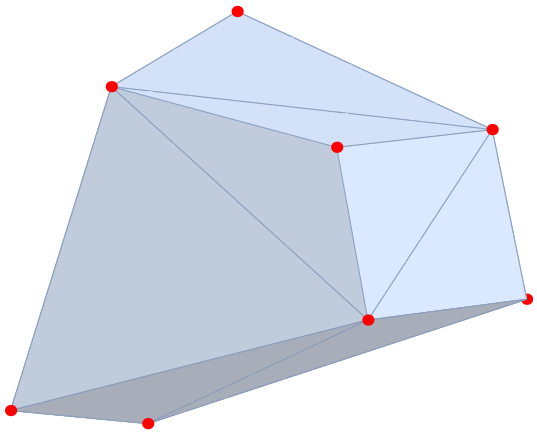

Figure 6.5: Convex hull of a four-level local diffusion problem represented in $\mathbb{R}^3$. Extreme points are denoted with red circles.

tuple appears: (B_{12}, B_{34}, B_{56}). In general, the n-level system contains only k-tuples satisfying $k \leq \lfloor n/2 \rfloor$.

Clearly, as n grows, the number of commuting k-tuples with $k \leq \lfloor n/2 \rfloor$ becomes large and direct counting becomes tedious, if not difficult. Fortunately, a general formula is available. Appropriating the notation of [Erdös and Straus, 1976], denote the number of commuting k-tuples as $A_k(n)$. Recalling that there are $n-1$ operators $B_{i,i+1}$ in the n-level problem, the number of extreme points for $n > 2$ levels is

$$1 + (n-1) + A_2(n) + A_3(n) + \cdots + A_{\lfloor n/2 \rfloor}(n), \tag{6.1}$$

where the leading 1 corresponds to the initial distribution ρ_0.

We can now attack the $A_k(n)$ in turn. Mapping each $B_{i,i+1}$ to the symbol i, $A_2(n)$ is the number of two-element subsets of $\{1, 2, \ldots, n-1\}$ which do not contain consecutive numbers. The total number of two-element subsets is $\binom{n-1}{2}$ and the number of subsets containing consecutive numbers is $n-2$. Therefore

$$A_2(n) = \binom{n-1}{2} - (n-2) = \frac{1}{2}(n-1)(n-2) = T_{n-3} \tag{6.2}$$

where T_n is the n^{th} triangular number (recall that the expression is restricted to $n > 2$). Proceeding analogously, $A_3(n)$ is seen to correspond to the tetrahedral numbers. In general, $A_k(n)$ can be identified with the set of regular k-polytopic numbers [Deza and Deza, 2012]. With the proper offsets, the formula for the number of extreme points for $n > 2$ is

$$n + \binom{n-2}{2} + \binom{n-3}{3} + \cdots = F_{n+1}, \tag{6.3}$$

where F_n is the n^{th} term of the Fibonacci sequence: 0, 1, 1, 2, 3 . . . with $F_0 = 0$. The identity is the statement that shallow diagonals of Pascal's triangle sum to Fibonacci numbers [Stover and Weisstein, n.d.].

$$\sum_{k=0}^{\lfloor n/2 \rfloor} \binom{n-k}{k} = F_{n+1}. \tag{6.4}$$

(Note that $\binom{n}{0} + \binom{n-1}{1} = n$.)

This result might have been anticipated because there are F_{n+2} unique subsets of $\{1, \ldots, n\}$ which do not contain consecutive numbers [Comtet, 1974]. For ex-

ample, there are three ($= F_4$) such subsets of {1, 2}: {$\varnothing$, {1}, {2}}. The problem of enumerating the extreme points is analogous: the n-level system contains $n-1$ operators, leading to F_{n+1} Fibonacci subsets.

The Fibonacci numbers are the solution to a similar problem in graph theory: F_{n+1} is the number of matchings in a path graph with n vertices [Prodinger and Tichy, 1982].

Thus the number of nonlocal extreme points in the case of P_n with operators $\{B_{12}, B_{23}, \ldots, B_{n-1,n}\}$ is F_{n+1}. Note these involve at most $\lfloor n/2 \rfloor$ operators (as opposed to up to $\binom{n}{2}$ in the case of K_n). All the other extreme points are asymptotic extreme points, involving averagings over 3 or more states.

6.5 Diffusion on the Cycle Graph C_n: Nonlocal Diffusion

Another possible restriction on the phase space connectivity results in a diffusion problem on the cycle graph C_n, Fig. 6.6 with allowed operators $\{B_{12}, B_{23}, \ldots, B_{n-1,n}\}$ as in the case of P_n studied before, and the single extra operator $B_{1,n}$ C_3 is isomorphic to K_3 and accordingly has the same diffusion polytopes; C_4 is the smallest case with a unique diffusion polytope.

Introducing the notation B_{ijk} for the operation of averaging over populations on the three vertices i, j, k (involving an infinite sequence of operations), Table 6.1 lists the 18 extreme points we have found for the C_4 diffusion polytope by brute force computation. We divide the points into 3 categories: those inherited from K_n, those

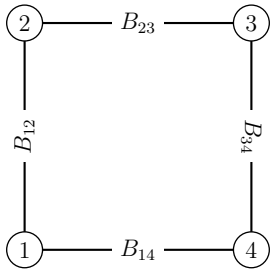

Figure 6.6: The cycle graph C_4

from K_4	shared P_4	C_4 only
ρ_0	$\rho_0 B_{123}$	$\rho_0 B_{123} B_{14}$
$\rho_0 B_{12}$	$\rho_0 B_{234}$	$\rho_0 B_{234} B_{14}$
$\rho_0 B_{23}$		$\rho_0 B_{123} B_{124}$
$\rho_0 B_{34}$		$\rho_0 B_{234} B_{134}$
$\rho_0 B_{12} B_{34}$		$\rho_0 B_{12} B_{34} B_{134}$
$\rho_0 B_{12} B_{34} B_{14}$		$\rho_0 B_{12} B_{34} B_{124}$
		$\rho_0 B_{234} B_{14} B_{12}$
		$\rho_0 B_{123} B_{14} B_{234}$
		$\rho_0 B_{234} B_{14} B_{123}$
		$\rho_0 B_{123} B_{23} B_{14} B_{34}$

Table 6.1: Extreme points for the diffusion problem on C_4.

shared with P_4 (by this we mean that these are extreme points for P_4 inherited from the C_4 case), and all others. In the case of C_4, as in the case of P_n that we solved explicitly, there are only nonlocal extreme points and asymptotic extreme points. We emphasize that in general there are also points involving a finite sequence of B_{ij} that are *not* inherited from K_n.

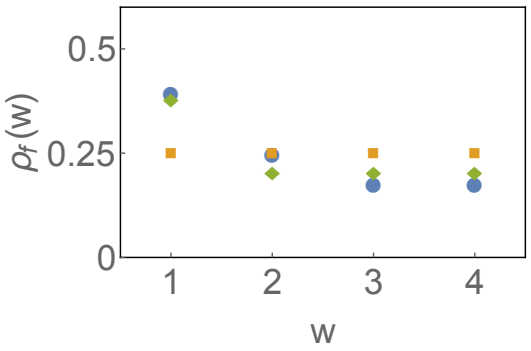

Figure 6.7: Comparison of minimal energy states for the diffusion problem with initial data $\rho_0 \propto (e^1, e^2, e^3, e^4)$ and $w = (1, 2, 3, 4)$. The blue circles label the level densities for the nonlocal problem (K_4), the green diamonds for the case C_4 and the yellow squares for the case P_4. Whereas in the nonlocal case the operations recovered 68% of the Gardner limit [Hay et al., 2015], the C_4 case recovered 63%, and in the P_4 case only 50% was recovered.

6.6 Discussion

In this work we have developed a non-standard diffusion model on a graph, explained the reason for looking at the associated diffusion polytope, and studied this in the cases where the graph is K_n, P_n and C_n. The case of P_n for which we have given a complete solution and the case of K_n should be regarded as extreme cases. Assuming increasing energy levels and initial densities, the nonlocal problem requires evaluation of the objective functional at a super-exponential number of points in the number of levels n, while for the local problem the solution is always the uniform distribution. We show in Fig. 6.7 the optimal population distribution with $w = (1, 2, 3, 4)$, $\rho_0 \propto (e^1, e^2, e^3, e^4)$ in the cases of K_4, P_4 (with operators B_{12}, B_{23}, B_{34}) and C_4 (with added operator B_{14}).

Although the diffusion problem on the complete graph is well-characterized, it is difficult to solve. The P_n model is an oversimplification, but it is possible that not much more complicated models may be useful. Some insight may be gained into the 'full' alpha particle diffusion problem by considering proximity in both position and energy space. As before, edges correspond to diffusion paths and vertices reference bins associated with the discretization of configuration and energy space. A particularly simple 2-D diffusion problem in x and ϵ can be visualized as in Fig. 6.8, on the composition of path graphs $P_m[P_n]$, $m \geq n$, essentially a grid graph with diagonal edges [Weisstein, n.d.a]. By judicious choice of the wave phase velocities, diffusion paths can be established between different parts of the phase space. Moving a particle in energy at constant location could be accomplished with a wave $k \to 0$, and vice versa, moving a particle without changing its energy with a wave $\omega \to 0$. The slopes of any diagonal diffusion paths are determined by intermediate ω/k [Herrmann and Fisch, 1997, Fisch and Herrmann, 1995]. Such an arrangement is characterized by degeneracy in both position and energy bins. A practical alpha channeling scheme would seek to maximize the density at a particular low-energy, large-radius sink node.

In general, one might consider diffusion problems on arbitrary subgraphs of the complete graph for $V = \{w\}$, of which the local problem is one solvable case (the path graph with $V = \{w\}$). These other problems will inherit some extreme points from the complete graph on the same number of vertices and should also have some unique ones depending on the particular graph structure. There may be rich physical significance for diffusion problems on more or less 'bottlenecked' graphs generally

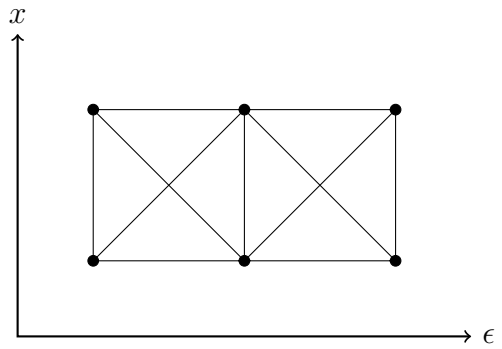

Figure 6.8: Diffusion problem on $G = P_3[P_2]$.

(in the sense of Cheeger), or e.g. the wheel graphs, k-regular trees, and complete bipartite graphs.

Our problem may be contrasted with other notions of (deterministic or stochastic) diffusion or spreading on graphs, for example in the context of spreading of epidemics [Keeling and Eames, 2005, Pastor-Satorras and Vespignani, 2001, Lloyd and May, 2001], or behavior [Christakis and Fowler, 2013]. In all such settings, the resulting behavior depends intimately on the character of the underlying graph. For example, disease transmission proceeds more slowly on a lattice than on small-world [Watts and Strogatz, 1998, Watts, 1999] or scale-free [Barabási and Albert, 1999, Pastor-Satorras and Vespignani, 2001] networks. Qualitative differences can also be observed in the context of classical graph diffusion [Monasson, 1999]. We expect to see similar differences in the context of our problem, though the computational task of verifying this is formidable.

Chapter 7

Alternate approaches to the diffusion problem

7.1 Word problem for the braid group $\mathcal{B}_n$

There is a surjection from the reduced words for a particular element of S_n to the extreme points with that permutation. That is, there are generally several sequences of B_{ij} leading to an extreme point of $ch(K)$. This fact suggests an interesting analogy to the braid group on n strands, $\mathcal{B}_n$, because in a very rough sense there are multiple 'braids' equivalent to the same 'permutation.'

The braid group generators are denoted σ_i, corresponding to crossing the neighboring strands i and $i+1$. The σ_i obey a couple of important relations [Artin,

1925]:

$$\sigma_i \sigma_j = \sigma_j \sigma_i \qquad |i-j| > 1 \tag{7.1}$$

$$\sigma_i \sigma_j \sigma_i = \sigma_j \sigma_i \sigma_j \qquad |i-j| = 1 \tag{7.2}$$

In words, the first identity states that crossing one set of strands and then a separate pair of strands can be accomplished in any order without affecting the braid. The second identity crops up in a number of contexts (Yang-Baxter equation in quantum and classical mechanics, knot theory) and goes by many names: long braid rule, third Reidemeister move, etc. It amounts to moving one strand from one side of two other strands' crossing to the other.

Note that these two relations, together with

$$\sigma_i^2 = e \tag{7.3}$$

form the rules under which the symmetric group S_n is generated by the adjacent transpositions.

There is a group homomorphism $f : \mathcal{B}_n \to S_n$ that amounts to ignoring the strand crossings and twists, regarding a braid as a permutation of the strands. The kernel of f consists of those braids containing only twists σ_i^2 and crossings that reduce to twists e.g. $(\sigma_i \sigma_j)^3 = \sigma_i^2 \sigma_j \sigma_i^2 \sigma_j = \sigma_j^2 = e$, where $|i-j| = 1$. In both cases, the symmetric group's generator relations reduce the braid word to the identity e.

This amounts to little more than neglecting the strands' torsion and crossings, such that a braid generated by the σ_i expresses merely a permutation on n let-

ters. In this light, the braid group's generators can be thought of as the symmetric group's generators: the 2-cycles $\sigma_i \doteq (i, i+1)$, $i \in \{1, 2 \ldots, n-1\}$. Recalling that an operation $B_{v(i),v(j)}$ corresponds to the 2-cycle (i, j), those representing adjacent transpositions (i.e. $B_{v(i),v(i+1)}$) correspond to the σ_i.

Taken together, the identities (7.2) and (7.3) suggest a tantalizing closeness between the diffusion problem and the *word problem* for the braid group (determining whether two words belong to the same commutation class using the above identities). The first identity conjures a distinction between the diffusion problem on K and the structure of B. The B_{ij} are *idempotent* ($B_{ij}^2 = B_{ij}$) on the density vector ρ, whereas 2-cycles are their own inverses, and so an even number of applications leaves the permutation unchanged. The first identity Eq. (7.2) holds for both systems, reflecting the fact that B_{ij} and σ_i commute if they do not operate on a shared state or letter, respectively. Of interest here is the second identity Eq. (7.3). For an extreme point of a given permutation, with a possible long braid move in the sequence of A, making that move will produce a new extreme point in ρ space with the *same* permutation.

7.2 Sorting networks

7.2.1 Bijection with the reduced words for $\pi \in S_n$

The number of inequivalent factorizations of the permutation $(n, n-1, \ldots, 2, 1)$ is equal to the number of primitive sorting networks on N elements [OEIS Foundation Inc., 2014a].

A sorting network is a fixed, 'oblivious' algorithm for sorting a word of known length, making comparisons and, possibly, swaps in a predetermined order [Knuth, 1992, 1997]. A sorting network consists of wires and comparators: each letter is assigned to a wire which may be crossed with another wire at a comparator if the two wires are 'out of order.' Formally, a comparator is a device which has two inputs x and y and two outputs: $x' = \min(x, y)$ and $y' = \max(x, y)$. (Without loss of generality—could have exchanged min and max) [Codish et al., 2014].

Another interesting problem is determining the optimal networks for words of a given length, i.e. the sorting network with minimal depth: the largest number of comparators any wire may pass through in the network. As of 2014, the depth-optimal networks are known for $N < 17$ [Bundala and Závodnỳ, 2014]. Because there are $N!$ permutations of N letters, testing a proposed sorting network against all inputs is a difficult problem. Although the number of test cases can be reduced to 2^N by the zero-one principle, verifying a network is known to be co-NP-complete [Knuth, 1997, Parberry, 1991].

A primitive sorting network contains only comparators that check *neighboring* wires. As the input length N tends to ∞, the upper bound on the number of such networks $P(N)$ is conjectured to be [Samuel, 2011a,b]

$$\log P(N) \leq \frac{1}{2}\binom{N}{2} \log 3. \tag{7.4}$$

Let's try to find a bijection between the extreme points with reverse permutations and the primitive sorting networks. For $N = 3$, the two extreme points are decomposed as $\sigma_1\sigma_2\sigma_1$ and $\sigma_2\sigma_1\sigma_2$, separated by a Yang-Baxter move. The two minimal

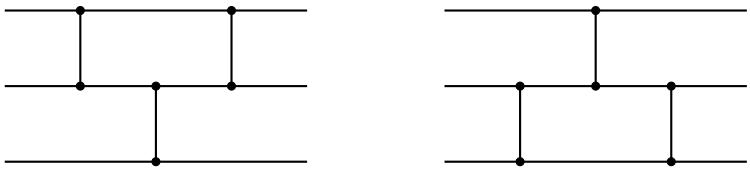

Figure 7.1: The two primitive sorting networks on three elements

primitive sorting networks on three elements are depicted in Figs. 1 and 2. The input is at the left hand side, and the sorted output is at the right hand side. Each element follows a wire left to right until a comparator is reached, depicted here as a vertical connection between two wires. In that case, the elements carried by each wire may be switched.

A naïve guess would be that the (looking top to bottom) the origin wire i of the comparator corresponds to the adjacent transposition σ_i. For $N = 3$, there is clearly a one-to-one correspondence between extreme points with the reverse permutation and primitive sorting networks. However, with $N = 4$ there are only eight (minimal) primitive sorting networks, each corresponding to a bold decomposition given above. Although there are 16 reduced decompositions for $(4, 3, 2, 1)$, two sorting networks with a 'short braid move,' i.e. sequential comparators on distinct pairs of wires, represent the same network. It makes no difference to the sorting algorithm whether these comparisons are made in either order, or simultaneously, as in parallel implementations.

Let's take a closer look. There are 16 reduced decompositions for the permutation $(4, 3, 2, 1)$:

(123121), (121321), (212321), (231231),

(213231), (123212), (312312), (132312),

(312132), (132132), (321232), (231213),

(213213), (232123), (323123), (321323),

where each numeral i corresponds to the adjacent transposition σ_i. However, there are at most eight unique extreme points in ρ-space. Here they are, labeled with the symbols $\mathcal{E}_j$:

$\mathcal{E}_1$: (123121), (**121321**)

$\mathcal{E}_2$: (**212321**)

$\mathcal{E}_3$: (231231), (213231), (231213), (**213213**)

$\mathcal{E}_4$: (**123212**), the 'cocktail-shaker'

$\mathcal{E}_5$: (312312), (132312), (312132), (**132132**)

$\mathcal{E}_6$: (**321232**)

$\mathcal{E}_7$: (**232123**)

$\mathcal{E}_8$: (323123), (**321323**).

The bold decompositions are those in the 'normal form' described by [Kawahara et al., 2011]. Upon inspection, it is clear that the short braid relation $\sigma_i\sigma_j = \sigma_j\sigma_i$, $|i-j| > 1$ is responsible for the multiplicity of decompositions for some extreme points.

7.2.2 Network isomorphisms and equivalent decompositions

These notions can be formalized by defining an isomorphism for sorting networks [Choi and Moon, 2002]. The zero-one principle asserts that a network on N wires which sorts all 2^N binary words in nondecreasing order will also sort any sequence of N numbers into nondecreasing order [Knuth, 1997, Choi and Moon, 2002]. Thus we can restrict our attention to binary words in counting sorting networks (this is a significant simplification from $N!$ words). Let a and $b \in \{0, 1\}$, noting $\min(a, b) = a \wedge b$ and $\max(a, b) = a \vee b$. Let x_k and y_k denote the 'input' and 'output,' respectively, on the k^{th} wire. Then any comparator network can be reduced to the logical information it encodes. Take for example the four-element sorting network in Fig. 7.2.

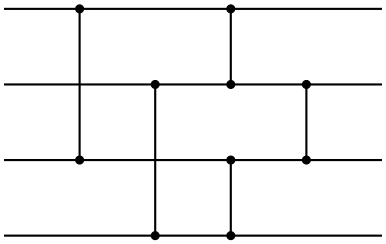

Figure 7.2: A sorting network on four elements

Top to bottom, the inputs are x_0, x_1, x_2, x_3, and the outputs are

$$y_0 = (x_0 \wedge x_2) \wedge (x_1 \wedge x_3) = x_0 \wedge x_1 \wedge x_2 \wedge x_3$$

$$y_1 = (x_0 \vee x_2) \wedge ((x_0 \wedge x_2) \vee (x_1 \wedge x_3)) = (x_0 \wedge x_1 \wedge x_3) \vee (x_0 \wedge x_2) \vee (x_1 \wedge x_2 \wedge x_3)$$

$$y_2 = (x_0 \vee x_2) \vee ((x_0 \wedge x_2) \vee (x_1 \wedge x_3)) = x_0 \vee x_2 \vee (x_1 \wedge x_3)$$

$$y_3 = (x_0 \vee x_2) \vee (x_1 \vee x_3) = x_0 \vee x_1 \vee x_2 \vee x_3$$

The last equality in each equation above has the y_i are expressed in disjunctive normal form (clauses containing only ANDs joined by ORs). This representation is useful because it simplifies the calculation of permutations. The permutation π of an expression in disjunctive normal form d is as follows:

$$\pi(d) = \bigvee_i \bigwedge_j \pi(x_{ij}), \tag{7.5}$$

where $d = \bigvee_i \bigwedge_j x_{ij}$. Now we are ready to define the network isomorphism [Choi and Moon, 2002]:

> Two sorting networks χ and χ' are isomorphic if and only if they contain the same number of comparators and there exists a permutation $\pi \in S_n$ that maps both inputs of each comparator in χ to those of the same comparator in χ':
>
> $$\pi(DI(c_i)) = DI(c_i') \ \ \forall i \in \{1, 2, \ldots, n\}$$

where c_i is the i^{th} comparator in χ and $DI(c_i)$ is the two-element set of inputs to c_i expressed in disjunctive normal form.

This notion is fundamental for us because a network containing a 'short braid move' is trivially isomorphic to the 'other' networks which order the comparators differently. Likewise, there is no possible isomorphism between networks expressing different sides of a 'long braid rule,' e.g. the networks depicted in Fig. 7.1. We see then that each network we count as unique has no isomorphism to any other unique network. The multiple networks associated with a given extreme point are in fact isomorphic to each other. An additional fact of interest: a network of wires and comparators (which may or may not sort) that is isomorphic to a sorting network is itself a sorting network.

Regarding the sorting network isomorphism as an equivalence relation, it is possible to neatly partition the set of reduced decompositions for a given permutation. Two networks are equivalent if, interpreting their comparators as the σ_i, they yield the same extreme point in ρ-space. The number of partitions is equal to the number of unique extreme points.

7.3 Order-theoretic perspective

Underlying the diffusion problem is the importance of the entropy of mixing, the loss of detailed microstate information as systems evolve. Diffusion operations on a state vector result in a final state more 'mixed' than the initial one. This notion can be related to a certain preorder on sets in $\mathbb{R}^n$, namely majorization [Marshall

et al., 2009]. If a vector y majorizes another vector x (written $y \succ x$), x is said to be more mixed than y. Because the entropy function s is Schur-concave, majorization has robust physical significance: if $y \succ x$, $s(y) \leq s(x)$. Illustratively, an equivalent condition is $x = yP$, where P is a doubly stochastic matrix: any diffusion operation can be expressed as an operator with this form. Although majorization is not antisymmetric ($y \succ x$ and $y \prec x \not\Rightarrow x = y$, only $y = x\pi$), the states attainable from diffusion operations nonetheless form a directed acyclic graph. It is generally impossible to return to an initial state by a series of diffusion operations, and the question of reachability from a particular state is nontrivial. Even if a target state is majorized by the initial state, it is possible that the bistochastic operator relating them cannot be decomposed into a product of diffusion operations.

However, reachability in the diffusion state space has a simple statement invoking the weak Bruhat order on S_n [Schröder, 2002, Björner and Brenti, 2005, Wei, 2010]. We will first need the notion of a partially ordered set (poset): a set P equipped with a partial ordering relation $\leq$ which is reflexive, antisymmetric, and transitive. The relation $\leq$ is 'partial' because P will generally contain pairs of elements which are incomparable; if every pair of elements is comparable, we have a *total* order. One example of a poset is the power set 2^S of a set S ordered by inclusion $\subseteq$. The real numbers $\mathbb{R}$ ordered by the usual 'less than or equal to' $\leq$ is an example of a totally ordered set.

The set of permutations $\pi \in S_n$ forms a poset when equipped with the weak Bruhat order $\leq$. Two permutations $u, v \in S_n$ satisfy the covering relation $u \lessdot v$ in the weak order if $v = us_i$ and $\ell(v) = 1 + \ell(u)$. The Coxeter length $\ell(\pi)$ is the

number of inversions in π. The reflexive and transitive closure of $\lessdot$ provides the ordering relation for the weak order [Cooper and Kirkpatrick, 2015]. In other words, $u \leq v$ if $\mathrm{Inv}(u) \subseteq \mathrm{Inv}(v)$, where $\mathrm{Inv}(\pi)$ is the set of inversions in the permutation π. The graph with all $\pi \in S_n$ as vertices and edges joining vertices satisfying the covering relation (i.e. permutations separated by exactly one adjacent transposition) results in the Hasse diagram for S_n. Fig. 7.3 is the Hasse diagram for S_3, indicating the reachability of each permutation from the others. Each edge corresponds to an adjacent transposition $(i, i+1)$ acting on the positions of the permutation e.g. $(2\,3)(213) = (231)$.

We can see from Fig. 7.3 that the weak order is a partial order on S_3 because e.g. (231) and (312) are incomparable. Explicitly,

$$\mathrm{Inv}(231) = \{(2,1),(3,1)\}$$
$$\mathrm{Inv}(312) = \{(3,1),(3,2)\},$$

and neither is a subset of the other. On the other hand, an extreme point with permutation w_1 can be reached from another extreme point with permutation w_0 by diffusion operations if

$$w_0 \in \Lambda_{w_1} = \{\pi \in S_n : \pi \leq w_1\},$$

that is, if w_0 is in the principal ideal of w_1. In other words, by applying a sequence of adjacent transpositions to w_0, each adding one inversion to the permutation, it is possible to reach w_1. [Ehresman, 1934] described a method for the efficient compar-

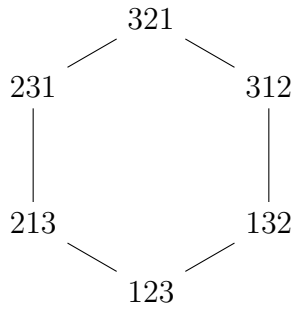

Figure 7.3: Hasse diagram for the weak order on S_3.

ison of two permutations in S_n that relies on each permutation's representation as a standard Young tableau [Stanley, 2011].

We will also need the related notion of a chain, a subset $C \subseteq P$ such that every pair of elements in C is comparable under the ordering relation: chains are totally ordered subsets of P. One example from Fig. 7.3 is the set $\{(123), (213), (231)\}$. A maximal chain is a chain with the property that the addition of any other element in the poset would destroy its total order. Maximal chains must contain a minimal and a maximal element of the poset. For chains in S_n, these correspond to the identity $(12 \cdots n)$ and the reverse permutation $(n \cdots 21)$. The example chain given above is not maximal because it remains totally ordered with the inclusion of (321). Because the reverse permutation contains $\binom{n}{2}$ inversions, the cardinality of a maximal chain in S_n is $\binom{n}{2} + 1$.

Fig. 7.4 is the Hasse diagram for the weak order on S_4. Whereas there are two maximal chains in the weak order on S_3, there are 16 in S_4 [OEIS Foundation Inc., 2011]. Additionally, some of these 16 chains are redundant in the sense that they correspond to equivalent decompositions of the reverse permutation (4321).

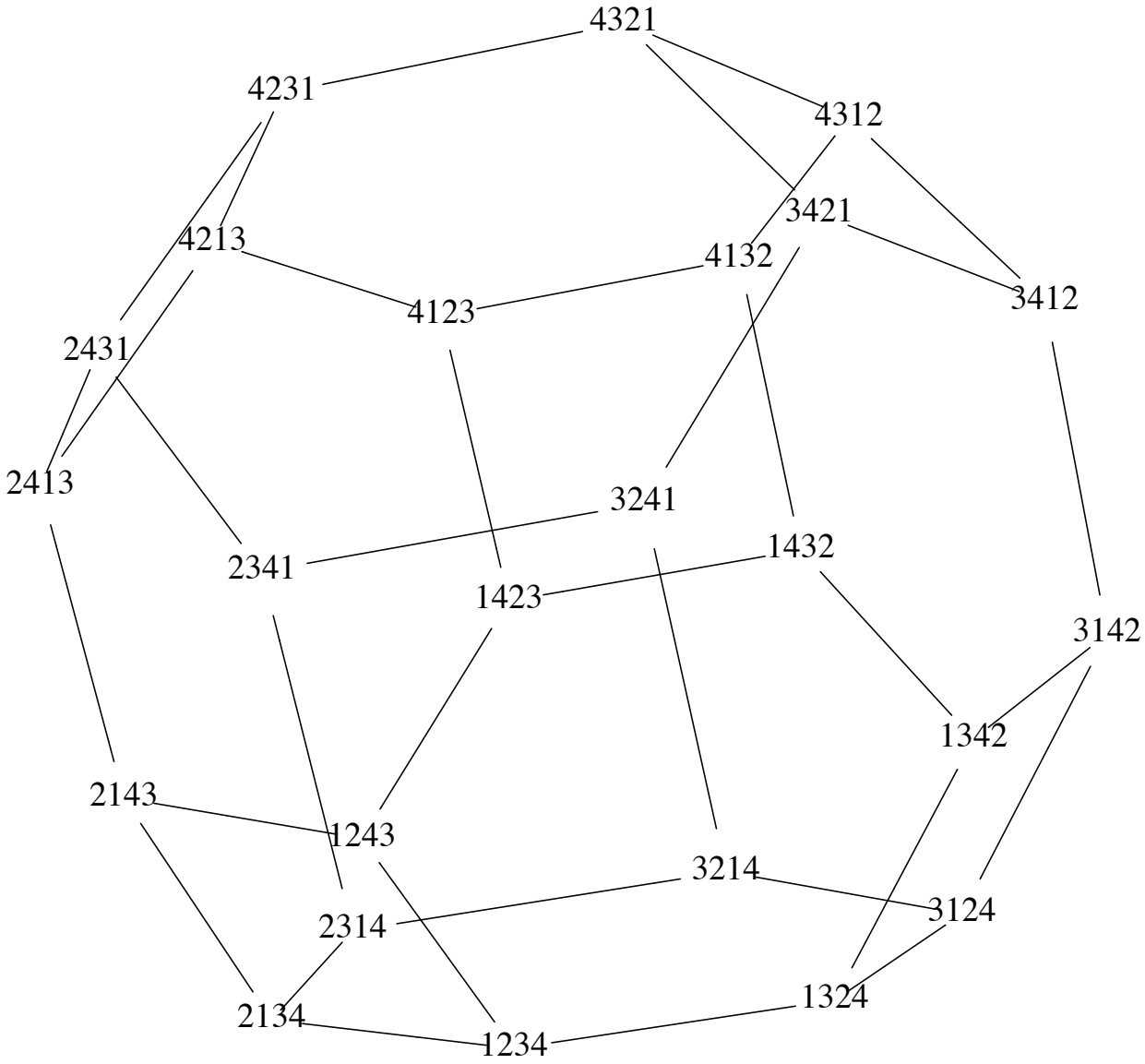

Figure 7.4: Hasse diagram showing the covering relations for S_4.

Another result with some significance for the diffusion problem is the finding that S_n equipped with the weak order is an *Eulerian* poset [Verma, 1971]. That is, each interval $[a, b] \doteq \{x \in S_n : a \leq x \leq b\}$ contains an equal number of odd- and even-ranked elements in the sense that $\ell(\pi)$ is either odd or even. Moreover, the poset $(S_n, \leq)$ is a lattice in the sense that each pair of elements has a unique supremum (join) and a unique infimum (meet) [Yanagimoto and Okamoto, 1969, Björner et al., 1990]. Eulerian lattices generalize the face lattices associated with convex polytopes, offering some hint as to the bijection between the inequivalent reduced decompositions and the vertices of the diffusion polytope K.

7.4 A few generalizations

Phase space conservation (Liouville's theorem) is a powerful constraint on wave-plasma coupling. [Levy et al., 2014] demonstrated that this constraint gives rise to fundamental limitations on a plasma's absorption of incident light at high intensities. The diffusion problem discussed here could shed light on the many dynamical systems whose evolution does not respect phase space conservation.

One generalization of the diffusion problem is the inclusion of a potential energy for each particle. Working with a gravitational potential, [Lynden-Bell, 1967] aimed to explain the violent relaxation observed in newly-formed elliptical galaxies. This model of 1-D gravitating sheets is governed by a Vlasov equation, which succeeded in explaining the evolution of the collisionless system towards a near-thermal distribution in energy [Yamaguchi, 2008].

In a similar vein, [Fetterman and Fisch, 2008] introduced the branching ratio f_E to describe the partitioning of alpha particle energy into kinetic and potential energy in rotating plasmas. In contrast with the wave-induced diffusion coupling position and kinetic energy (Ch. 2), the wave-particle interaction in rotating plasmas may also be engineered to change the particle's potential energy $q\Delta\Phi = v_E \Delta W / v_{ph}$, where v_E is the $E \times B$ velocity [Fetterman, 2012]. If a finite f_E is necessary, the extraction of both kinetic and potential energy could be an interesting extension of the diffusion problem discussed here.

In plasmas, the diffusion problem envisioned takes place on a collisionless timescale, before the system can relax to a thermal distribution. Another generalization might incorporate weakly collisional effects. In the quasilinear regime, the rate of diffusion is proportional to the amplitude of the mode [Vedenov et al., 1962]

$$D_v = 2\pi \frac{e^2}{m^2} \sum_k |E_k|^2 \delta(\omega_k - kv).$$

For a specified collisional timescale, the energy extraction efficiency of an imposed spectrum of waves would depend on the speed with which the particles are diffused between the various levels. Such a restriction could prioritize some level mixings over others, resulting in an optimum distinct from those discussed earlier. For example, an $n-$level system is resonant with up to $\binom{n}{2}$ modes, each of which is associated with

a particular energy difference between levels:

$$\hbar\,\omega_{ij} = |\epsilon_i - \epsilon_j|,\ i, j \in \{1, 2, \ldots n\}.$$

One would expect substantially different optima for spectra decaying with mode energy $|E_k|^2 \sim 1/\omega_k$ or peaked around a particular value $|E_k|^2 \sim \delta(\epsilon - \hbar\,\omega_k)$.

Another means of introducing collisional effects is treating the spectral line broadening due to collisions (pressure broadening) [Rybicki and Lightman, 1985]. As a result, the line shape has a Lorentizian profile

$$\phi(\nu) = \frac{1}{\pi}\frac{\alpha_L}{(\nu - \nu_0)^2 + \alpha_L^2}.$$

In nearly-degenerate systems, with multiple level spacings close in magnitude, a finite line width could lead to the mixing of several states simultaneously. This effect could prove particularly useful in such collisional systems, in which a finite amount of time is allotted for wave-particle manipulation.

Another natural extension of the diffusion problem would be moving to a nonlinear objective function, as would be the case if one included a potential energy function in the optimization. In this case, the results about K's starlike nature could prove crucial. Yet another extension would be optimizing the free energy of a system of countable particles, requiring integer programming. These two extensions could be combined to study e.g. the behavior of fermions in a pumped system.

Chapter 8

Conclusions and future work

8.1 Key accomplishments

In Chapter 3, we identified a solution to a persistent problem, the production of shaped plasmas in vacuum. These plasmas have enormous implications for Raman amplification and other laser-plasma methods. In order to identify the solution, a new theory of aerosol focusing was described, which was verified by experiment. This description of dense aerodynamic focusing will be invaluable for future workers designing structured targets for radiation generation and fusion experiments.

In Chapter 4, we constrained the possible reactivity gains from alpha channeling to a light ion beam in DT and p-^{11}B plasmas. Although the p-^{11}B reactivity was not improved, we have proposed a possible solution for helium ash removal, a pivotal consideration for p-^{11}B fusion energy. Moreover, we identified a new metric for beam utility which will aid in the search for operating points using other fusion reactions.

In Chapter 5, we solved a longstanding academic question: the precise plasma free energy that may be tapped with waves. The linear programming approach allowed us to make definitive conclusions about the optimal sequences of injected waves. In particular, we proved that neither truncating the wave diffusion nor heating the plasma results can result in a minimum energy state.

In Chapter 6, we defined and contextualized the plasma wave diffusion problem in the language of network theory. Unfortunately, our study of other regimes of phase space connectedness revealed that there are very few general statements which can be made about diffusion problems on arbitrary graphs. Nonetheless, we succeeded in completely characterizing the state space under the local diffusion constraint.

Finally, in Chapter 7, we have suggested additional context for the diffusion problem which may aid in a definitive resolution of the nonlocal problem.

8.2 Future work

Aerosol plasmas are nonequilibrium systems which may have many interesting transport properties. Their relation to dusty and strongly-coupled plasmas should be established. The theory developed in Chapter 3 should be extended to account for this new physics, which may be important in designing structured aerosol targets for MagLIF experiments on Z. Their true utility as shaped plasmas will be borne out by experiment.

Regarding alpha channeling in p-^{11}B plasmas, more sophisticated calculations could revise conclusions made about the utility of a monoenergetic proton beam.

In particular, direct simulation of the 0-D equilibrium, i.e. with a velocity space particle-in-cell code, could yield equilibria which the model did not identify. Moreover, a proper treatment of p-^{11}B ICF requires at least 1-D radiation hydrodynamics calculations which anticipate the significance of radiative transfer in p-^{11}B plasmas.

Because our ultimate interest in the diffusion problem lies in its application to plasmas, a solution for continuous distribution functions is desirable. As posed in [Fisch and Rax, 1993], this is tantamount to calculating the optimal kernel $K(v, v', t)$ governing the evolution of the particle distribution, to wit

$$\frac{\partial f}{\partial t} = \int K(v, v', t)[f(v', t) - f(v, t)]dv',$$

such that the energy functional

$$W(t) = \int \epsilon(v) f(v, t) dv$$

is minimized for $t \to \infty$. The solution may lie in a variational approach, perhaps requiring optimal control methods [Todorov, 2006].

There is much work to be done placing the discrete diffusion problem on firmer mathematical foundations. In particular, characterizing and enumerating the extreme points may yield to a direct, algebraic approach [Samuel, 2011a,b, Armstrong, 2009]. Another path is further developing the analogy between primitive sorting networks and ladder lotteries [Kawahara et al., 2011]. Apart from the connection to Eulerian lattices, another possible explanation for the link between the combinatorial origin of the extreme points and convexity could be provided by sorting networks

[Knuth, 1997, 1992, Armstrong, 2009]. Perhaps there is an intuitive explanation for why the B_{ij} sequences we've identified must yield a convex set in density space. Identifying bijections with the inequivalent factorizations could place a sharper constraint on the computational complexity of the nonlocal optimization problem.

I hope with these three applications I have given the reader an idea of the ubiquity and possibilities for nonthermal plasmas, and nonequilibrium systems generally. Understanding the natural world as it exists depends on our thoughtful study of these systems.

Appendix A

Auxiliary calculations for Chapter 4

A.1 Maintaining a monoenergetic beam

There are several possible model choices for the recirculated power required to maintain the proton beam. [Rider, 1995] calculated the amount of power necessary to prevent velocity space spreading of the beam past a prescribed thermal width $v_{th} \ll v_b$. This spread results primarily from beam-beam collisions; the Rider estimate of the recirculated power is proportional to n_b^2. This calculation is applicable when the beam lies far outside the thermal proton population and the velocity width of the beam is important.

In general, P_{recirc} must also counteract beam collisions on the thermal population, involving terms proportional to $n_b n_p$, $n_b n_B$, and $n_b n_e$. A more precise calculation

would include both beam-beam and beam-thermal collisions and evaluate the reactivity integrals with a realistic slowing down distribution for the beam protons. In pursuing an upper bound of the gains realizable from alpha channeling, it has been assumed that the monoenergetic beam collides only with thermal particles.

A.1.1 Collisional evolution of beam

The Fokker-Planck equation governs the collisional evolution of an initially monoenergetic beam. Drag and velocity space diffusion induced by each of the thermal species contribute to the beam's eventual thermalization. We invoke a test particle analysis to argue for the validity of the model employed here. Consider, for example, the case of a 600 keV proton slowing in a plasma with $T_p = T_B = 120\,\mathrm{keV}$ and $T_e = 80\,\mathrm{keV}$. The number ratio is $n_B/n_p = 0.20$ and $n_e = 3.5 \times 10^{13}\,\mathrm{cm}^{-3}$. Although the beam slows primarily on thermal protons until an energy scattering time has passed, the fusion rate falls significantly from its original value on a collisionless time scale.

A similar DT case would have a 125 keV deuteron slowing in a plasma with $T_D = T_T = 11\,\mathrm{keV}$ and $T_e = 24\,\mathrm{keV}$. The number ratio is $n_T/n_D = 1.25$ and $n_e = 7.5 \times 10^{13}\,\mathrm{cm}^{-3}$. The picture is altered here because the ideal beam energy (maximizing the beam-thermal *reactivity*[Mikkelsen, 1989]) is somewhat larger than the fusion resonance, such that most of the beam fusion events come after about one collision time. However, the fusion rate remains larger than the thermal ion collision times throughout the slowing down process.

In all cases, the beam remains well outside the thermal ion distributions, and most fusion events occur on a collisionless timescale. We do not anticipate that collisional spreading of the beam will modify the power balance laid out here.

A.1.2 Collisionless instability

Let us expand on comments made in the Introduction concerning the stability of the monoenergetic beams. In particular, we will present suggestive criteria for ion beams propagating in either cold or warm plasmas. A more detailed stability analysis for a collisional three-component plasma is beyond the scope of this work.

In a collisionless two-component plasma, the stability threshold for Langmuir waves in the presence of an ion beam is[Fried and Wong, 1966]

$$\mathcal{D}(u) = Z'(u) + n\alpha^2 Z'[\alpha(u - V)] - 2(n + 1)T = 0, \tag{A.1}$$

where Z' is the first derivative of the plasma dispersion function[Fried and Conte, 1961], $u = \omega/kv_{th,i}$ is a dimensionless phase velocity, $\alpha = v_{th,i}/v_{th,b}$ describes the 'coldness' of the beam, $V = V_b/v_{th,i}$ measures the beam's separation in velocity from the bulk ions, and $n = n_b/n_i$ is the dimensionless beam density, and $T = T_i/T_e$. Generally speaking, V is $\mathcal{O}(1)$ in all configurations and T is larger for p-^{11}B than DT plasmas (greater electron-ion temperature separation).

Taking asymptotes of Eq. (A1), we can get some general notions of the stability of the beam-plasma configurations to be presented.[Fried and Wong, 1966] We will present the stability threshold as a curve in (V, α) space parametric in the phase

velocity u. For $V \gg 1$, corresponding to a beam well outside of the thermal ion bulk (cold plasma), the stability threshold is

$$V = (\alpha + 1)\sqrt{\frac{n}{2(n+1)T}}, \tag{A.2}$$

and likewise for $V \ll 1$, a beam embedded in the thermal bulk (warm plasma),

$$V = \xi(1 + n\alpha^3 e^{-\alpha^2\xi^2}), \tag{A.3}$$

with

$$\xi = \sqrt{\frac{n/2}{T(n+1)+1}}. \tag{A.4}$$

In practice, these criteria may be regarded as a minimum amount of thermal spread intrinsic to the beam. Cold beams with little thermal spread (large α) lying above these curves are unstable.

For example, we consider a case typical of the configurations to follow, a DT plasma with $n = 0.1$ and $T = 0.5$. In both DT and p-^{11}B plasmas, $V \gtrsim 1$, so we will proceed cautiously using the $V \gg 1$ asymptote. Then a stable beam has

$$\alpha < \sqrt{11}V - 1. \tag{A.5}$$

For a representative $V = 4$, $\alpha < 4\sqrt{11} - 1 \approx 12$, corresponding to a minimum beam temperature for stability of 100 eV in DT. (Typical beam energies are in the neighborhood of 127 keV, the center of mass energy at the fusion cross section

peak.) Compare a typical case in p-^{11}B , with $n = 0.1$ and $T = 2$. We assume the beam-plasma interaction largely ignores the boron ions. The corresponding stability criterion is $\alpha < \sqrt{110}V - 1 \approx 20$ for a typical $V = 2$. The minimum thermal spread is then 1 keV, compared to a beam energy of about 627 keV.

In these representative examples, quasi-monoenergetic beams are well within the stability threshold. However, as the beam fraction is increased, the necessary stabilizing thermal spread may approach the beam energy in some scenarios.

A.2 Optimized reactivity subject to maximum pressure

In pressure-limited systems, the greatest achievable reactivity is an important experimental parameter that establishes confinement criteria. In the absence of a fast beam, the maximum of the function

$$n_A n_B \langle \sigma v \rangle (T) \,|\, n_A T + n_B T + n_e T < p_0 \tag{A.6}$$

is of interest. n_A and n_B are the number densities of the reacting ion species, such that $n_e = Z_A n_A + Z_B n_B$. p_0 denotes the maximum allowed pressure and $n_A/n_B = \epsilon$. Equivalently, one can maximize the Lagrange function

$$L = n_A n_B \langle \sigma v \rangle - \lambda(n_A T + n_B T + n_e T - p_0). \tag{A.7}$$

The components of the gradient are

$$\frac{\partial L}{\partial n_e} = (1 + Z_B + \epsilon(1 + Z_A))T\lambda + 2\frac{n_e\epsilon \langle\sigma v\rangle}{Z_B + Z_A\epsilon} \tag{A.8}$$

$$\frac{1}{n_e}\frac{\partial L}{\partial \epsilon} = (Z_B - Z_A)T\lambda + \frac{Z_B - Z_A\epsilon}{Z_B + Z_A\epsilon} n_e \langle\sigma v\rangle \tag{A.9}$$

$$\frac{1}{n_e}\frac{\partial L}{\partial T} = (1 + Z_B + \epsilon(1 + Z_A))\lambda + \frac{n_e\epsilon \langle\sigma v\rangle'(T)}{Z_B + Z_A\epsilon} \tag{A.10}$$

$$\frac{\partial L}{\partial \lambda} = \frac{1 + Z_B + \epsilon(1 + Z_A)}{Z_B + Z_A\epsilon} n_e T - p_0 \tag{A.11}$$

Considering the complementarity condition, $\lambda = 0$ implies $n_e\epsilon \langle\sigma v\rangle = 0$, which cannot hold in a finite-temperature plasma. Proceed, fixing $p = p_0$. Then

$$\epsilon = \frac{1 + Z_B}{1 + Z_A} \tag{A.12}$$

$$n_e = \frac{(Z_A + Z_B + 2Z_AZ_B)}{2(1 + Z_A)(1 + Z_B)}\frac{p_0}{T} \tag{A.13}$$

$$\langle\sigma v\rangle'(T) = 2\frac{\langle\sigma v\rangle(T)}{T} \tag{A.14}$$

where the final equation can be solved implicitly for the $T = T_0$ which maximizes the reactivity.

A.3 Evaluation of burn fraction ϕ

Without loss of generality, suppose initial number densities n_{A0} and n_{B0} such that $n_{A0} + n_{B0} = n_0$ and $n_{A0}/n_{B0} = \epsilon$. Then

$$n_{A0} = \frac{\epsilon}{1+\epsilon} n_0 \tag{A.15}$$

$$n_{B0} = \frac{1}{1+\epsilon} n_0 \tag{A.16}$$

and

$$n_A(t) = \frac{\epsilon}{1+\epsilon} n_0 - n \tag{A.17}$$

$$n_B(t) = \frac{1}{1+\epsilon} n_0 - n \tag{A.18}$$

where $n = n(t)$ is the cumulative number of binary fusion reactions. Defining $\phi \doteq 2n/n_0$,

$$\frac{dn}{dt} = \frac{n_0}{2}\frac{d\phi}{dt} = n_A n_B \langle\sigma v\rangle \tag{A.19}$$

$$= \frac{n_0^2 \langle\sigma v\rangle}{4(1+\epsilon)^2}((\epsilon+1)\phi - 2)(\epsilon(\phi-2)+\phi)$$

which is a Riccati equation for ϕ. Assuming constant T_e and T_i during burn, integrate over the confinement time, $R/3c_s$, to obtain the implicit equation

$$\frac{1+\epsilon}{1-\epsilon} \log\left[\frac{\epsilon(\phi(\epsilon+1)-2)}{\epsilon(\phi-2)+\phi}\right] = \frac{R}{3c_s} n_0 \langle\sigma v\rangle \tag{A.20}$$

This can be inverted to obtain

$$\phi = \frac{2}{\epsilon+1}\left[1 - \frac{\epsilon-1}{\epsilon\exp\left(\frac{2}{H_B}\frac{\epsilon-1}{\epsilon+1}\rho R\right)-1}\right] \tag{A.21}$$

where $\rho = m_A n_{A0} + m_B n_{B0}$, $H_B = 6c_s m/\langle\sigma v\rangle$, and $m = (\epsilon m_A + m_B)/(\epsilon+1)$.

Appendix B

Auxiliary calculations for Chapter 5

B.1 Extreme point geometry

[Thon and Wallace, 2004] proved that their algorithm generates the full set of extreme points for an arbitrary number of energy levels N. However, the $N = 3$ case admits a straightforward geometric proof. All states resulting from the application of a B_{ij} lie along the line $n_i = n_j$. This constrains the possible paths through state space. In particular, the slope of the line joining any two points p_1 and p_2 such that $p_2 = p_1 B_{ij}$ is -1 if $(i, j) = (1, 2)$, 0 if $(i, j) = (1, 3)$, or ∞ if $(i, j) = (2, 3)$.

Fig. B.1 plots the extreme points and the three lines covering K as well as these constrained trajectories. One extreme point is given (n, the initial data), and the other six are generated from choosing one of two routes through state space. Note

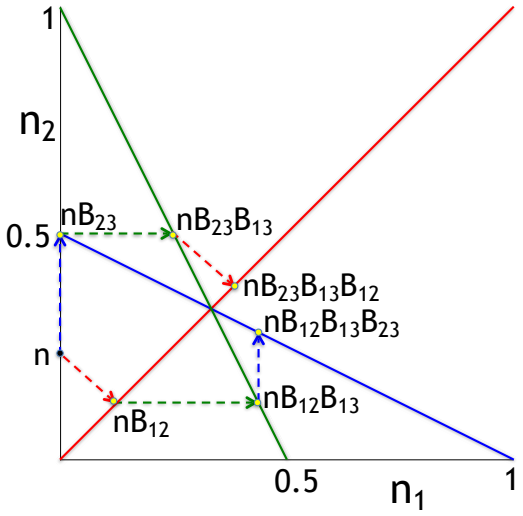

Figure B.1: Geometric construction of K. Extreme points of $ch(K)$ (yellow dots) depicted with lines $n_i = n_j$ (solid) and lines joining extreme points (dashed).

that extreme points are only obtained by moving directly to a line $n_i = n_j$, without crossing any other such line. The lines are color-coded. Thus, for example, the partial relaxation along a red dotted line terminates on the red solid line; the red solid indicates complete relaxation of levels n_1 and n_2, while all the states traversed along the dotted line are reachable. It can be seen from this geometrical representation that no extreme points are obtained by revisiting the same line: each diffusive transformation B_{ij} reduces the distance of the state from the uniform distribution e. Thus, a state that revisits a line would necessarily be interior to the first state reached on that line.

B.2 Combinatorial methods

Thon and Wallace[Thon and Wallace, 2004] simplified the structures of many proofs by making use of the combinatorial features of the Dalton transfer problem. In particular, they introduced the permutation of the individuals whose incomes were to be redistributed. In their notation, the initial permutation is denoted $v = (v(1), v(2), \ldots, v(N))$, where $v(i) = k$ is interpreted to mean that the individual numbered k is the i^{th} poorest. This representation is equivalent to the common *two-line notation*:

$$\begin{pmatrix} 1 & 2 & \cdots & N \\ v(1) & v(2) & \cdots & v(N) \end{pmatrix},$$

where the first row lists indices of the permutation and the second row identifies the individuals. Note that the ordering of the columns is immaterial. The first column could be read as "individual $v(1)$ is the poorest, listed first."

In their problem, as in ours, it is assumed that the individuals (levels) are ordered initially from poorest (least populated) to richest (most populated), yielding an initial permutation $v(i) = i$. Because the diffusion operations treated in this work transfer level densities but leave the level energies unchanged, we lose no generality by specializing to such a permutation, which we denote $\{1, 2, \ldots, N\}$, reflecting $n_0^1 \leq n_0^2 \leq \cdots \leq n_0^N$. (This is the *ordered arrangement* or *one-line* representation of the level density permutation.) In concordance with Ref. [Thon and Wallace, 2004], we describe the levels nearest in population as *neighbors*, e.g. n_2 is neighbors with n_1 and n_3 only. It turns out that the extreme points of $ch(K)$ can be reached only

by sequences of B_{ij} averaging such neighboring levels (*Prop. 2* of Ref. [Thon and Wallace, 2004]).

Hoping for greater simplicity, we discuss separately the permutation of the level energies, denoted $\{w(1), w(2), \ldots, w(N)\}$, with $w(i) = k$ meaning the level with the k^{th} lowest energy has initially the i^{th} smallest population. For example, if there is a complete population inversion, the highest-energy levels are initially most populated and $\epsilon \sim \{1, 2, \ldots, N\}$. If instead $N = 3$ and the second-highest energy level is most populated, followed in turn by the lowest and highest energy levels, one has $\epsilon \sim \{3, 1, 2\}$, or, in two-line notation:

$$\begin{pmatrix} 3 & 2 & 1 \\ 2 & 1 & 3 \end{pmatrix} = \begin{pmatrix} 1 & 2 & 3 \\ 3 & 1 & 2 \end{pmatrix}.$$

(Recall our assumption $i = v(i)$, so that the first row of the two-line representation of the energy permutation identifies the states ordered by initial level populations. Thus the columns of the two-line representation could be parsed "greatest density in second-highest energy level, second-highest density in the lowest energy level, and least density in highest-energy level.")

Apart from equalizing the populations of levels i and j, one can consider the effect of the B_{ij} on these permutations. As mentioned previously, the B_{ij} have no effect on the permutation of level energies, which remains fixed throughout the problem. However, each B_{ij} changes the permutation of level populations, with the result that the numberings are exchanged, so that e.g. $n_0 B_{13}$ has permutation $\{3, 2, 1\}$. Considering the problem in n_1-n_2 space, one realizes that the effect of a B_{ij} is to

move the system state to another of the $N! = 6$ cells in $ch(K)$, each corresponding to a specific permutation of the level populations (cf. Fig. 1 of Ref. [Thon and Wallace, 2004]). The cells are separated by rays from e to six of extreme points in $ch(K)$ (n_0 excluded).

One of the key insights of this approach is the connection between population inversions and inversions in the permutation of level densities vis-á-vis the energy permutation. Using only the B_{ij}, it is possible to reorder the entire set of level populations, so that the final distribution is decreasing with energy (we term the permutations corresponding to such distributions *stopping* permutations).

In fact, there is a unique stopping permutation in a given problem: the *reverse* of the energy permutation, i.e. $\{w(N), w(N-1), \ldots, w(1)\}$, obtained from the composition of $\mathbf{w}$ with the order-reversing permutation. Let $\mathbf{w}^r$ denote the reverse of the permutation $\mathbf{w}$. In two-line notation, one has

$$\mathbf{w}^r = \begin{pmatrix} 1 & 2 & \cdots & N \\ w(1) & w(2) & \cdots & w(N) \end{pmatrix} \begin{pmatrix} 1 & 2 & \cdots & N \\ N & N-1 & \cdots & 1 \end{pmatrix}$$

$$= \begin{pmatrix} N & N-1 & \cdots & 1 \\ w(N) & w(N-1) & \cdots & w(1) \end{pmatrix} \begin{pmatrix} 1 & 2 & \cdots & N \\ N & N-1 & \cdots & 1 \end{pmatrix}$$

$$= \begin{pmatrix} 1 & 2 & \cdots & N \\ w(N) & w(N-1) & \cdots & w(1) \end{pmatrix}.$$

Note that the reverse operation is an involution, such that $(\mathbf{w}^r)^r = \mathbf{w}$. For example, $\{1, 2, 3\}$ and $\{3, 2, 1\}$ are reverse permutations. In our previous example, the level

energy permutation was $\{3, 1, 2\}$ such that $\epsilon_3 \leq \epsilon_1 \leq \epsilon_2$ for $\epsilon = (\epsilon_1, \epsilon_2, \epsilon_3)$ and $n_0 = (n_0^1, n_0^2, n_0^3)$. The reverse of the ϵ permutation is $\{2, 1, 3\}$. Thus any stopping state has $n_2 \leq n_1 \leq n_3$, such that the final population in the highest-energy level ('level 2,' when ordered by initial population) is smallest, and so on.

By identifying the level energies' permutation and its reverse, the search for the correct sequence of B_{ij} can be greatly narrowed because only extreme points with the stopping permutation need be considered.

Appendix C

The S_A are the complete set of extreme points

The local state space is the set of states accessible from the initial state ρ_0, after an arbitrary finite sequence of transformations $B_{i,i+1}$ has been applied. We claim that the convex hull of (the closure of) this space has 2^{n-1} extreme points in bijection with the power set of $\{1, 2, \ldots, n-1\}$. Denote these points S_A, where the index A runs over all subsets of $\{1, 2, \ldots, n-1\}$.

The bijection has a simple description. The empty set $\varnothing$ corresponds to the initial state ρ_0. The point S_A corresponding to the set A has the property that for each $i \in A$ the i'th and $(i+1)$'th components of S_A are equal, and its components are obtained by averaging over subsets of components of ρ_0. So, for example, in a seven-level system, $S_{\{1,2,3,6\}}$ is the point (x, x, x, x, y, z, z) where x is the average of the first four components of ρ_0, y is the fifth component, and z is the average of the

sixth and seventh components. In greater generality, whenever A contains a sequence of k consecutive integers $i, i+1, \ldots, i+k-1$ then the $k+1$ components of S_A from i to $i+k$ are equal to the average of the corresponding components of ρ_0.

Lemma 1. *The S_A are contained in the closure of the local state space.*

Proof. Fix a subset $A \subseteq \{1, 2, \ldots, n-1\}$ corresponding to a particular S_A. Suppose $i, i+1, \ldots, i+k-1$ is a maximal sequence of k consecutive integers in A, i.e. all these are in A, but $i-1$ and $i+k$ are not, and consider the quantity $\rho_{i+k} - \rho_i$. This is non-negative, and, if it is non-zero, strictly decreases when the operator $B_{i+k-1,i+k} \ldots B_{i+1,i+2} B_{i,i+1}$ is applied to the state ρ. Furthermore it is unchanged when the corresponding operator for a different maximal sequence of consecutive integers is applied to ρ. It follows that by repeated application of such operators the initial state ρ_0 can be brought arbitrarilly close to the extreme point S_A. Thus the points S_A are in the closure of the local state space. □

Lemma 2. *No point S_A can be written as a nontrivial convex combination of the others.*

Proof. Consider a convex combination $\sum a_A S_A$, with $a_A \geq 0$ and $\sum a_A = 1$. Let $\rho_{A,i}$ denote the component densities of the point S_A. Suppose $\sum a_A S_A = S$, with densities ρ_i. Because an arbitrary sequence of local operators $B_{i,i+1}$ cannot achieve a population inversion, we have $\rho_{A,i} \leq \rho_{A,i+1}$ for all A and i. Therefore $\rho_i = \rho_{i+1}$ if and only if $\rho_{A,i} = \rho_{A,i+1}$ for all A with $a_A > 0$. Thus any convex combination yielding the point S has only one summand, S itself. □

Lemma 3. *Any point in the local state space can be written as a convex combination of the S_A.*

Proof. We wish to show that every accessible state ρ can be written as a convex combination of the extreme points, i.e. that we can write

$$\rho = \sum_A \lambda_A S_A \ , \qquad \text{where} \ \ \lambda_A \geq 0 \ , \sum_A \lambda_A = 1.$$

Every accessible state can be obtained by applying an arbitrary finite sequence of $B_{i,i+1}$ to the initial state $\rho_0 = S_\varnothing$. We proceed by induction on the number of $B_{i,i+1}$ operators to be applied. To prove the inductive step it is necessary to check that for every A and for every i, $S_A B_{i,i+1}$ can be written as a convex combination of extreme points. If $i \in A$, then $S_A B_{i,i+1} = S_A$ is an extreme point. If $i \notin A$ then the i'th and $(i+1)$'th components of S_A may be different. S_A then takes the form

$$(\ldots, x, \ldots, x, x, y, y, \ldots y, \ldots) \ .$$

where there is a string of $k > 0$ x's ending in the i'th position and a string of $l > 0$ y's starting in the $(i+1)$'th position. The entries on the left of the string of x's and on the right of the string of y's remain fixed and identical for all the points that appear in the forthcoming calculation, and thus do not play any role. It is assumed that the entry immediately on the left of the x's (if there is such) is strictly less than x, and the entry immediately on the right of the y's (if it exists) is strictly greater than y.

Applying $B_{i,i+1}$ we have

$$S_A B_{i,i+1} = (\ldots, x, \ldots, x, \frac{x+y}{2}, \frac{x+y}{2}, y, \ldots, y, \ldots)$$

where now the strings of x's and y's are of length $k-1$ and $l-1$ respectively. It should be emphasized that except in the case $k = l = 1$ *this is not an extreme point*, as although the values in the i'th and $(i+1)$'th positions are equal, they have been determined by components of the initial density ρ_0 from outside these positions, and full averaging over the relevant subset has not been achieved. However we will now show it is a convex combination of four extreme points of the following form:

$$S_1 = (\ldots, X, \ldots X, X, X, X, \ldots X, \ldots),$$
$$\text{with } k+l \text{ } X\text{'s},$$
$$S_2 = (\ldots, X_1, \ldots, X_1, X_1, X_1, Y_1, \ldots, Y_1, \ldots),$$
$$\text{with } k+1 \text{ } X_1\text{'s and } l-1 \text{ } Y_1\text{'s},$$
$$S_3 = (\ldots, X_2, \ldots, X_2, Y_2, Y_2, Y_2, \ldots, Y_2, \ldots),$$
$$\text{with } k-1 \text{ } X_2\text{'s and } l+1 \text{ } Y_2\text{'s, and}$$
$$S_4 = (\ldots, X_2, \ldots, X_2, Z, Z, Y_1, \ldots, Y_1, \ldots),$$
$$\text{with } k-1 \text{ } X_2\text{'s and } l-1 \text{ } Y_1\text{'s}.$$

(These four points are only distinct on the assumption $k, l > 1$. The cases $k = l = 1$, $k = 1, l > 1$, and $k > 1, l = 1$ should be considered separately but are simpler — in particular in the case $k = l = 1$ all four points coincide and the resulting

point is extreme. We omit the details of the cases $k = 1, l > 1$ and $k > 1, l = 1$.) The quantities $x, y, X, X_1, Y_1, X_2, Y_2, Z$ appearing here are not independent, as they are obtained from averaging over certain entries of ρ_0. Denote the average value of entries $i-(k-1), \ldots, i-1$ of ρ_0 as R_1, the value of entry i as R_2, the value of entry $i+1$ as R_3 and the average of entries $i+2, \ldots, i+l$ as R_4. Then

$$\begin{aligned}
x &= \frac{(k-1)R_1 + R_2}{k} \\
y &= \frac{R_3 + (l-1)R_4}{l} \\
X &= \frac{(k-1)R_1 + R_2 + R_3 + (l-1)R_4}{k+l} \\
X_1 &= \frac{(k-1)R_1 + R_2 + R_3}{k+1} \\
Y_1 &= R_4 \\
X_2 &= R_1 \\
Y_2 &= \frac{R_2 + R_3 + (l-1)R_4}{l+1} \\
Z &= \frac{R_2 + R_3}{2}
\end{aligned}$$

Our aim is to find $\lambda_1, \lambda_2, \lambda_3, \lambda_4 \geq 0$ such that

$$S_A B_{i,i+1} = \sum_{i=1}^{4} \lambda_i S_i \quad \text{and} \quad \sum_{i=1}^{4} \lambda_i = 1$$

Solving these linear equations gives three constraints between the λ_i, which can be written in the form

$$\begin{aligned}\lambda_1 &= C_1\lambda_4 + D_1\\ \lambda_2 &= C_2\lambda_4 + D_2\\ \lambda_3 &= C_3\lambda_4 + D_3\end{aligned}$$

where $C_1, C_2, C_3, D_1, D_2, D_3$ are complicated expressions involving k, l and R_1, R_2, R_3, R_4. However, it follows from $R_1 \leq R_2 \leq R_3 \leq R_4$ that $C_1 > 0$ and $C_2, C_3 < 0$. (Expressions for C_1, C_2, C_3 are given later.) Thus for nonnegativity of the λ_i we need

$$\max\left(0, -\frac{D_1}{C_1}\right) \leq \lambda_4 \leq \min\left(-\frac{D_2}{C_2}, -\frac{D_3}{C_3}\right) \tag{C.1}$$

Expressions for $-\frac{D_1}{C_1}, -\frac{D_2}{C_2}, -\frac{D_3}{C_3}$ are given later, from which it can be seen that $-\frac{D_2}{C_2}, -\frac{D_3}{C_3}$ are both nonnegative and not less than $-\frac{D_1}{C_1}$. Thus the inequalities (C.1) can always be satisfied. Note that the quantity $-\frac{D_1}{C_1}$ is of indeterminate sign. When it is negative it is possible to take $\lambda_4 = 0$ and thus write $S_A B_{i,i+1}$ as a convex combination of just three extreme points. However, in general, four are needed. □

Theorem 1. *The convex hull of the closure of the local state space has* 2^{n-1} *extreme points in bijection with the power set of* $\{1, 2, \ldots, n-1\}$.

Proof. By **Lemma 1**, the S_A are all contained in the closure of the local state space and thus in its convex hull. Thus the convex hull of the points S_A is contained in the

convex hull of the closure of the local state space. By **Lemma 2**, no point S_A can be expressed as a nontrivial convex combination of the others. Thus the convex hull of the points S_A has all the 2^{n-1} points S_A as extreme points. By **Lemma 3**, any point in the local state space can be expressed as a convex combination of the S_A. Thus the local state space is contained in the convex hull of the points S_A, which is a closed convex set, so must therefore also contain the convex hull of the closure of the local state space. Combining these results we conclude that the convex hull of the closure of the local state space can be identified with the convex hull of the points S_A and these are a complete set of extreme points. □

Corollary 1. *The extreme points of the local state space for the n-level diffusion problem form an* $(n-1)$*-dimensional hypercube.*

Proof. By **Theorem 1**, the total number of extreme points is 2^{n-1}; these correspond to the vertices of an $(n-1)$-dimensional hypercube.[Weisstein, n.d.b] Choose a particular vertex corresponding to the subset $A \subseteq \{1, 2, \ldots, n-1\}$. Because each vertex corresponds to an element of the power set of $\{1, 2, \ldots, n-1\}$, there are $n-1$ edges from the vertex associated with A in correspondence with the $n-1$ sets differing from A by the inclusion or exclusion of a single element. □

Expressions for C_i and D_i

$$
\begin{aligned}
C_1 &= \frac{(p_2 + 2\,p_3)\,(p_2 + 2\,p_1)\,(k+l)}{2\,((k-1)p_1 + kp_2 + (k+1)p_3)} \\
&\quad \times \frac{1}{(l+1)p_1 + lp_2 + (l-1)p_3} \\
C_2 &= -\frac{(p_2 + 2\,p_3)\,(k+1)}{2\,((k-1)p_1 + kp_2 + (k+1)p_3)} \\
C_3 &= -\frac{(p_2 + 2\,p_1)\,(l+1)}{2\,((l+1)p_1 + lp_2 + (l-1)p_3)}
\end{aligned}
$$

Here

$$
\begin{aligned}
p_1 &= R_2 - R_1 \\
p_2 &= R_3 - R_2 \\
p_3 &= R_4 - R_3
\end{aligned}
$$

with $p_i \geq 0$. Also

$$
\begin{aligned}
-\frac{D_1}{C_1} &= \big((k-1)lp_1p_2 + klp_2^2 \\
&\quad + k(l-1)p_2p_3 - 2(l+k)p_1p_3\big) \\
&\quad \times \frac{1}{(p_2 + 2\,p_3)\,(p_2 + 2\,p_1)\,kl} \\
-\frac{D_2}{C_2} &= \frac{(k-1)lp_1 + klp_2 + k(l-1)p_3}{(p_2 + 2p_3)\,kl} \\
-\frac{D_3}{C_3} &= \frac{(k-1)lp_1 + klp_2 + k(l-1)p_3}{(p_2 + 2p_1)\,kl}
\end{aligned}
$$

To see the inequalities (C.1) can be satisfied observe that $-\frac{D_2}{C_2}, -\frac{D_3}{C_3} > 0$ and

$$-\frac{D_2}{C_2} - \left(-\frac{D_1}{C_1}\right) = \frac{2p_1\ ((k-1)p_1 + kp_2 + (k+1)p_3)}{k\,(p_2+2p_3)\,(p_2+2p_1)} > 0$$

$$-\frac{D_3}{C_3} - \left(-\frac{D_1}{C_1}\right) = \frac{2p_3\ ((l+1)p_2 + lp_2 + (l-1)p_3)}{l\,(p_2+2p_3)\,(p_2+2p_1)} > 0$$

Bibliography

R. Aboudi and D. Thon. Second degree Pareto dominance. *Soc. Choice Welfare*, 30: 475–493, 2008.

D. Armstrong. The sorting order on a Coxeter group. *J. Combin. Theory Ser. A*, 116:1285–1305, 2009.

E. Artin. Theorie der zöpfe. In *Abhandlungen aus dem Mathematischen Seminar der Universität Hamburg*, volume 4, pages 47–72. Springer, 1925.

S. Atzeni and J. Meyer-ter-Vehn. *The Physics of Inertial Fusion*. Clarendon, Oxford, 2004.

A.-L. Barabási and R. Albert. Emergence of scaling in random networks. *Science*, 286(5439):509–512, 10 1999. URL `http://science.sciencemag.org/content/286/5439/509.abstract`.

I. Barth, I. Y. Dodin, and N. J. Fisch. Ladder climbing and autoresonant acceleration of plasma waves. *Phys. Rev. Lett.*, 115:075001, 2015.

R. Bédard. On commutation classes of reduced words in Weyl groups. *Europ. J. Combinatorics*, 20:483–505, 1999.

A. Berenstein, S. Fomin, and A. Zelevinsky. Parametrizations of canonical bases and totally positive matrices. *Adv. Math.*, 122:49–149, 1996.

G. Berkolaiko and J. Irving. Inequivalent factorizations of permutations. *J. Combin. Theory Ser. A*, 140:1–37, 2016.

I. B. Bernstein. Waves in a plasma in a magnetic field. *Phys. Rev.*, 109(1):10, 1958.

N. L. Biggs, E. K. Lloyd, and R. J. Wilson. *Graph Theory 1736–1936*. Oxford U. P., Oxford, 1976.

M. Binderbauer and T. Tajima. Conversion of high-energy photons into electricity, May 2013. URL http://www.google.com/patents/US20130125963. US Patent App. 13/521,220.

M. W. Binderbauer, T. Tajima, L. C. Steinhauer, E. Garate, M. Tuszewski, L. Schmitz, H. Y. Guo, A. Smirnov, H. Gota, D. Barnes, B. H. Deng, M. C. Thompson, E. Trask, X. Yang, S. Putvinski, N. Rostoker, R. Andow, S. Aefsky, N. Bolte, D. Q. Bui, F. Ceccherini, R. Clary, A. H. Cheung, K. D. Conroy, S. A. Dettrick, J. D. Douglass, P. Feng, L. Galeotti, F. Giammanco, E. Granstedt, D. Gupta, S. Gupta, A. A. Ivanov, J. S. Kinley, K. Knapp, S. Korepanov, M. Hollins, R. Magee, R. Mendoza, Y. Mok, A. Necas, S. Primavera, M. Onofri, D. Osin, N. Rath, T. Roche, J. Romero, J. H. Schroeder, L. Sevier, A. Sibley, Y. Song, A. D. Van Drie, J. K. Walters, W. Waggoner, P. Yushmanov, K. Zhai, and T. Team. A high performance field-reversed configurationa). *Phys. Plasmas*, 22(5):056110, 2015. doi: http://dx.doi.org/10.1063/1.4920950. URL http://scitation.aip.org/content/aip/journal/pop/22/5/10.1063/1.4920950.

A. Björner and F. Brenti. *Combinatorics of Coxeter Groups*. Graduate Texts in Mathematics. Springer, New York, 1st edition, 2005.

A. Björner, P. H. Edelman, and G. M. Ziegler. Hyperplane arrangements with a lattice of regions. *Discrete Comput. Geom.*, 5(3):263–288, 1990. ISSN 0179-5376. doi: 10.1007/BF02187790. URL http://dx.doi.org/10.1007/BF02187790.

A. Björner, L. Lovász, and P. W. Shor. Chip-firing games on graphs. *Europ. J. Combinatorics*, 12(4):283–291, 1991.

A. Bondy and U. S. R. Murty. *Graph Theory*. Graduate Texts in Mathematics. Springer-Verlag, London, 1st edition, 2008.

T. Brabec and F. Krausz. Intense few-cycle laser fields: Frontiers of nonlinear optics. *Rev. Mod. Phys.*, 72(2):545–591, 2000.

A. E. Bugrov, S. Y. Gus'kov, V. B. Rozanov, I. N. Burdonskiĭ, V. V. Gavrilov, A. Y. Gol'tsov, E. V. Zhuzhukalo, N. G. Koval'skiĭ, M. I. Pergament, and V. M. Petryakov. Interaction of a high-power laser beam with low-density porous media. *JETP*, 84:497, 1997.

D. Bundala and J. Závodnỳ. Optimal sorting networks. In *Language and Automata Theory and Applications*, pages 236–247. Springer, 2014.

V. Y. Bychenkov and V. F. Kovalev. Coulomb explosion in a cluster plasma. *Plasma Phys. Reports*, 31:178–183, 2005.

G. J. Caporaso. A general-class of self-similar power-driven expansions. *Phys. Fluids*, 25:436, 1982.

B. V. Chirikov. A universal instability of many-dimensional oscillator systems. *Phys. Rep.*, 52:263–379, 1979.

S. Choi and B. R. Moon. Isomorphism, normalization, and a genetic algorithm for sorting network optimization. In *Proceedings of the Genetic and Evolutionary Computation Conference*, GECCO '02, pages 327–334, San Francisco, 2002. Morgan Kaufmann. ISBN 1-55860-878-8. URL `http://dl.acm.org/citation.cfm?id=646205.682480`.

N. A. Christakis and J. H. Fowler. Social contagion theory: examining dynamic social networks and human behavior. *Stat. Med.*, 32(4):10.1002/sim.5408, 2013.

F. R. K. Chung. *Spectral graph theory*. Number 92 in Conference Board of the Mathematical Sciences: Regional Conference Series. American Mathematical Society, Providence, Rhode Island, 2009.

M. Codish, L. Cruz-Filipe, and P. Schneider-Kamp. The Quest for Optimal Sorting Networks: Efficient Generation of Two-Layer Prefixes. *ArXiv e-prints*, Apr. 2014.

R. Cohen, K. Erez, D. ben-Avraham, and S. Havlin. Resilience of the Internet to random breakdowns. *Phys. Rev. Lett.*, 85:4626, 2000.

L. Comtet. *Advanced Combinatorics*. D. Reidel, Dordrecht, The Netherlands, 1974.

J. Cooper and A. Kirkpatrick. Computing the Size of Intervals in the Weak Bruhat Order. *ArXiv e-prints*, July 2015.

S. Davidovits and N. J. Fisch. Fusion utility in the Knudsen layer. *Phys. Plasmas*, 21:092114, 2014.

J. M. Dawson. *Fusion*, volume 1. Academic Press, New York, 1981.

J. F. de la Mora and P. Riesco-Chueca. Aerodynamic focusing of particles in a carrier gas. *J. Fluid Mech.*, 195:1, 1988.

T. Desmet, R. Morent, N. D. Geyter, C. Leys, E. Schacht, and P. Dubruel. Nonthermal plasma technology as a versatile strategy for polymeric biomaterials surface modification: A review. *Biomacromolecules*, 10(9):2351–2378, 2009. doi: 10.1021/bm900186s. URL http://dx.doi.org/10.1021/bm900186s. PMID: 19655722.

E. Deza and M. M. Deza. *Figurate Numbers*. World Scientific, Hackensack, NJ, 2012.

D. Dhar. Self-organized critical state of sandpile automaton models. *Phys. Rev. Lett.*, 64:1613, 1990.

D. Dhar. The abelian sandpile and related models. *Physica A*, 263:4–25, 1999.

A. Di Piazza, C. Müller, K. Z. Hatsagortsyan, and C. H. Keitel. Extremely high-intensity laser interactions with fundamental quantum systems. *Rev. Mod. Phys.*, 84:1177–1228, Aug 2012. doi: 10.1103/RevModPhys.84.1177. URL http://link.aps.org/doi/10.1103/RevModPhys.84.1177.

R. Diestel. *Graph Theory*. Graduate Texts in Mathematics. Springer-Verlag, Berlin, 4th edition, 2010.

P. A. M. Dirac. The quantum theory of the emission and absorption of radiation. *Proc. R. Soc. Lond. A*, 114:243–265, 1927.

T. Ditmire, T. Donnelly, R. W. Falcone, and M. D. Perry. Strong x-ray emission from high-temperature plasmas produced by intense irradiation of clusters. *Phys. Rev. Lett.*, 75:3122–3125, Oct 1995. doi: 10.1103/PhysRevLett.75.3122. URL http://link.aps.org/doi/10.1103/PhysRevLett.75.3122.

T. Ditmire, J. W. G. Tisch, E. Springate, M. B. Mason, N. Hay, R. A. Smith, J. Marangos, and M. H. R. Hutchinson. High-energy ions produced in explosions of superheated atomic clusters. *Nature*, 386(6620):54–56, 03 1997. URL http://dx.doi.org/10.1038/386054a0.

T. Ditmire, J. Zweiback, V. P. Yanovsky, T. E. Cowan, G. Hays, and K. B. Wharton. Nuclear fusion from explosions of femtosecond laser-heated deuterium clusters. *Nature*, 398(6727):489–492, 04 1999. URL http://dx.doi.org/10.1038/19037.

I. Y. Dodin. Geometric view on noneikonal waves. *Phys. Lett. A*, 378:1598–1621, 2014.

I. Y. Dodin and N. J. Fisch. Variational formulation of the Gardner's restacking algorithm. *Phys. Lett. A*, 341:187, 2005.

D. Dragoman and M. Dragoman. *Quantum-Classical Analogies*. Springer, Berlin, 2004.

H. Dreicer. Electron and ion runaway in a fully ionized gas. I. *Phys. Rev.*, 115(2): 238, 1959.

C. Ehresman. Sur la topologie de certains éspaces homogènes. *Ann. Math.*, 35: 396443, 1934.

S. Eliezer and J. M. Martinez-Val. Proton-boron-11 fusion reactions induced by heat-detonation burning waves. *Laser Part. Beams*, 16:581, 1998.

G. A. Emmert, L. A. El-Guebaly, G. L. Kulcinski, J. F. Santarius, I. N. Sviatoslavsky, and D. M. Meade. Improvement in fusion-reactor performance due to ion channeling. In *11th Topical Meeting on the Technology of Fusion Energy*, pages 1158–1162, New Orleans, 1994.

P. Erdös and E. G. Straus. How abelian is a finite group? *Linear and Multilinear Algebra*, 3(4):307–312, 1976.

E. Esarey, C. B. Schroeder, and W. P. Leemans. Physics of laser-driven plasma-based electron accelerators. *Rev. Mod. Phys.*, 81:1229–1285, Aug 2009. doi: 10.1103/RevModPhys.81.1229. URL `http://link.aps.org/doi/10.1103/RevModPhys.81.1229`.

A. J. Fetterman. *Wave-driven rotation and mass separation in rotating magnetic mirrors*. PhD thesis, Princeton University, Jan 2012.

A. J. Fetterman and N. J. Fisch. Alpha channeling in a rotating plasma. *Phys. Rev. Lett.*, 101:205003, 2008.

N. J. Fisch. Transport in driven plasmas. *Phys. Fluids*, 29(1):172, 1986.

N. J. Fisch. Theory of current drive in plasmas. *Rev. Mod. Phys*, 59:175, 1987.

N. J. Fisch. Alpha channeling using ion Bernstein waves. *Phys. Plasmas*, 2:2375, 1995.

N. J. Fisch. Physics of alpha channeling and related TFTR experiments. *Nucl. Fusion*, 40:1095, 2000.

N. J. Fisch. Alpha channeling in mirror machines. *Phys. Rev. Lett.*, 97:225001, 2006.

N. J. Fisch. Alpha channeling in mirror machines and in tokamaks. *Trans. Fusion Science and Technology*, 51:1, 2007.

N. J. Fisch. Elementary processes underlying alpha channeling in tokamaks. *AIP Conf. Proc.*, 1478(1):80–90, 2012.

N. J. Fisch. Some unsolved challenges in radio-frequency heating and current drive. *Fusion Sci. Technol.*, 65, 2014.

N. J. Fisch. Pushing particles with waves: Current drive and α-channeling. *Plasma Fusion Res.*, 11:2101010, 2016.

N. J. Fisch and M. C. Herrmann. Utility of extracting alpha-particle energy by waves. *Nucl. Fusion*, 34:1541, 1994.

N. J. Fisch and M. C. Herrmann. Alpha power channeling with two waves. *Nucl. Fusion*, 35(12):1753, 1995.

N. J. Fisch and M. C. Herrmann. A tutorial on alpha-channeling. *Plasma Phys. Control. Fusion*, 41:A221, 1999.

N. J. Fisch and C. F. F. Karney. Asymptotic analysis of radio frequency heated collisional plasma. *Phys. Fluids*, 28(10):3107, 1985.

N. J. Fisch and J.-M. Rax. Current drive by lower hybrid waves in the presence of energetic alpha-particles. *Nucl. Fusion*, 13:549, 1992a.

N. J. Fisch and J.-M. Rax. Interaction of energetic alpha particles with intense lower hybrid waves. *Phys. Rev. Lett.*, 69:612–615, 1992b.

N. J. Fisch and J.-M. Rax. Free energy in plasmas under wave-induced diffusion. *Phys. Fluids B*, 5(6):1754, 1993.

N. J. Fisch, M. G. Gladush, Y. V. Petrushevich, P. Quarati, and A. N. Starostin. Enhancement of fusion rates due to quantum effects in the particles' momentum distribution in nonideal plasma media. *Eur. Phys. J. D*, 66:154, 2012.

J. P. Freidberg. *Plasma physics and fusion energy.* Cambridge U., Cambridge, 2007.

B. D. Fried and S. Conte. *The Plasma Dispersion Function.* Academic, New York, 1961.

B. D. Fried and A. Y. Wong. Stability limits for longitudinal waves in ion beam-plasma interaction. *Phys. Fluids*, 9:1084, 1966.

N. A. Fuchs. *The Mechanics of Aerosols*. MacMillan, New York, 1964.

C. S. Gardner. Bound on the energy available from a plasma. *Phys. Fluids*, 6:839, 1963.

V. I. Geyko, I. Y. Dodin, N. J. Fisch, and G. M. Fraiman. Supra-bubble regime for laser acceleration of cold electron beams in tenuous plasma. *Phys. Plasmas*, 17: 023105, 2010.

A. N. Gorban. Thermodynamic tree: The space of admissible paths. *SIAM J. Appl. Dyn. Syst.*, 12:246–278, 2013.

S. Gordienko and A. Pukhov. Scalings for ultrarelativistic laser plasmas and quasi-monoenergetic electrons. *Phys. Plasmas*, 12:043109, 2005.

M. Grech, R. Nuter, A. Mikaberidze, P. Di Cintio, L. Gremillet, E. Lefebvre, U. Saalmann, J. M. Rost, and S. Skupin. Coulomb explosion of uniformly charged spheroids. *Phys. Rev. E*, 84:056404, Nov 2011. doi: 10.1103/PhysRevE.84.056404. URL `http://link.aps.org/doi/10.1103/PhysRevE.84.056404`.

X. Guan, H. Qin, and N. J. Fisch. Phase-space dynamics of runaway electrons in tokamaks. *Phys. Plasmas*, 17:092502, 2010.

H. Y. Guo, M. W. Binderbauer, T. Tajima, R. D. Milroy, L. C. Steinhauer, X. Yang, E. G. Garate, H. Gota, S. Korepanov, A. Necas, T. Roche, A. Smirnov, and E. Trask. Achieving a long-lived high-beta plasma state by energetic beam injection. *Nat. Commun.*, 6, 04 2015. URL `http://dx.doi.org/10.1038/ncomms7897`.

M. J. Hay and N. J. Fisch. Ignition threshold for non-maxwellian plasmas. *Phys. Plasmas*, 22:112116, 2015.

M. J. Hay, E. J. Valeo, and N. J. Fisch. Geometrical optics of dense aerosols: Forming dense plasma slabs. *Phys. Rev. Lett.*, 111:188301, 2013.

M. J. Hay, J. Schiff, and N. J. Fisch. Maximal energy extraction under discrete diffusive exchange. *Phys. Plasmas*, 22:102108, 2015.

M. J. Hay, J. Schiff, and N. J. Fisch. Available free energy under local phase space diffusion. *ArXiv e-prints*, Apr. 2016.

M. C. Herrmann. *Cooling Alpha Particles with Waves*. PhD thesis, Princeton University, 1998.

M. C. Herrmann and N. J. Fisch. Cooling energetic alpha particles in a tokamak with waves. *Phys. Rev. Lett.*, 79:1495, 1997.

F. L. Hinton and R. D. Hazeltine. Theory of plasma transport in toroidal confinement systems. *Rev. Mod. Phys.*, 48(2):239, 1976.

H. Hora. *Laser Plasmas and Nuclear Energy*. Plenum, New York, 1975.

F. Horn. Attainable and non-attainable regions in chemical reaction techniques. In *Proceedings of the 3rd European Symposium on Chemical Reaction Engineering*, pages 1–10. Pergamon, 1964.

J. D. Huba. *NRL Plasma Formulary*. Naval Research Laboratory, Washington, 2007.

S. Ichimaru. Nuclear fusion in dense plasmas. *Rev. Mod. Phys.*, 65:255–299, Apr 1993. doi: 10.1103/RevModPhys.65.255. URL `http://link.aps.org/doi/10.1103/RevModPhys.65.255`.

G. Kaniadakis, A. Lavagno, and P. Quarati. Generalized statistics and solar neutrinos. *Phys. Lett. B*, 369:308–312, 1996.

C. F. F. Karney. Stochastic ion heating by a lower hybrid wave: II. *Phys. Fluids*, 22:2188, 1979.

C. F. F. Karney and N. J. Fisch. Numerical studies of current generation by radio-frequency traveling waves. *Phys. Fluids*, 22(9):1817–1824, 1979.

J. Kawahara, T. Saitoh, R. Yoshinaka, and S. Minato. Counting primitive sorting networks by πdds. TCS Technical Report TCS-TR-A-11-54, Hokkaido University, 2011.

M. J. Keeling and K. T. D. Eames. Networks and epidemic models. *J. R. Soc. Interface*, 2(4):295–307, 2005.

W. Kernbichler, R. Feldbacher, and M. Heindler. Parametric analysis of p-^{11}B as advanced reactor fuel. In *Proc. 10th Int. Conf.*, pages IAEA–CN–44/I–I–6, Vienna, 1987. IAEA.

D. E. Knuth. Axioms and hulls. *Lect. Notes Comput. Sci.*, 606, 1992.

D. E. Knuth. *The Art of Computer Programming, Volume 3: Sorting and Searching*. Addison-Wesley, 2 edition, 1997.

R. I. Kondor and J. Lafferty. Diffusion kernels on graphs and other discrete input spaces. In *Proc. Int'l Conf. on Machine Learning*, 2002.

M. Kraitchik. *Mathematical Recreations*, chapter 8.4.1, pages 209–211. W. W. Norton, New York, 1942.

N. A. Krall and A. W. Trivelpiece. *Principles of Plasma Physics*. McGraw-Hill, New York, 1973.

C. Labaune, C. Baccou, S. Depierreux, C. Goyon, G. Loisel, V. Yahia, and J. Rafelski. Fusion reactions initiated by laser-accelerated particle beams in a laser-produced plasma. *Nat. Commun.*, 4, 10 2013. URL `http://dx.doi.org/10.1038/ncomms3506`.

C. Labaune, C. Baccou, V. Yahia, C. Neuville, and J. Rafelski. Laser-initiated primary and secondary nuclear reactions in boron-nitride. *Sci. Rep.*, 6:21202, 2016. URL `http://dx.doi.org/10.1038/srep21202`.

S. Lang. *Algebra*. Graduate Texts in Mathematics. Springer, New York, rev. 3rd edition, 2002.

G. Lapenta and P. Quarati. Analysis of non-maxwellian fusion reaction rates with electron screening. *Z. Phys. A*, 346:243–250, 1993.

J. Lauer, H. Herold, H. Ruder, and G. Wunner. Bremsstrahlung in strong magnetic-fields: I. the elementary process. *J. Phys. B*, 16:3673, 1983.

J. D. Lawson. Some criteria for a power producing thermonuclear reactor. *Proc. Phys. Soc. B*, 70:6, 1957.

P. T. Leon, S. Eliezer, J. M. Martinez-Val, and M. Piera. Fusion burning waves in degenerate plasmas. *Phys. Lett. A*, 289:135, 2001.

E. Lerner and A. Blake. Method and apparatus for producing x-rays, ion beams and nuclear fusion energy, Aug 2007. URL `http://www.google.com/patents/US20070201598`. US Patent App. 11/365,105.

M. C. Levy, S. C. Wilks, M. Tabak, S. B. Libby, and M. G. Baring. Petawatt laser absorption bounded. *Nat. Commun.*, 5:4149, 2014.

M. A. Lieberman and A. J. Lichtenberg. *Principles of Plasma Discharges and Materials Processing*. Wiley, Hoboken, 2nd edition, 2005. ISBN 978-0-47172-425-4.

J. Lindl. Development of the indirect-drive approach to inertial confinement fusion and the target physics basis for ignition and gain. *Phys. Plasmas*, 2:3933, 1995.

P. Liu, P. J. Ziemann, D. B. Kittelson, and P. H. McMurry. Generating particle beams of controlled dimensions and divergence: I. theory of particle motion in aerodynamic lenses and nozzle expansions. *Aerosol Sci. Tech.*, 22:293, 1995a.

P. Liu, P. J. Ziemann, D. B. Kittelson, and P. H. McMurry. Generating particle beams of controlled dimensions and divergence: Ii. experimental evaluation of particle motion in aerodynamic lenses and nozzle expansions. *Aerosol Science and Technology*, 22(3):314–324, 1995b. doi: 10.1080/02786829408959749. URL `http://dx.doi.org/10.1080/02786829408959749`.

A. L. Lloyd and R. M. May. How viruses spread among computers and people. *Science*, 292(5520):1316–1317, 05 2001. URL `http://science.sciencemag.org/content/292/5520/1316.abstract`.

D. Lynden-Bell. Statistical mechanics of violent relaxation in stellar systems. *Mon. Not. R. astr. Soc.*, 136:101–121, 1967.

V. M. Malkin and N. J. Fisch. Extended propagation of powerful laser pulses in focusing Kerr media. *ArXiv e-prints*, June 2016.

V. M. Malkin, G. Shvets, and N. J. Fisch. Fast compression of laser beams to highly overcritical powers. *Phys. Rev. Lett.*, 82:4448, 1999.

V. M. Malkin, Z. Toroker, and N. J. Fisch. Laser duration and intensity limits in plasma backward raman amplifiers. *Phys. Plasmas*, 19(2):023109, 2012. doi: http://dx.doi.org/10.1063/1.3683558. URL `http://scitation.aip.org/content/aip/journal/pop/19/2/10.1063/1.3683558`.

W. Manheimer. Fusion breeding for mid-century sustainable power. *J. Fusion Energy*, 33:199–234, 2014.

A. W. Marshall, I. Olkin, and B. C. Arnold. *Inequalities: Theory of Majorization and Its Applications*. Springer, New York, 2nd edition, 2009.

J. M. Martinez-Val, S. Eliezer, M. Piera, and G. Velarde. Fusion burning waves in proton-boron-11 plasmas. *Phys. Lett. A*, 216:142, 1996.

P. E. Mason, F. Uhlig, V. Vaněk, T. Buttersack, S. Bauerecker, and P. Jungwirth. Coulomb explosion during the early stages of the reaction of alkali metals with water. *Nat. Chem.*, 7(3):250–254, 03 2015. URL `http://dx.doi.org/10.1038/nchem.2161`.

D. R. Mikkelsen. Approximation for non-resonant beam target fusion reactivities. *Nucl. Fusion*, 29:1113, 1989.

G. S. Miller, E. E. Salpeter, and I. Wasserman. Deceleration of infalling plasma in the atmospheres of accreting neutron-stars: I. isothermal atmospheres. *Astrophys. J.*, 314:215, 1987.

K. Molvig, N. M. Hoffman, B. J. Albright, E. M. Nelson, and R. B. Webster. Knudsen layer reduction of fusion reactivity. *Phys. Rev. Lett.*, 109:095001, 2012.

R. Monasson. Diffusion, localization and dispersion relations on "small-world" lattices. *Eur. Phys. J. B*, 12:555–567, 1999.

P. J. Morrison and D. Pfirsch. Free-energy expressions for Vlasov equilibria. *Phys. Rev. A*, 40:3898–3910, 1989.

P. J. Morrison and D. Pfirsch. The free energy of Maxwell-Vlasov equilibria. *Phys. Fluids B*, 2:1106–1113, 1990.

P. J. Morrison and D. Pfirsch. Dielectric energy versus plasma energy, and Hamiltonian action-angle variables for the Vlasov equation. *Phys. Fluids B*, 4:3038–3057, 1992.

G. Mourou, N. Fisch, V. Malkin, Z. Toroker, E. Khazanov, A. Sergeev, T. Tajima, and B. L. Garrec. Exawatt-zettawatt pulse generation and applications. *Optics Communications*, 285(5):720 – 724, 2012. ISSN 0030-4018. doi: http://dx.doi.org/10.1016/j.optcom.2011.10.089. URL `http://www.sciencedirect.com/science/article/pii/S0030401811012338`.

T. Nakamura, J. K. Koga, T. Z. Esirkepov, M. Kando, G. Korn, and S. V. Bulanov. High-power γ-ray flash generation in ultraintense laser-plasma interactions. *Phys. Rev. Lett.*, 108:195001, May 2012. doi: 10.1103/PhysRevLett.108.195001. URL `http://link.aps.org/doi/10.1103/PhysRevLett.108.195001`.

W. M. Nevins. A review of confinement requirements for advanced fuels. *J. Fusion Energy*, 17:25, 1998.

W. M. Nevins and R. Swain. The thermonuclear fusion rate coefficient for p-b-11 reactions. *Nucl. Fusion*, 40:865, 2000.

J. Nuckolls, J. Lindl, W. Mead, A. Thiessen, L. Wood, and G. Zimmerman. Laser driven implosion of hollow pellets. Technical Report UCRL 75538, Univ. of CA. Livermore, Nov 1974.

I. E. Ochs, N. Bertelli, and N. J. Fisch. Coupling of alpha channeling to parallel wavenumber upshift in lower hybrid current drive. *Phys. Plasmas*, 22:082119, 2015a.

I. E. Ochs, N. Bertelli, and N. J. Fisch. Alpha channeling with high-field launch of lower hybrid waves. *Phys. Plasmas*, 22:112103, 2015b.

OEIS Foundation Inc. The On-Line Encyclopedia of Integer Sequences. `http://oeis.org/A005118`, 2011. [Online; accessed 13-Aug-2015].

OEIS Foundation Inc. The On-Line Encyclopedia of Integer Sequences. `http://oeis.org/A006245`, 2014a. [Online; accessed 11-Jan-2016].

OEIS Foundation Inc. The On-Line Encyclopedia of Integer Sequences. `http://oeis.org/A246865`, 2014b. [Online; accessed 13-Aug-2015].

OEIS Foundation Inc. The On-Line Encyclopedia of Integer Sequences. `http://oeis.org/A239568`, 2014c. [Online; accessed 13-Aug-2015].

I. Parberry. On the computational complexity of optimal sorting network verification. In *Proc. PARLE '91: Parallel Architectures and Languages Europe, Volume I: Parallel Architectures and Algorithms*, pages 252–269, Eindhoven, The Netherlands, 1991.

R. Pastor-Satorras and A. Vespignani. Epidemic spreading in scale-free networks. *Phys. Rev. Lett.*, 86:3200–3203, Apr 2001. doi: 10.1103/PhysRevLett.86.3200. URL `http://link.aps.org/doi/10.1103/PhysRevLett.86.3200`.

Y. Ping, W. Cheng, S. Suckewer, D. S. Clark, and N. J. Fisch. Amplification of ultrashort laser pulses by a resonant Raman scheme in a gas-jet plasma. *Phys. Rev. Lett.*, 92:175007, 2004.

P. Porshnev, S. Bivona, and G. Ferrante. Evolution of the electron distribution function in intense laser-plasma interactions. *Phys. Rev. E*, 50(5):3943, 1994.

R. F. Post. Mirror systems: Fuel cycles, loss reduction and energy recovery. In *Proc. Brit. Nucl. Energy Soc. Conf. Nucl. Fusion Reactors*, page 88, Culham, England, 1969. UKAEA, Culham Laboratory.

H. Prodinger and R. F. Tichy. Fibonacci numbers of graphs. *Fibonacci Q.*, 20:16–21, 1982.

T. H. Rider. *Fundamental Limitations on Plasma Fusion Systems Not in Thermodynamic Equilibrium*. PhD thesis, Massachusetts Institute of Technology, 1995.

M. D. Rosen, P. L. Hagelstein, D. L. Matthews, E. M. Campbell, A. U. Hazi, B. L. Whitten, B. MacGowan, R. E. Turner, R. W. Lee, G. Charatis, G. E. Busch, C. L. Shepard, and P. D. Rockett. Exploding-foil technique for achieving a soft x-ray laser. *Phys. Rev. Lett.*, 54:106–109, Jan 1985. doi: 10.1103/PhysRevLett.54.106. URL `http://link.aps.org/doi/10.1103/PhysRevLett.54.106`.

D. E. Ruiz, L. M. Gunderson, M. J. Hay, E. Merino, E. J. Valeo, S. J. Zweben, and N. J. Fisch. Aerodynamic focusing of high-density aerosols. *J. Aerosol Sci.*, 76: 115–125, 2014.

G. B. Rybicki and A. P. Lightman. *Radiative Processes in Astrophysics*. Wiley-VCH, Weinheim, Germany, 1985.

E. E. Salpeter. Electron screening and thermonuclear reactions. *Austr. J. Phys.*, 7 (3):373 – 388, 1954.

M. J. Samuel. Word posets, complexity, and Coxeter groups. *ArXiv e-prints*, Jan. 2011a.

M. J. Samuel. Word posets, with applications to Coxeter groups. *ArXiv e-prints*, Aug. 2011b.

V. I. Savchenko, N. J. Fisch, A. A. Panteleev, and A. N. Starostin. Role of quantum interference in thermodynamic equilibrium. *Phys. Rev. A*, 59(1):708, 1999.

P. F. Schmit and N. J. Fisch. Driving sudden current and voltage in expanding and compressing plasma. *Phys. Rev. Lett.*, 108:215003, 2012.

P. F. Schmit, I. Y. Dodin, and N. J. Fisch. Controlling hot electrons by wave amplification and decay in compressing plasma. *Phys. Rev. Lett.*, 105:175003, 2010.

B. S. W. Schröder. *Ordered Sets: An Introduction*. Birkhäuser, Boston, 1st edition, 2002.

F. Schwabl. *Quantum Mechanics*. Springer, Berlin, 4 edition, 2007.

J. Schwinger. On gauge invariance and vacuum polarization. *Phys. Rev.*, 82(5): 664–679, 1951.

J. K. Shultis and R. E. Faw. *Fundamentals of Nuclear Science and Engineering*. CRC Press, Boca Raton, 2 edition, 2007.

S. A. Slutz and R. A. Vesey. High-gain magnetized inertial fusion. *Phys. Rev. Lett.*, 108:025003, 2012.

G. R. Smith and A. N. Kaufman. Stochastic acceleration by a single wave in a magnetic field. *Phys. Rev. Lett.*, 34:1613–1616, Jun 1975. doi: 10.1103/PhysRevLett.34.1613. URL `http://link.aps.org/doi/10.1103/PhysRevLett.34.1613`.

R. A. Snavely, M. H. Key, S. P. Hatchett, T. E. Cowan, M. Roth, T. W. Phillips, M. A. Stoyer, E. A. Henry, T. C. Sangster, M. S. Singh, S. C. Wilks, A. MacKinnon, A. Offenberger, D. M. Pennington, K. Yasuike, A. B. Langdon, B. F. Lasinski, J. Johnson, M. D. Perry, and E. M. Campbell. Intense high-energy proton beams from petawatt-laser irradiation of solids. *Phys. Rev. Lett.*, 85:2945–2948, Oct 2000. doi: 10.1103/PhysRevLett.85.2945. URL `http://link.aps.org/doi/10.1103/PhysRevLett.85.2945`.

S. Son and N. J. Fisch. Aneutronic fusion in a degenerate plasma. *Phys. Lett. A*, 329:76, 2004.

S. Son and N. J. Fisch. Pycnonuclear reaction and possible chain reactions in an ultra-dense dt plasma. *Phys. Lett. A*, 337:397–407, 2005.

R. P. Stanley. On the number of reduced decompositions of elements of Coxeter groups. *Europ. J. Combinatorics*, 5:359–372, 1984.

R. P. Stanley. *Enumerative Combinatorics, Volume I*. Cambridge Studies in Advanced Mathematics. Cambridge U. P., New York, 2 edition, 2011.

A. N. Starostin, V. I. Savchenko, and N. J. Fisch. Effect of quantum uncertainty on the rate of nuclear reactions in the Sun. *Phys. Lett. A*, 274:64–68, 2000.

S. Stave, M. W. Ahmed, R. H. France, S. S. Henshaw, B. Muller, B. A. Perdue, R. M. Prior, M. C. Spraker, and H. R. Weller. Understanding the $^{11}B(p,\alpha)\alpha\alpha$ reaction at the 0.675 MeV resonance. *Phys. Lett. B*, 696:26, 2011.

J. R. Stembridge. On the fully commutative elements of Coxeter groups. *J. Algebraic Combin.*, pages 353–385, 1996.

T. H. Stix. *Waves in Plasmas*. Springer-Verlag, New York, 1992.

C. Stover and E. W. Weisstein. Pascal's triangle. From *MathWorld*—A Wolfram Web Resource, n.d. Last visited 6/21/2016.

H. Sze, J. Banister, B. H. Failor, J. S. Levine, N. Qi, A. L. Velikovich, J. Davis, D. Lojewski, and P. Sincerny. Efficient radiation production in long implosions of structured gas-puff z pinch loads from large initial radius. *Phys. Rev. Lett.*, 95: 105001, 2005.

M. Tabak, J. Hammer, M. E. Glinsky, W. L. Kruer, S. C. Wilks, J. Woodworth, E. M. Campbell, M. D. Perry, and R. J. Mason. Ignition and high gain with ultrapowerful lasers. *Phys. Plasmas*, 1:1626–1634, 1994.

T. Tajima and J. M. Dawson. Laser electron accelerator. *Phys. Rev. Lett.*, 43:267–270, Jul 1979. doi: 10.1103/PhysRevLett.43.267. URL `http://link.aps.org/doi/10.1103/PhysRevLett.43.267`.

T. Tanizawa, G. Paul, R. Cohen, S. Havlin, and S. E. Stanley. Optimization of network robustness to waves of targeted and random attacks optimization of network robustness to waves of targeted and random attacks. *Phys. Rev. E*, 71:047101, 2005.

D. Thon and S. W. Wallace. Dalton transfers, inequality and altruism. *Soc. Choice Welfare*, 22:447, 2004.

A. N. Tkachev and S. I. Yakovlenko. Coulomb explosion of a laser plasma. *Quantum Electron.*, 23(11):972–974, 1993.

E. Todorov. *Optimal control theory*. Bayesian Brain. MIT, Cambridge, MA, 2006.

Z. Toroker, V. M. Malkin, A. A. Balakin, G. M. Fraiman, and N. J. Fisch. Geometrical constraints on plasma couplers for Raman compression. *Phys. Plasmas*, 19: 083110, 2012.

E. R. Tracy, A. J. Brizard, A. S. Richardson, and A. N. Kaufman. *Ray Tracing and Beyond: Phase Space Methods in Plasma Wave Theory*. Cambridge U. P., New York, 2014.

V. N. Tsytovich. *Nonlinear Effects in Plasma*. Plenum, New York, 1970.

E. J. Valeo and N. J. Fisch. Excitation of large k_θ ion-Bernstein waves in tokamaks. *Phys. Rev. Lett.*, 73:3536, 1994.

A. A. Vedenov, E. P. Velikhov, and R. Z. Sagdeev. The quasi-linear theory of plasma oscillationss. *Nucl. Fusion Suppl.*, 2:465, 1962.

D. N. Verma. Möbius inversion for the Bruhat ordering on a Weyl group. *Ann. Sci. École Norm. Sup.*, 4:393–398, 1971.

X. Wang and P. H. McMurry. An experimental study of nanoparticle focusing with aerodynamic lenses. *International Journal of Mass Spectrometry*, 258(1–3):30 – 36, 2006. ISSN 1387-3806. doi: http://dx.doi.org/10.1016/j.ijms.2006.06.008. URL `http://www.sciencedirect.com/science/article/pii/S138738060600306X`. Aerosols/Microparticles Special Issue.

D. J. Watts. Networks, dynamics and the small-world phenomenon. *Am. J. Sociol.*, 105(2):493–527, 1999.

D. J. Watts and S. H. Strogatz. Collective dynamics of 'small-world' networks. *Nature*, 393(6684):440–442, 06 1998. URL `http://dx.doi.org/10.1038/30918`.

F. Wei. The Weak Bruhat Order and Separable Permutations. *ArXiv e-prints*, Sept. 2010.

E. W. Weisstein. Graph composition. From *MathWorld*—A Wolfram Web Resource, n.d.a. Last visited 6/21/2016.

E. W. Weisstein. Hypercube. From *MathWorld*—A Wolfram Web Resource, n.d.b. Last visited 6/21/2016.

E. Wigner. On the quantum correction for thermodynamic equilibrium. *Phys. Rev.*, 40:749–759, Jun 1932. doi: 10.1103/PhysRev.40.749. URL `http://link.aps.org/doi/10.1103/PhysRev.40.749`.

Y. Y. Yamaguchi. One-dimensional self-gravitating sheet model and Lynden-Bell statistics. *Phys. Rev. E*, 78:041114, 2008.

T. Yamamoto and M. Okubo. *Nonthermal Plasma Technology*, pages 135–293. Humana Press, Totowa, NJ, 2007. ISBN 978-1-59745-173-4. doi: 10.1007/978-1-59745-173-4_4. URL `http://dx.doi.org/10.1007/978-1-59745-173-4_4`.

T. Yanagimoto and M. Okamoto. Partial orderings of permutations and monotonicity of a rank correlation statistic. *Ann. Institute Statistical Math.*, 21:489–506, 1969.

M. Yannakakis. Expressing combinatorial optimization problems by linear programs. *J. Comput. Syst. Sci*, 43:441–466, 1991.

A. I. Zhmoginov and N. J. Fisch. Flux control in networks of diffusion paths. *Phys. Lett. A*, 372:5534–5541, 2008.

C. Zylka. A note on the attainability of states by equalizing processes. *Theor. Chim. Acta*, 68:363, 1985.